Universitetet i Stavanger

FACULTY OF SCIENCE AND TECHNOLOGY

MASTER'S THESIS

Study programme/specialisation: Offshore Technology / Marine and Subsea Technology	Spring semester, 2017 Open/~~Confidential~~
Author: Bjarte Knapstad	Bjarte Knapstad ..... (signature of author)
Programme coordinator: Professor Daniel Karunakaran, University of Stavanger and Subsea7 **Supervisor:** Professor Daniel Karunakaran	
Title of master's thesis: Optimisation of Steel Lazy Wave Risers	
Credits (ECTS): 30	
Keywords: Steel Lazy Wave Riser, Optimisation, DNV-OS-F201, Extreme Response Analysis, Wave Induced Fatigue, Ultra-Deep Water	Number of pages: 74 + enclosure: 19 Stavanger: 13th of July 2017

Optimisation of Steel Lazy Wave Risers

Master Thesis

Offshore Technology

Marine and Subsea Technology

Bjarte Knapstad

Spring 2017

Abstract

The objective of this thesis is to optimise the performance of an initial Steel Lazy Wave Riser (SLWR) configuration with regards to the combined loading criteria in the Offshore Standard DNV-OS-F201: Dynamic Risers. This is done by conducting large scale parameter variations for the configuration using the programming interface in the OrcaFlex analysis software. The study considers the implementation of SLWRs in ultra-deep waters, in conjunction with a Floating Production Storage and Offloading (FPSO) vessel.

Being connected to a spread moored FPSO in a water depth of 2800 meters, the riser configurations are analysed for typical extreme environmental conditions found in the Santos basin off the coast of Brazil. By analysing the vessel response for different 100-year waves, the worst conditions are determined in terms of the largest downward velocities experienced at hang-off point. These parameters are used in combination with a 10-year current to study the extreme response behaviour for the different configurations analysed.

From the design basis, an initial SLWR configuration is established and it is verified that it meets the stated design criteria for combined loading and the wave induced fatigue. This configuration is then subjected to parameter variations by altering the hang-off angle, total net buoyancy force and length of buoyancy section. A total of 75 different configurations are created and analysed under extreme environmental conditions to determine a better configuration in terms of the combined loading utilisation. The findings are presented and a comparison of selected configurations are given to better understand the effect of the parameter variations.

The optimisation results show that all the configurations meet the Ultimate Limit State (ULS) design criteria, and that the maximum utilisation experienced in the different cases varies significantly. With tension being the main contributor for the combined loading in these water depths, it is found that a combination of reduced hang-off angle and increased net buoyancy force will improve the performance of the configuration. From the optimisation study, the best configuration is determined and assessed for wave induced fatigue life. The fatigue results show an increase in fatigue life, which also reflects the importance of reducing the top tension.

The work presented in this thesis provides information on how different parameters for a SLWR in ultra-deep water affects the combined loading utilisation, and it is proven that this concept is feasible for use in conjunction with a FPSO in these water depths.

Acknowledgment

First, I would like to thank Professor Daniel Karunakaran for the opportunity to write this thesis under his guidance. He has always been available for any enquiry and been a very supportive mentor through this whole period. His positive attitude and constructive feedback has been vital for the progress and finalisation of this thesis.

Subsea7 for making me feel welcome and giving me a desk space in their office at Forus, this gave me an opportunity to be close to the needed expertise on the many subjects and access to analysis programs needed for this thesis.

Øystein Døskeland, Senior Engineer at Subsea7, the OrcaFlex and Python guru who time and time again helped with programming and theoretical understanding to help with the progress of this thesis.

Yuri Vladimirovic Novoseltsev for giving a basic introduction to the OrcaFlex-Python interface and programming.

I would like to thank Professor Ove Tobias Gudmestad for helping me with defining the project scope in the Marine Operations course, which led me to the topic for this Master thesis.

Adekunle Peter Orimolade, fellow at the University of Stavanger, for providing me with answers for any questions regarding the topic and the use of the OrcaFlex software.

Abraham Aimuth Tewolde, my fellow student from UiS, I could not ask for a more supportive and helpful desk mate. Thanks for all the good discussions and for increasing my skills in table soccer.

A big thank you to Svein Erik Nuland for taking the time to proofread and give feedback on my work, and for helping me with the finalising of the thesis setup.

And to all my fellow students and lecturers at the University of Stavanger, thanks for the many good memories over the past two years.

Stavanger, 13th of July 2017
Bjarte Knapstad

Table of contents

List of figures

*Remark: Figures without references are made by the author.

List of tables

Abbreviations

BHR	Bundled Hybrid Riser
CRA	Corrosion Resistant Alloy
DLL	Dynamic Link Library
DNV	Det Norske Veritas
DoF	Degrees of Freedom
FPU	Floating Production Unit
GoM	Gulf of Mexico
LF	Low Frequency
LRFD	Load and Resistance Factor Design
N/A	Not Applicable
NPV	Net Present Value
OS	Offshore Standard
OSS	Offshore Service Specifications
RFC	Rain Flow Counting
RP	Recommended Practice
SCR	Steel Catenary Riser
SHR	Single Hybrid Riser
SLWR	Steel Lazy Wave Riser
TLP	Tension Leg Platform
TTR	Top-Tensioned Riser
VIV	Vortex Induced Vibration
WF	Wave Frequency

Chapter 1 Introduction

1.1 Background

In the offshore oil and gas industry, the evolution has gone from a well being drilled off a pier on the coast of California, to steel-jacket platforms and large gravity based structures in water depths of several hundred meters (SPE International, 2015). These fixed platforms have an economic and structural limit in which they are feasible (Odland, 2015), which has resulted in the development of floating solutions for use in deeper waters. Since floating production units (FPU) are to some extent able to move in all six Degrees of Freedom (DoF), there are challenges related to the dynamic forces on connected equipment. Thus, the wellhead and valve-tree is often moved from the topside and onto the seabed, known as a subsea solution, and from there the well-stream is transported topside using a suitable pipe, called a riser.

Being the link between topside facilities and the subsea equipment, the riser is a key component in the offshore oil and gas industry. From the early stage of exploration through to the production, import and export of hydrocarbons, the riser plays a vital part. Therefore, it is paid a lot of attention to ensure high availability while meeting all the stringent safety requirements set for offshore oil and gas production (Kirkemo et al., 1999).

As the demand for energy has increased (U.S. Energy Information Administration, 2016), the search for new hydrocarbon reservoir has pushed the frontier of oil and gas production into deeper water in harsher environment. This has led to new riser solutions, and adaptation of conventional riser technology to cope with the forces associated with floater motion and the increased depth.

In Figure 1, different production concepts are shown, ranging from fixed platforms in shallow waters through to FPUs in deep and ultradeep waters. In this thesis, shallow water will be referred to as being below 500 m, deep waters in the range of 500 m to 2000 m and ultradeep is more than 2000 m deep.

When going in to water depths greater than 450 m the choice of platform, as a rule of thumb, is a FPU of some sort. The selection of type of platform depends on a range of factors such as net-present-value (NPV) of development, motion characteristics, loadbearing and storage abilities and many more considerations (Odland, 2015). Selection of production riser, is in turn based on the type of host platform, water depth, environmental conditions, design pressure and temperature, with the dynamic behaviour of the FPU as the main design driver.

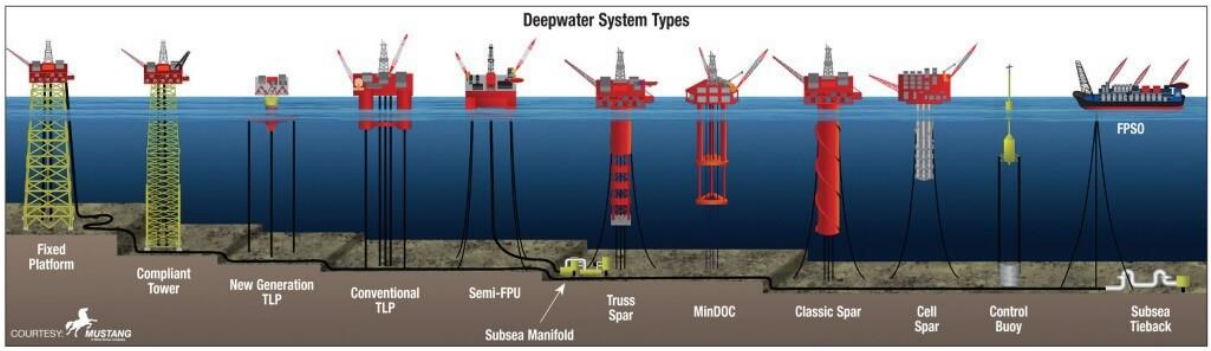

Figure 1: Different deep-water platforms and production concepts (Offshore Magazine, 2015)

Production risers can be divided into two categories, rigid and flexible risers, and a combination of these two is called a hybrid riser solution (Bai and Bai, 2012). Traditionally the flexible riser solution has been the preferred solution for FPUs in shallow to deep-water field development, whereas the rigid steel risers has been used for fixed platforms or as a top-tensioned riser solution (TTR) for floating platforms with desirable motion characteristics, such as a Spar or Tension-Leg Platform (TLP). Flexible risers can be laid in a wide range of configurations which decouples the motion induced forces of the surface facility from affecting the touchdown region by geometrical changes in the configuration, known as a compliant configuration. Even though the flexible riser offers a range of beneficial properties and easy instalment, it has limitations regarding large diameter bore in deeper waters and is much more expensive per meter than a rigid steel solution (Phifer et al., 1994).

Targeting these issues, the use of compliant rigid steel risers has gained popularity lately and become an attractive solution. One such being the steel catenary riser (SCR) concept, which in its simplest form is a steel pipe suspended by its own weight in a near vertically direction from a platform and then curves out into the horizontal plane at the seabed. These risers offer larger production diameter at a lower cost, and has proven to be a good solution in combination with low motion platforms. The first SCR was installed on the Auger TLP in the Gulf of Mexico (GoM) in 1994 (Carter and Ronalds, 1998), and have since been applied in harsher environments in combination with platforms with favourable motion characteristics. The limitation of the SCR, is its ability to withstand vertical motions causing compression and fatigue damages in the touchdown region, especially in combination with floaters in harsh environments. A study conducted by (Karunakaran et al., 2002) targeted this problem by varying the weight along the riser, using different types of coating with different densities, which improved the dynamic performance of the concept. Still, the use of SCRs in combination with large motion vessels in harsh environments poses a great challenge (Legras et al., 2013).

For application in harsh environments in conjunction with large motion vessels, the SCR concept can be further modified by increasing its length and adding buoyancy elements over a section of the riser, creating a wave configuration known as a Steel Lazy Wave Riser (SLWR). This significantly improves its dynamic performance by allowing the wave section of the configuration to comply with the motion of the topside vessel, thus absorbing a large part of the forces and keeping them from reaching the touchdown area. By combining good dynamic behaviour with the desired material properties needed for deep and ultradeep field development, the use of the SLWR concept has been gaining popularity around the world.

As for all types of riser solutions, they must meet project requirements set by the oil company and follow the design criteria specified in all relevant standards before realisation. This involves studies where the design and configuration is analysed to verify the feasibility of different solutions. In this process, many simulations and trials are executed to determine the best possible configuration for each riser, which can be a time-consuming process if done manually, but it doesn't necessarily lead to an optimum solution. Consequently, there have lately been an increased focus on optimising the SLWR configuration to obtain a best possible solution by use of more automated solutions (Andrade et al., 2010). One such solution is to use programming interfaces in the analysis software, which allows for programmed scripts to create files, change parameters within the analysis software and collect the results in a systematic way.

1.2 Objective and Scope

The main objective for this thesis is to optimise an initial SLWR configuration by use of the Python programming interface for OrcaFlex. The optimisation criteria will be based on improving the utilisation factor in terms of the combined loading criteria presented in the premise. All cases are considered for use in conjunction with a spread moored FPSO located in the ultra-deep waters off the coast of Brazil.

The scope includes a brief presentation of different deep-water riser concepts with proven merits currently in operation. An introduction to the reference standard, DNV-OS-F201: Dynamic Risers, is given together with a presentation of the limit state design criteria used in this study. A detailed description of each limit state is given along with the parameters used in the analyses.

From listed material and field specific parameters, an initial SLWR configuration is determined and extreme response and fatigue analyses are conducted based on given environmental conditions. Methodology for determining the environmental parameters to be used for the

extreme response behaviour analyses are presented in detail. The environmental data selected based on typical 100-year sea states in combination with a 10-year current found in this region.

The extreme response and fatigue results are presented and discussed to better understand the dynamics of the system, and it is verified that the configuration meets the design criteria stated. The end result will be a presentation of the findings done in the optimisation study. These design cases are conducted by varying buoyancy length, buoyancy force and hang-off angle to determine a more optimum configuration in terms of the combined loading utilisation for the ULS design criteria. Discussion and conclusions will be done based on these results to better understand the driving design factors in determining a best possible configuration for SLWRs in ultra-deep waters.

1.3 Justification

With decreasing oil prices, the demand for more cost saving and optimised solutions in the oil and gas industry has been in focus the last couple of years. This approach can be applied for riser engineering by using more automated procedures in the engineering analyses.

The traditional way of analysing the global behaviour of a riser configuration has been to make individual cases manually for all the different parameter changes, and then run simulation for each case and manually do the post processing and comparison of the obtained results.

An emerging approach for large batch processing, is the use of programming interfaces which allows for an easy and fast way of doing analysis. By use of a programming language, a script can be made to create new files in the analysis software, change parameters and do post-processing by collecting the results. This saves a lot of time in engineering hours and is a convenient way of sorting out all undesired configurations, thus making it easy to focus on the ones that gives the most promising results. This thesis will not address the optimisation in terms of cost, installation and dimensioning of buoyancy modules, but rather focus on increasing the performance of the SLWR based on the ULS criteria given in the reference standard.

Chapter 2 Deepwater Riser Systems

2.1 Introduction

The riser plays a part in the entire lifecycle of an offshore field development and can be divided into the following concepts:

- Drilling riser
- Production riser
- Export riser
- Injection riser

The drilling riser is a rigid steel riser involved in exploration, completion, workover and plugging operations and play a crucial role in the development and service of a well. This riser is only in use for temporarily operations, whereas the remaining three concepts are installed on a more permanent basis. The production, export and injection risers are in principle the same, but serve different purposes in the field development and they are either made up of rigid steel risers, flexible risers or a combination of the two, called a hybrid riser. For a field development, the selection of riser concept depends on several factors, like cost, topside facility, water depth and environmental conditions. In deep- and ultra-deep waters, where the topside facility consists of a FPU, the main design driver will be the floater motions.

The riser arrangement is subjected to both internal and external loads, and must be design such that it has a sufficient safety margin to withstand all subjected loads, such as:

- Platform/Vessel motions
- Pressure
- Weight
- Current
- Wave forces and fatigue
- Vortex Induced Vibrations (VIV)
- Interference with auxiliary equipment and other risers

2.2 Flexible Risers

Flexible risers are pipes with high axial stiffness and low bending stiffness. These risers are made up of several individual layers and can be divided in to two different categories, un-bonded and bonded type. The difference being that the layers in the un-bonded riser is free to move in relation to each other, whereas the bonded type "lock" the different layers together by use of a polymer material. Bonded flexible pipes are usually only used for shorter sections, such as topside jumpers. The un-bonded flexible riser has historically been the preferred solution for production risers in combination with FPUs in shallow waters. With an operational history of over 40 years, the concept has evolved to meet the demand for larger production bore, and the challenges faced with the implementation in increased water depth. And as of 2014, there are flexible risers certified for water depths of 3000m (Luppi et al., 2014).

A conventional un-bonded flexible riser, as shown in Figure 2, consists of a metallic inner carcass to withstand the outer environmental pressure and a plastic pressure sheath to keep the production fluids from mitigating to the annulus. For pressure containment, a hoop layer is spun around the pressure sheath, then follows a paired tension layer that is spun in opposite directions with wear-protective layers in between. The outer sheath consists of a thermoplastic material that protects the metallic layers from the outside environment.

Due to its low bending stiffness and high axial strength, the flexible riser can be installed in many different configurations and is able to take large motions and withstand the wave induced motions from an FPU over time, ensuring good fatigue resistance (DNV, 2010b). It also offers other benefits such as easy instalment, and it can be relocated and used again after decommissioning. In recent years, composite materials have been introduced in the production of flexibles to reduce weight, save cost and improve corrosion protection (Kalman et al., 2014).

Even though the flexible riser provides many desired properties and has an extensive track record, it has its limitations when it comes to deep waters. Due to the increased external pressure, the production bore is limited in these depths (Carter and Ronalds, 1998). This needs to be taken into consideration in concept selection, together with the cost of construction, which is much higher than compared to rigid steel risers.

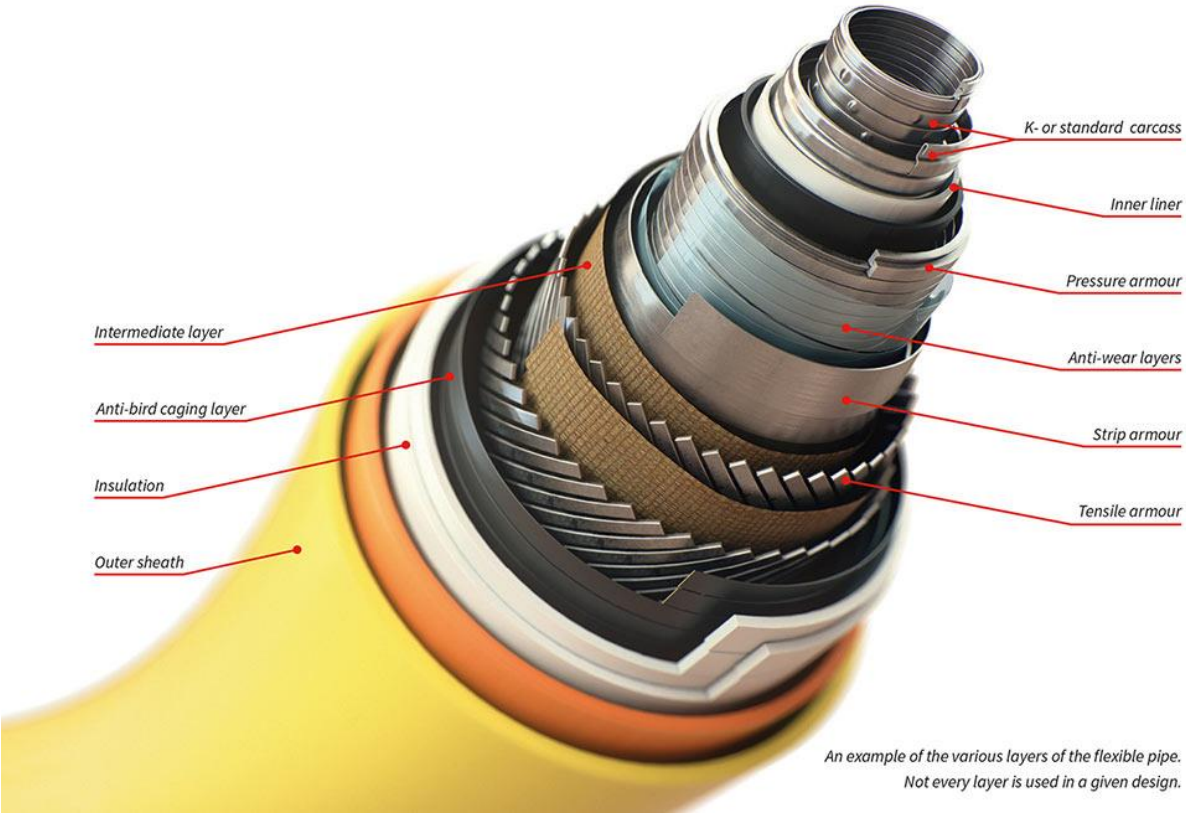

Figure 2: Multilayer Flexible Pipe (NOV, 2017).

2.3 Rigid Steel Risers

Rigid steel risers are sections of pipe that are joined together to a desired length by welding, flanges, threads or other means, and have traditionally been used in combination with fixed platforms where they are supported laterally by the substructure (Chakrabarti, 2005). When using FPUs and moving into deeper waters, the dynamic forces become more prevailing and the implementation of rigid steel risers becomes more challenging. In this section, the two main types of rigid steel riser concepts for deep-water production will be presented.

2.3.1 Steel Catenary Risers

The Steel Catenary Riser (SCR) is a single pipe that is coupled directly to the topside facility, where it is suspended by its own weight from a near vertical direction topside to the horizontal plane at the seabed. The shape of the configuration follows the catenary equation in static state, hence the name, and the desired curve and shape of the configuration is determined by the applied top tension of the riser. Figure 3 depicts the configuration and a typical composition of the SCR in conjunction with a TLP. Due to its simple design and cost effectiveness in construction, the SCR has become an attractive choice for deep-water field developments in conjunction with low motion floaters.

This riser concept is categorised as a compliant riser, meaning that any floater motion is absorbed by geometrical changes in the riser configuration without any motion compensation equipment such as heave compensators (Voie and Sødahl, 2013).

For deep-water wet tree solutions, the SCR concept is a preferred solution since it can offer large production bore at a low cost (Bai and Bai, 2005). The riser consists of steel segments that are welded together and the steel quality and wall thickness is selected based on these specifications:

- Weldability
- External pressure
- Reservoir properties: pressure, temperature and corrosive well fluid
- Cost and installation methods
- Fatigue performance
- Topside weight budget

The riser is connected to the host platform by a flex joint at the top and can either be terminated by a subsea termination module at the bottom, or be welded directly to the subsea flowline.

This concept has been gaining popularity since its first installation at the Auger field in the GoM in 1994, and have later been installed in other regions such as Brazil, Indonesia and West of Africa. It has proven merits in combination with various low motion floaters, such as TLP and Spars, in these areas.

However, the use of SCRs in harsher environment has been challenging due to large floater motions from waves and increased vessel offsets (Legras et al., 2013). Large heave, surge and sway motions induce increased bending forces and poses great buckling issues in the touchdown area and fatigue challenges resulting from riser-soil interactions. These design challenges can be addressed by varying the weight along the riser using different density for the applied coating. A study conducted by (Karunakaran et al., 2005) showed that increasing weight in the upper section of the riser and having a light as possible cross-sectional weight in the touch down area significantly improved dynamic behaviour of the SCR. Still there is a limit in which the floater motions are to large and the SCR concept no longer will be a feasible solution. Another design challenge is high hang-off tension in deep and ultra-deep waters.

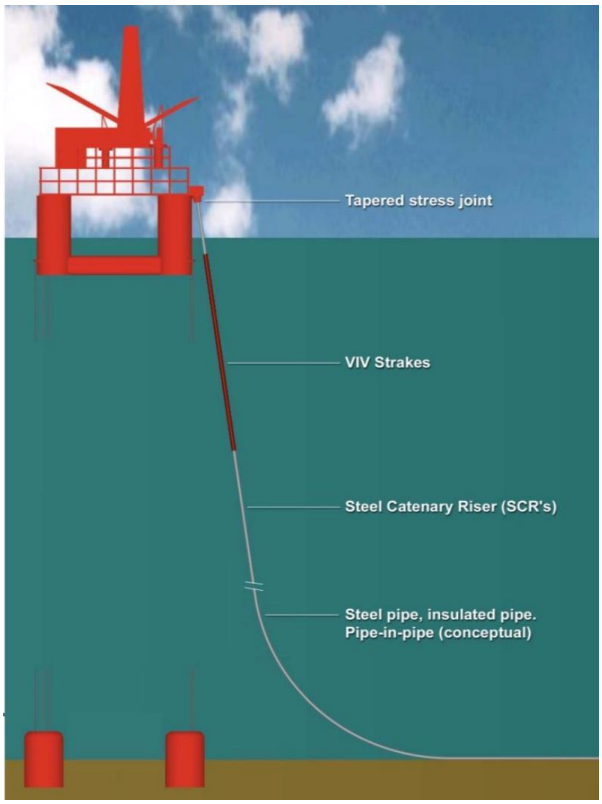

Figure 3: SCR configuration (Subsea7, 2017)

2.3.2 Steel Lazy Wave Risers

To improve the dynamic performance of the SCR concept, it can be made with buoyancy modules fitted along a part of the lower riser section. This creates a low lazy wave with the ability to absorb the vertical motion of the FPU, thus preventing the forces from affecting the touchdown area of the riser, and at the same time take some of the payload off the topside vessel. This concept decouples the forces exerted by the FPU, thus significantly improving its fatigue life and is known as a Steel Lazy Wave Riser (SLWR). For a best possible configuration, a low curvature in the hog and sag bend is desired, as it limit the static stresses in this section (Karunakaran et al., 1996). Since its first installation in the BC-10 field off the coast of Brazil in 2008, it has been gaining popularity and have since been installed at several other field developments around the world (Karunakaran and Frønsdal, 2016).

A schematic description of the SLWR is shown in Figure 4, and the length of the configuration can be divided into four sections:

1. Upper catenary section
2. Buoyancy section
3. Lower catenary section
4. Bottom section

The upper section is mainly supported by the host vessel and is terminated at the hang-off point with a desired angle in its static state, this section usually constitutes most of the riser length. The buoyancy section is the part that provides lift force by attaching buoyancy modules along a given length. The lower catenary section is the short section from the end of the buoyant part to the touchdown point (TDP) on the seabed. Along the seabed, from the TDP to connection point or riser-flowline transition point, lies the bottom section (Hoffman et al., 2010). The height between the highest point on the hog bend and the lowest point on the sag bend is described as the wave height of the riser.

This concept offers the many beneficial properties of the SCR while significantly improving its dynamic behaviour, and is considered a suitable configuration for implementation in deep waters and harsh environments in conjunction with large motion floaters. Compared to a SCR, which normally has a horizontal spread of around 1-1.5 times the water depth, the SLWR will consequently demand a larger spreading area due to its buoyant section. Having a longer spread means that the increase in length will give larger fabrication and installation cost, and also the added buoyancy elements contributes to a more complex and expensive design.

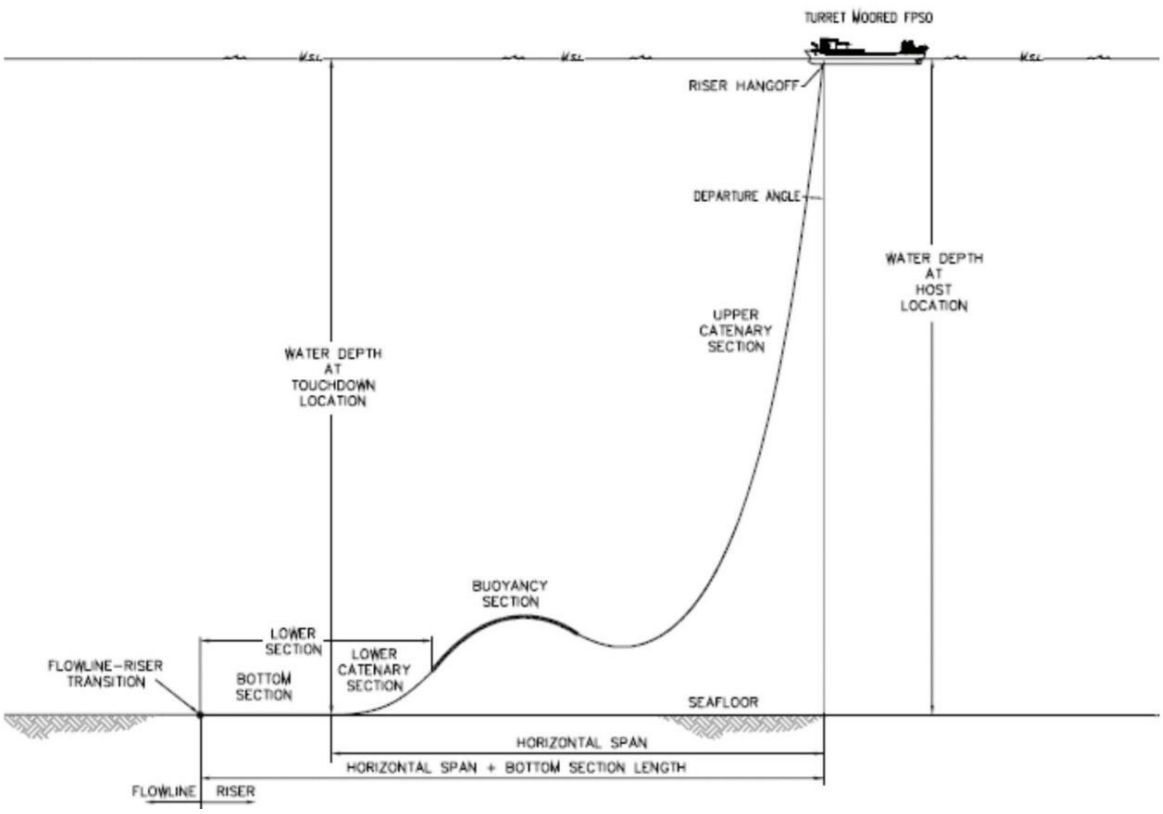

Figure 4: SLWR Configuration (Hoffman et al., 2010)

2.4 Hybrid Risers

A combination of rigid steel risers and flexibles is known as a hybrid solution. The first installation of a hybrid riser was done at the Green Canyon Block 29 project in the GoM, 1988 (Fisher and Berner, 1988), and as of today there are a variety of different hybrid riser concepts developed and installed, where the two main concepts are the Single Hybrid Riser (SHR) and the Bundled Hybrid Riser (BHR). The SHR consists of a single independent steel riser solution, whereas the BHR groups several lines together.

The principle for all hybrid riser concepts are the same, where a steel riser section is kept in tension by use of a buoyancy tank at the top. And a flexible pipe links the FPU to the steel riser, this decouples the dynamics of the vessel from affecting the steel riser. The basic principle of this concept is shown in Figure 5, and consists of a suction anchor or gravity base, flexible joint, steel riser tower, buoyancy section and a flexible pipe/umbilical connection at the top.

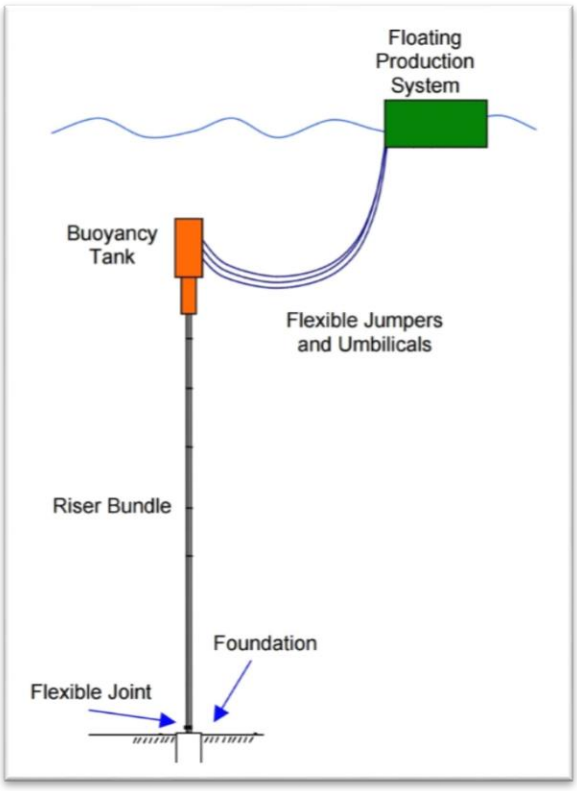

Figure 5: Hybrid riser principle (Sworn, 2005)

Benefits of using hybrid riser solutions are that they significantly reduce the payload on the FPU, offer a small subsea footprint ensuring a good seabed layout, and they can be installed before the topside facility is in place. The system can be assembled onshore where it is possible to ensure better quality inspection, but onshore construction involves a tow-out of the riser, which can affect the fatigue life significantly and also represent a risk of damage or loss of the

riser. Hybrid solutions are also very complicated systems that consists of many individual parts and components, which adds to the cost. Typically, the overall cost of hybrid solutions tends to be between the choice of the SCR/SLWR and Flexible risers, where the SCR usually is the cheapest solution (Sworn, 2005).

Other installed hybrid concepts:

- Buoyancy Supported Riser (BSR), combines several SCRs with flexibles by use of a large buoyancy module tethered to the seabed, see Figure 6. This concept has been installed by Subsea7 in a water depth of 2200 meters for the Guara Lula project off the coast of Brazil.
- Grouped Single Line Offset Riser (SLOR), groups several SHR together at a fixed distance by use of a buoyant frame on top.
- Catenary Offset Buoyant Riser Assembly (COBRA), which consists of a SCR supported by a buoyancy tank that is tethered to the seabed. This concept provides the advantages of the SCR while removing the need for complicated bottom assemblies usually needed for hybrid solutions.

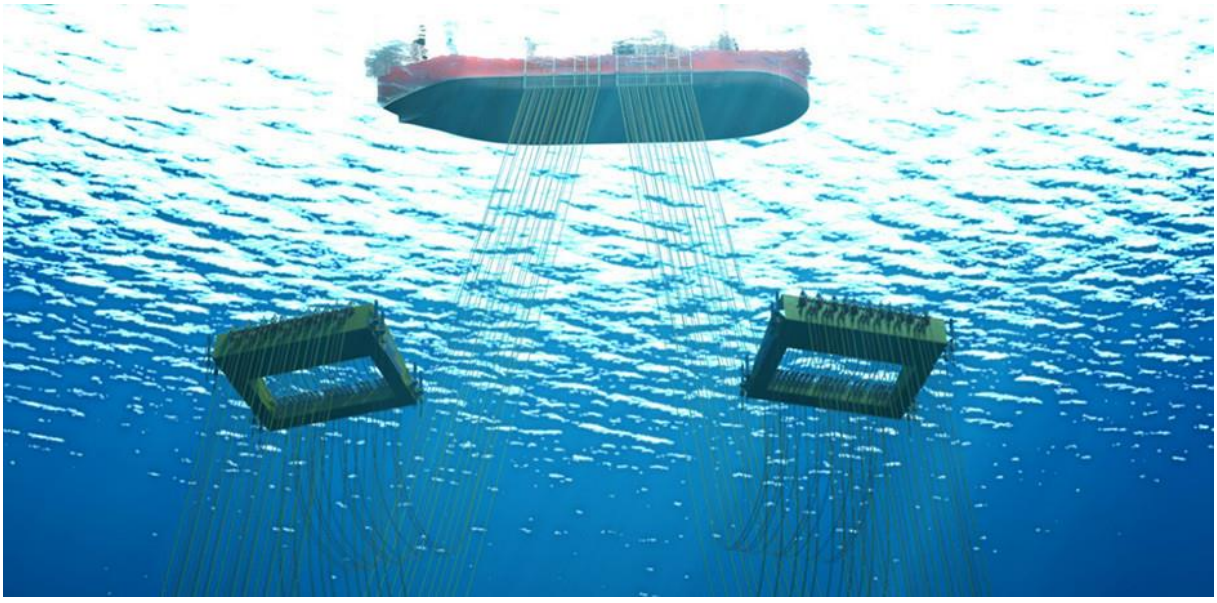

Figure 6: Buoyancy Supported Risers (Subsea7 for Petrobras, 2015)

Chapter 3 Design Code

3.1 Introduction

In standard industry practice, the structural safety of risers in combination with floating production systems has been designed to meet the Working Stress Design (WSD) criteria according to standards, such as API RP 2RD, by using a single safety factor. This approach accounts for all uncertainties by use of one single factor applied to the nominal yield strength, thus the reliability and safety margin will rely on the selected factor applied (Kavanagh et al., 2003). This design approach is accepted for well-known riser concepts and have long been the practice, but the safety level of the design will vary a lot depending on the load condition. And as new riser concepts came into operation while moving into deeper waters, a standard for more specific design criteria and analysis procedures for all riser systems was needed.

As a result, the DNV-OS-F201 standard was developed from a Joint Industry Project (JIP) between DNV, Sintef, several major oil and industry companies to make a standard that can be applied to all riser concepts. It is also applicable for modifications, operation and upgrading of existing risers, and is intended to serve as a common reference for designers, manufacturers and end-users (Katla et al., 2001). This standard includes both a Load and Resistance Factor Design (LRFD) approach and a more conservative WSD format. The partial safety factors for loads and strength in the LRFD approach are established by reliability analyses and are calibrated to give a high reliability without compromising the safety of the system (Kavanagh et al., 2003). In this chapter, the different limit states will be described and the design basis for a dynamic riser with reference to the DNV-OS-F201 standard is presented.

3.2 DNV-OS-F201

"This standard gives criteria, requirements and guidance on structural design and analysis of riser systems exposed to static and dynamic loading for use in the offshore petroleum and natural gas industries." [DNV-OS-F201: Dynamic Risers]

Design according to this standard provide a state-of-the-art limit state design for the riser that is based on accepted practice with consensus in the industry. Figure 7 shows the design approach for risers according to the reference standard. The Load and Resistance Factor Design (LRFD) is a reliability-based design format with partial safety factors used to ensure that the effects of the factorised design loads do not exceed the factored design resistance for the considered limit states.

Design criteria is provided for the following limit states:

- Serviceability Limit State (SLS): Requiring the riser to remain in service and operate as intended.

  Limit state:

  - Clearance
  - Excessive angular response
  - Mechanical function

- Ultimate Limit State (ULS): Requiring that the riser must remain intact and avoid rupture, but not necessary be able to operate. In operational condition, this corresponds to the maximum resistance against applied loads with an annual exceedance probability of 10^{-2}.

  Limit state:

  - Burst
  - Hoop buckling (collapse)
  - Propagating buckling
  - Gross plastic deformation and local buckling
  - Gross plastic deformation, local buckling and hoop buckling
  - Unstable fracture and gross plastic deformation
  - Liquid tightness
  - Global buckling

- Accidental Limit State (ALS): Same as for ULS, but for accidental loads.

  Limit state:

  - Same as SLS and ULS

- Fatigue Limit State (FLS): An ultimate limit state due to damage from cyclic loading or excessive fatigue crack growth.

  Limit state:

  - Fatigue failure

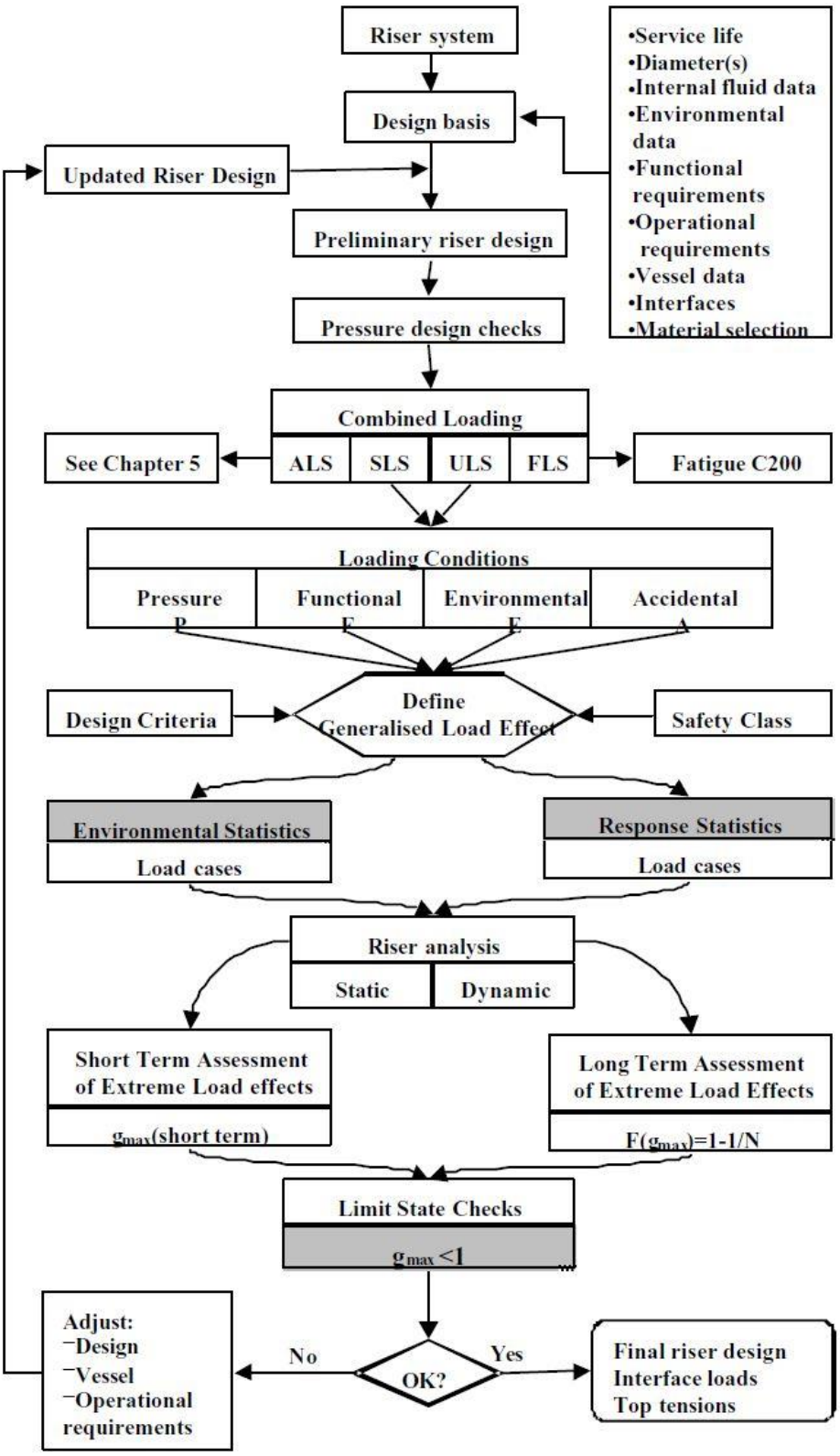

Figure 7: Design approach (DNV, 2010a)

3.3 Design Load and Resistance Effect Factors

3.3.1 Design Load Effects

In design checks, the load effect factors are used to account for extreme load effects with a precise enough margin when checking the utilisation of the cross-section of the riser, in terms of bending moment and effective tension in the combined loading criteria. The load effects are specified in terms of Pressure, Functional, Environmental and Accidental load effects which are categorised in the reference standard as shown in Table 1, and the listed factors for the different limit states are given in Table 2.

Table 1: Description of loads according to DNV-OS-F201 (DNV, 2010a)

F-loads	*E-loads*	*P-loads*[7]
Weight and buoyancy[6] of riser, tubing, coatings[6], marine growth[2], anodes, buoyancy modules, contents and attachments Weight of internal fluid Applied tension for top-tension risers Installation induced residual loads or pre-stressing Pre-load of connectors Applied displacements and guidance loads, including active positioning of support floater Thermal loads Soil pressure on buried risers Differential settlements Loads from drilling operations Construction loads and loads caused by tools	Waves Internal waves and other effects due to differences in water density. Current Earthquake[4] Ice[3] Floater motions induced by wind, waves and current, i.e.: — Mean offset including steady wave drift, wind and current forces — Wave frequency motions — Low frequency motions	External hydrostatic pressure Internal fluid pressure: hydrostatic, static and dynamic[5] contributions, as relevant Water Levels

NOTES
1) Accidental loads, both size and frequency, for a specific riser and floater may be defined by a risk analysis.
2) For temporary risers, marine growth can often be neglected due to the limited duration of planned operations.
3) Ice effects shall be taken into account in areas where ice may develop or drift.
4) Earthquake load effects shall be considered in the riser design for regions considered being seismically active.
5) Slugs and pressure surges may introduce global load effects for compliant configurations.
6) Includes also absorbed water.
7) Possible dynamic load effects from P-loads and F-loads shall be treated as E-loads, e.g. slug flow.

Table 2: Load effect factors (DNV, 2010a)

Limit State	**Functional load effect factor**	**Environmental load effect factor**	**Accidental load effect factor**
	γ_F	γ_E	γ_A
ULS	1.1	1.3	NA
FLS	1.0	1.0	NA
SLS and ALS	1.0	1.0	1.0

3.3.2 Resistance Factors

There are two different safety factors implemented in the combined loading case, one is linked to the actual safety class of the pipe in question, γ_{SC}, and the other accounts for any material and resistance uncertainties, γ_m. The safety class is defined based on consequence of failure

regarding human life, environmental and economic consequences inn range of Low, Medium or High. Safety class and material resistance factors are listed in Table 3.

Table 3: Safety class and material resistance factor (DNV, 2010a)

Safety class resistance factor, γ_{SC}		
Low	*Medium*	*High*
1.04	1.14	1.26
Material resistance factor, γ_m		
ULS and ALS	*SLS and FLS*	
1.15	1.0	

3.4 Serviceability Limit State

As stated before, this limit state sets the requirements for normal operating condition in terms of clearance, angular response and mechanical function. Acceptable limits are often set by the owner, but it is also important that the designer evaluates the serviceability of the riser to determine relevant criteria for the riser. FMEA and HAZOP are useful tools when identifying limitations and determining consequences of exceeding the limitations. Operating procedures shall clearly state all limitations and the assumptions they are based on. Some SLS with regard to global riser behaviour are displacement, deflection, rotation and ovalisation of the pipe. Excessive ovalisation of the pipe is not allowed and limitations shall be documented, such that the total out-of-roundness is limited to 3% as stated in the following criteria:

$$f_0 = \frac{D_{max} - D_{min}}{D_0} \leq 0.03 \qquad \textit{Eq. 1}$$

Some examples of SLS are listed in Section 5 of DNV-OS-F201, where one such criteria can be weather limitations during riser installation to avoid riser interference.

3.5 Ultimate Limit State

Ultimate limit state ensures that the design can withstand the failure modes listed in section two of this chapter and the checks emphasis on load controlled conditions.

3.5.1 Burst Criterion

To ensure the pipe integrity when subjected to net internal overpressure it must be designed to satisfy the following criteria for all cross sections:

$$(p_{li} - p_e) \leq \frac{p_b(t_1)}{\gamma_m * \gamma_{SC}} \qquad \textit{Eq. 2}$$

Where:

p_{li} = Local incidental pressure

= $p_{inc} + \rho_i * g * h$

ρ_i = Density of internal fluid

p_{inc} = Incidental pressure

= $1.1 * p_{design}$

p_e = External pressure

$p_b(t_1)$ = Burst resistance

= $\frac{2}{\sqrt{3}} * \frac{2*t_1}{D-t_1} \min\left(f_y; \frac{f_u}{1.15}\right)$

t_1 = Local incidental pressure

= $t_{nom} - t_{fab}$

t_{nom} = Nominal/Specified wall thickness

t_{fab} = Fabrication negative tolerance

3.5.2 Hoop Buckling

If subjected to external overpressure, the pipe must be designed to satisfy the following criteria:

$$(p_e - p_{min}) \leq \frac{p_c(t_1)}{\gamma_m * \gamma_{SC}} \qquad \textit{Eq. 3}$$

Where:

p_{min} = Minimum internal pressure

$p_c(t)$ is the resistance against hoop buckling given in DNV-OS-F101 as:

$$(p_c(t) - (p_{el}(t)) * \left(p_c^2(t) - p_p^2(t)\right) = p_c(t) * p_{el}(t) * p_p(t) * f_0 * \frac{D}{t}$$

Where:

$p_{el}(t)$ = Elastic collapse pressure

$= \frac{2*E*\left(\frac{t}{D}\right)^2}{1-v^2}$

E = Elastic modulus

t = Wall thickness of pipe

D = Pipe diameter

v = Poisson ratio

$p_p(t)$ = Plastic collapse pressure

$=2 * \frac{t}{D} * f_y * \alpha_{fab}$

f_y = Material yield strength

α_{fab} = Manufacturing process reduction factor

f_0 = Initial ovality of pipe, not to be taken less than 0.5%

$= \frac{D_{max}-D_{min}}{D}$

3.5.3 Combined Loading Criteria

The acceptance criteria for combined loading, where the pipe is subjected to bending moment, effective tension and net internal overpressure, the design needs to satisfy the equation described as followed:

$$\{\gamma_{SC} * \gamma_m\}\left\{\left(\frac{|M_d|}{M_k} * \sqrt{1-\left(\frac{p_{ld}-p_e}{p_b(t_2)}\right)^2}\right)+\left[\frac{T_{ed}}{T_k}\right]^2\right\}+\left(\frac{p_{ld}-p_e}{p_b(t_2)}\right)^2 \leq 1 \qquad \textit{Eq. 4}$$

Where:

M_d = Design bending moment

$= \gamma_F M_F + \gamma_E M_E + \gamma_A M_A$

$\gamma_{F/E/A}$ = Load effect factors for Functional/Environmental/Accidental

$M_{F/E/A}$ = Bending moment from Functional/Environmental/Accidental loads

T_{ed} = Design effective tension

= $\gamma_F T_{eF} + \gamma_E T_{eE} + \gamma_A T_{eA}$

$T_{eF/eE/eA}$ = Effective tension from Functional/Environmental/Accidental loads

T_k = Plastic axial force resistance

= $M_k = f_y * \alpha_c * \pi * (D - t_2)^2 * t_2$

M_k = Plastic bending moment resistance

= $M_k = f_y * \alpha_c * (D - t_2)^2 * t_2$

t_2 = Nominal wall thickness

f_y = Material yield strength

D = Outer diameter

α_c = Flow stress parameter accounting for strain hardening

T_k = Plastic axial force resistance

$p_b(t_2)$ = Burst resistance

= $\frac{2}{\sqrt{3}} * \frac{2*t_2}{D-t_2} \min\left(f_y; \frac{f_u}{1.15}\right)$

t_2 = $t_{nom} - t_{corr}$

t_{nom} = Nominal/Specified pipe wall thickness

t_{corr} = Corrosion/Wear/Erosion allowance

f_u = Ultimate yield strength

p_{ld} = Local internal design pressure

p_e = Local external pressure

In the case of combined loading where the pipe is subjected to net over pressure, bending moment and effective tension, the following equation applies:

$$\{\gamma_{SC} * \gamma_m\}^2 \left\{\frac{|M_d|}{M_k} + \left[\frac{T_{ed}}{T_k}\right]^2\right\}^2 + \{\gamma_{SC} * \gamma_m\}^2 \left(\frac{p_{ld} - p_e}{p_c(t_2)}\right)^2 \leq 1 \qquad \textit{Eq. 5}$$

Where:

$p_c(t_2)$ = Hoop buckling capacity

3.6 Fatigue Limit State

This ensures that the riser has adequately safety against fatigue damage over its intended lifetime and ensures that all cyclic loadings in danger of causing fatigue damage is accounted for.

The standard lists two types of fatigue assessments that can be conducted to verify sufficient fatigue resistance, these are:

- S-N curves:

$$D_{fat} * DFF \leq 1 \qquad \textit{Eq. 6}$$

Where:

D_{fat} = Accumulated fatigue damage (Palmgren-Miner rule)

DFF = Design fatigue factor according to Table 4.

- Crack propagation curves:

$$\frac{N_{tot}}{N_{cg}} * DFF \leq 1 \qquad \textit{Eq. 7}$$

Where:

N_{tot} = Total number of applied stress cycles during service or to in-service inspection

N_{cg} = Number of stress cycles necessary to increase the defect from initial to the critical size

DFF = Design fatigue factor according to Table 4.

Table 4: Design Fatigue Factors (DNV, 2010a)

Safety classes		
Low	***Medium***	***High***
3	6	10

3.7 Accidental Limit State

ALS considers loads caused by abnormal conditions, technical failure or incorrect operation and are loads that typically result from unplanned occurrences (DNV, 2010a). These loads are typically discrete events that occurs with an annual frequency of less than 10^{-2}. Other loads that might be present at the time of an accidental incident shall be accounted for, and based on risk analyses and experience, all relevant failure criteria and accidental loads shall be determined. In Section 5 of DNV-OS-F201, several accidental loads are categorised and listed, and design against accidental loads are further described.

Chapter 4 Methodology and Design Premise

4.1 Introduction

Methodology and design parameters presented in this chapter will serve as the basis for establishing an initial SLWR configuration in conjunction with an FPSO in the ultra-deep waters off the coast of Brazil. Environmental data for typical extreme weather conditions found in this area are presented, and the procedure for determining the worst sea state based on vessel response is described. The data and methodology for calculating the fatigue life due to wave induced fatigue is given, and the design cases to be conducted in the thesis are listed. Based on the provided data in this chapter, the initial configuration will be modelled in OrcaFlex and all environmental data are implemented in the analyses to verify that the design meets the stated acceptance criteria. Thus, the design premise will be the verification of a safe design in accordance with the reference standard, based on parameters and methodology given in this chapter. This initial configuration will then be subjected an optimisation process with the aim of improving the overall riser performance for the combined loading utilisation within the ULS design criteria.

In addition to the reference standard, the following standards and technical specifications are used:

- DNV-OS-F101: Submarine Pipeline Systems
- DNV-RP-C203: Fatigue Design of Offshore Steel Structures
- DNV-OSS-302: Offshore Riser Systems
- NORSOK N-003:2017: Actions and actions effects

4.2 General Description

The chosen area for this study is the Santos basin, off the coast of Brazil. This region is located several hundred kilometres from shore and stretches over an area of approximately 350 000 km^2. The water depth in the Santos Basin ranges from 1900 m to 3000 m, and has shown to be the most promising area for offshore exploration and production in the last decade.

For this thesis, a water depth of 2800 meters is chosen to study the behaviour of a SLWR in ultra-deep waters. And being a field development located in ultra-deep waters far from shore, the topside facility will be a spread moored Floating Production, Storage and Offloading (FPSO) vessel with riser termination points along the sides.

4.3 Design Basis and Analyses

4.3.1 Environmental Data

4.3.1.1 Waves and Current

The extreme sea states used for all analyses are described by typical 100-year waves and an associated 10-year current found in this region. To determine the worst wave condition for the SLWR a vessel response analysis is conducted, this is described in Section 4.3.2.2. The velocity profile for the current used is shown in Figure 8.

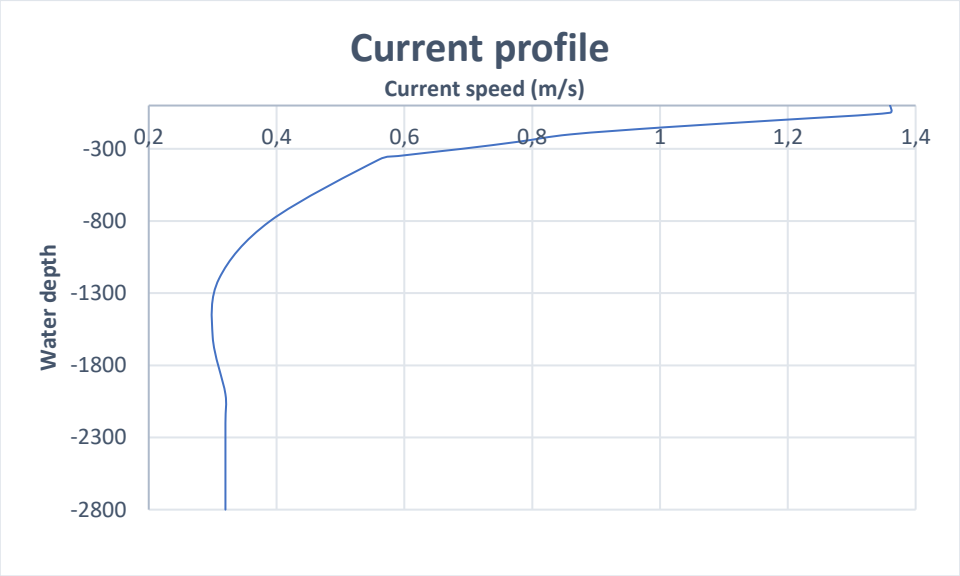

Figure 8: 10-year current profile

4.3.1.2 Wave Spectrum

As the sea surface is composed of many various random waves of different lengths and with varying periods, it can be difficult to describe the actual sea surface process. Waves being a random phenomenon, it is generally described by probabilistic methods. For marine structure design, there are two different methods to describe the wave environment, either by a deterministic or a stochastic design method (Felisita, 2016). As for this thesis, a stochastic design approach is used, where the sea surface is described by a wave spectrum, namely the JONSWAP spectrum. The random waves modelled in OrcaFlex, will follow the JONSWAP spectrum with a peak shape parameter, γ, that is adjusted for the Santos basin. This adjusted shape parameter describes the extreme wave conditions experienced in the Santos basin. Where single peak waves occur when strong winds are blowing with a long fetch in the same direction as the dominant wave direction. And because of non-linear wave interactions, the high frequency energy gradually feeds the lower frequencies and merges it into a single peak sea state.

4.3.1.3 Soil Stiffness

Oscillatory loads caused by vessel motions and current affects the overall performance of the riser configuration, and can have significant impact on the fatigue life in the TDP region. This is a result of complex riser-soil interactions, such as pipe penetrating into the soil and thus increasing the soil resistance (Karunakaran et al., 2005). It is therefore important to implement this interaction in the analyses by selecting a suitable model. The commonly used linear friction model is selected for this thesis, and it treats the seabed as a linear spring in the normal and shear directions. This results in a normal resistance that is proportional to the penetration of the riser into the seabed, and the lateral displacement of the nodes along the riser from its initial position. Suitable friction parameters were determined and are listed in Table 5.

Table 5: Friction factors

Riser-Soil Parameters		
	Value	Unit
Normal	50	$\frac{\mathrm{kN/m}}{\mathrm{m^2}}$
Shear	200	$\frac{\mathrm{kN/m}}{\mathrm{m^2}}$
Normal Friction Coefficient	0.5	N/A
Axial Friction Coefficient	0.5	N/A

4.3.2 Vessel Data

The selected vessel is a typical spread moored FPSO used in this region. It is implemented in the analyses with associated Response Amplitude Operators (RAOs) to accurately describe the vessel motion, the RAOs are confidential and not presented in this thesis. Using vessel specific RAOs are important in riser design since they describe the vessels motional behaviour for the different sea states. The origin of the RAOs is located at the centre of gravity of the vessel.

Figure 9 depicts the riser hang-off point and vessel heading, where the direction of the bow is set to a South-SouthWest direction at 195° in clockwise direction from North. The local coordinate system for the FPSO is located midship and the axis directions are listed in Table 6, along with riser hang-off point with reference to the local coordinate system.

Table 6: Local coordinate system for the FPSO and riser hang-off point

Axis	Description	Riser hang-off (m)
X	Bow direction	0
Y	Portside direction	31
Z	Upward direction	11.6

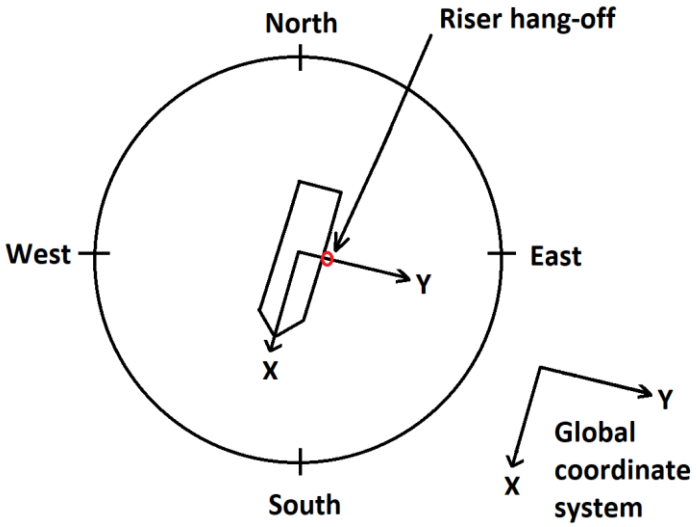

Figure 9: Local vessel and global coordinate system in reference to the four cardinal directions

4.3.2.1 Vessel Motion

Vessel motion contributes to both static and dynamic loading on the riser and DNV-OS-F201 lists three main design data needed for riser design:

1. **Static offset:**

For station keeping, the vessel is moored in place by catenary mooring lines at each corner of the ship. These lines ensure that the vessel will not drift off, but it allows for some movement from its nominal position, this is known as vessel offset and is caused by the combination of wave loads, current and wind.

For accidental situations, where there is failure in one or more of the mooring lines, the offset can be larger and these offsets need to be considered when analysing the riser to ensure safe operation at all times. For a riser, the most critical situations are when the vessel is subjected to wind, waves and current that moves in the same direction as the riser length, either away or towards the subsea connection, known as far or near offset respectively. Figure 10 shows the

nominal position of the FPSO in comparison with the near and far offsets for the intact mooring condition.

The mean static offsets used in this study for the intact and accidental mooring condition is set to 5.5% and 6.6% of the water depth, as presented in Table 7. Where the accidental case is considered as complete loss of one mooring line.

Table 7: Operational and accidental offsets

Condition	Offset in % of water depth	Offset in meters
Intact	5.5	154
Accidental	6.6	184.4

2. Wave Frequency motions:

Wave Frequency (WF) motions are a direct result of first order waves acting on the vessel in periods between 3-25 seconds and are usually given as the vessels RAOs (DNV, 2010a). The behaviour of the vessel in different sea states are described by its RAOs, which is a transfer function for converting wave forces into vessel motion in all six degrees. Having its origin at the centre of gravity of the vessel, it transforms the wave energy spectrum to response spectrum at any point in reference to its origin (Gemilang, 2015).

3. Low Frequency motions:

The Low Frequency (LF) motions are motions due to wind gust and second order wave forces, and is typically ranging in periods between 30 to 300 seconds. These are response frequencies below wave frequency that can be harmonic with the eigenperiod of the floater (DNV, 2010a).

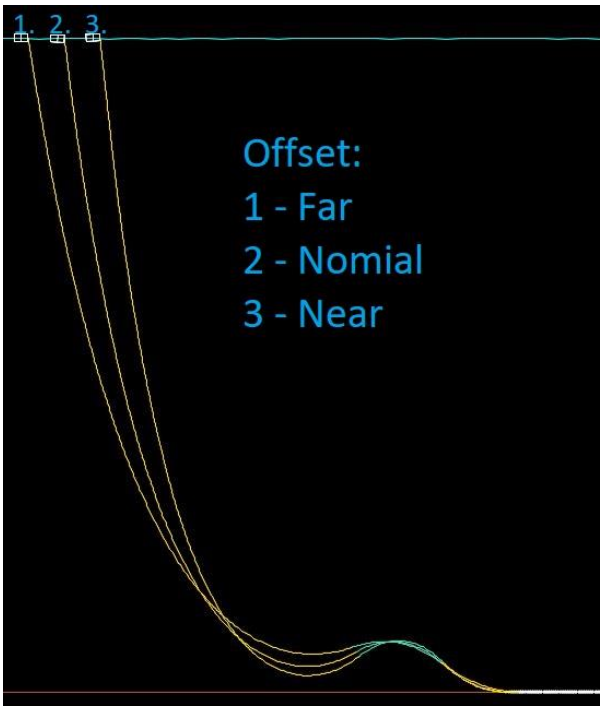

Figure 10: Illustration of the far, nominal and near offset position for the operational condition

4.3.2.2 Vessel Response Analysis

The SLWR is sensitive to downward forces exerted by the motion of the topside vessel (Kim and Kim, 2015). These forces contribute to increased bending moment in the hog-bend and can cause compressive forces in the touchdown region. Thus, it is important to determine under which conditions the largest downward forces are experienced, and these forces occur when the vessel is moving with a high velocity in the downward vertical direction.

To determine under which sea states this occurs, the 100-year wave contour for all directions must be assessed against the vessels RAOs. This is important to accurately capture which combination of sea state and wave heading results in the largest downward velocity for the hang-off point in question. Consequently, a set of typical 100-year wave parameters were studied to determine under which conditions the riser hang-off point experienced the largest downward velocity. The results presented in Table 8 were found for the Near and Far offset position in accordance with the wave directions provided by Subsea7.

Table 8: Worst sea state for the different offsets based on RAOs

	Hs (m)	Tp (s)	Wave direction
Near	6.6	11.5	East-SouthEast
Far	6.5	12.5	West-NorthWest

4.3.2.3 Extreme Response Methodology

As the riser is sensitive to large downward velocities, it is important to determine under which modelled sea-states these velocities occur. By registering the response maxima for several realisations, sufficient statistical confidence can be provided determine under which conditions this occurs.

The wave generator in OrcaFlex creates a time history of wave heights. This wave spectrum is divided into several sine waves of constant amplitude and pseudo-random phases that are generated by a random number generator and a seed number. This means that for a given seed number, the wave will always have the same phase and result in the same wave-train in the software. Consequently, several seed numbers are assigned to determine the worst combination for the two sea states. For this study, it was done by running 3 hours simulations with increments of 5 for the seed numbers between 200 and 600. With 80 different realisations, the results were studied and the largest downward velocity at hang-off point was registered. According to NORSOK N-003:2017, at least 30 simulations should be conducted to provide adequate statistical confidence when fitting the observed extremes to a probabilistic model.

By fitting the observed maxima to a Gumbel distribution, the target extreme value was estimated for a 90% percentile of the fitted distribution. This approach is in accordance with NORSOK-N003:2017 for sea states with an annual exceedance probability of 10^{-2}. The graphs in Figure 11 shows the linearized cumulative Gumbel distribution of the downward velocity maxima for the two sea states in question. The associated seed number for the closest maxima above the target value was determined and the time of occurrence in the simulation was registered for both cases. These results will be used for running short-term simulations over the worst sea-states found, thus saving time in analyses. This approach is in accordance with the reference standard and provides an adequate statistical confidence in the extreme response analyses.

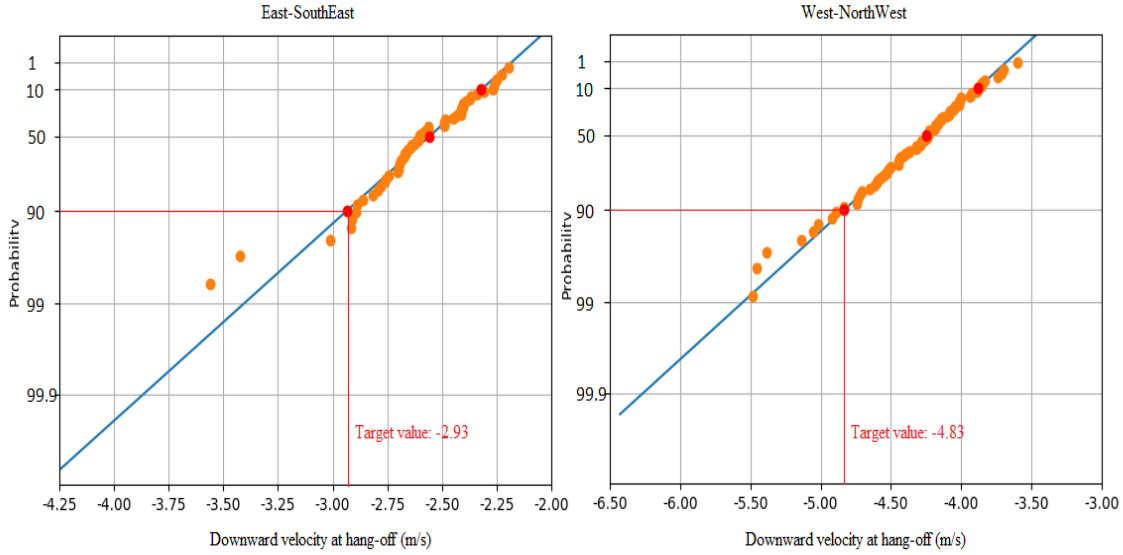

Figure 11: Linearized cumulative Gumbel distribution of downward velocities maxima at hang-off point. From these results, the associated seed number and time of occurrence for the worst sea state was determined.

4.3.3 Design Data

4.3.3.1 Riser Properties and Design Life

The properties presented in Table 9 will serve as the basis for all riser configurations and a design life of 25 years is chosen for this thesis. Selected riser material is made up of regular carbon steel in accordance with the API Specification 5L – Steel pipe for pipeline transportation systems, where the API X65 steel grade is chosen.

In this field development, the presence of H_2S- and CO_2-gas is assumed in the well-stream, which are chemical compositions known to react to regular carbon steel, thus the riser must be designed for sour service by using internal cladding, known as Corrosion Resistant Alloy (CRA) cladding. In the analyses, the cladding will be modelled with applicable material properties, but not given any structural strength.

Table 9: Riser properties

Description:	Value:	Unit:
Internal diameter	254	mm
Internal Cladding thickness	3	mm
Riser wall thickness 1	30	mm
Riser wall thickness 2	28	mm
Riser wall thickness 3	25	mm
Steel material density	7850	kg/m^3
Specified Minimum Yield Strength (SMYS)	448,2	MPa
Specified Minimum Tensile Strength (SMTS)	530,9	MPa
Design Pressure	50	MPa
Elastic modulus	207	GPa
Poisson ratio	0,3	–
Internal cladding density	8440	kg/m^3
External coating thickness	40	mm
External coating density	850	kg/m^3

4.3.3.2 Flex Joint

The riser will be connected to the FPSO by use of a flex joint which allows the riser to rotate with minimum bending moment (Bai and Bai, 2005). These joints usually incorporate an alternating lamination of spherically shaped steel and rubber components inside a steel structure that is welded to the riser, see Figure 12. This composition allows for rotational movement about both a vertical and horizontal axis (Grealish et al., 2007). The limitation for the angular deflections about its initial longitudinal axis, known as the cocking angle, is typically ± 20°.

In the analyses, the flex joint will be modelled as a pinned joint with no rotational stiffness in the global analysis of the riser, since it will not influence the riser response in extreme loading conditions. Whereas for the fatigue analysis, the rotational stiffness will influence the fatigue response and will be implemented (Legras et al., 2013). For this analysis, the rotational stiffness is set to 20 kN*m/degree and is considered to be good representation of the actual stiffness in a conventional flex joint.

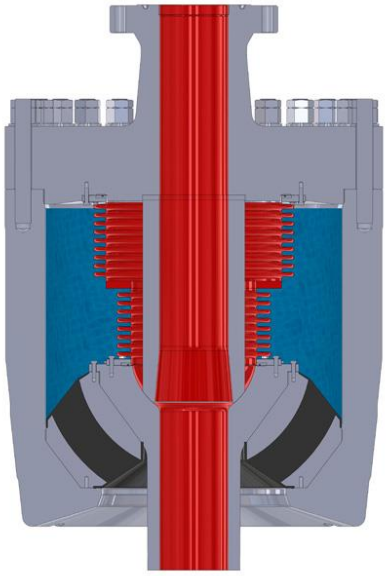

Figure 12: Flex joint (Hutchinson oil & gas, 2017)

4.3.3.3 Internal Fluid Data

For this study, the internal fluid considered has a density of 800 kg/m^3 and its associated design pressure at the seabed is set to 50 MPa.

4.3.3.4 Buoyancy Elements

To reduce the payload of the riser and to improve fatigue life, the riser is fitted with buoyancy elements along a section of the riser. These elements are usually made up of syntactic foam with a much lower density than water and each module is fitted with a clamp to secure them in place. To achieve the desired lazy wave configuration, these modules are spread out over a section of the pipe at a given interval, known as pitch, and provide enough buoyancy force to carry the weight of the riser and its content.

For the initial case, a total net buoyancy force of 150 tonnes is used and the dimensions of the modules are listed in Table 10. In the Orcaflex model, the buoyant section is modelled as an equivalent line with the same total buoyancy force as exerted by the total number of buoyancy modules. The optimum number and dimensions of the buoyancy modules will not be addressed in this thesis, and the pitch will be fixed at 6 meters for all cases. For the optimisations studies, the length of each module is also fixed and the outer diameter is adjusted for the total buoyancy force needed in each case.

Table 10: Properties of buoyancy elements

Description	Value	Unit
Length	3	m
Inner diameter	0.39	m
Outer diameter	1.3	m
Material density	395	kg/m3
Clamp weight	25	kg
Pitch	6	m

4.3.3.5 Hydrodynamic Coefficients

For slender structures, the hydrodynamic loading can be expressed by the Morison equation in terms of fluid velocities and acceleration (DNV, 2010a). The Morison equation is derived from experiments and includes two coefficients, one for drag and one for mass. These coefficients depend on several parameters, including both Keulegan-Carpenter and Reynolds number and surface roughness of the body. This means that the coefficient will change in terms of varying velocities, wave periods and the presence of marine growth. As a conservative approach, the use of a constant value for the entire length of the riser can be opted (Orimolade, 2014).

In the standard used for this study, the approximation of steady flow over a bare circular pipe recommends a drag coefficient between 0.7 and 1.0 and 1.0 for added mass. The inertia, or mass, coefficient is taken as $C_{Inertia} = C_{Added} + 1$ in accordance with DNV-OS-F201.

The conservative approach is selected for this study and it is assumed that the coefficients used accounts for any marine growth on the riser. Added mass and drag coefficients used, for both riser and buoyancy modules, are given in Table 11. To account for the installation of strakes in the top section of the riser, a higher drag coefficient is implemented for a length of 1950 meters for the initial configuration.

Table 11: Drag and mass coefficients

	Drag Coefficients			Added Mass Coefficients	
Description:	**Normal**	**Axial Form**	**Axial Skin**	**Normal**	**Axial**
Riser	1	-	-	1	-
Riser with strakes	1.4	-	-	1	-
Buoyancy module	1	1	0.01	1	0.5

4.4 Wall Thickness Sizing

Determining the needed wall thickness is crucial to verify the pipes ability to withstand both internal and external overpressure in the system. This is done by use of the Pipeline Engineering Tool (PET), which is a software developed by DNV for calculating needed wall thickness in accordance with DNV-OS-F101: Offshore standard for pipeline systems.

The results were obtained by implementing the material inputs from and the design and test pressures set for this thesis, see Table 12. Calculated wall thickness determines the minimum required wall thickness with respect to propagation buckling, burst and collapse pressure.

Table 12: Design and test pressure for wall thickness sizing

Description	Input (MPa)	Ref. from sea-level (m)	Content density (kg/m3)
Design Pressure	50	-2800	800
Test pressure	57.77	-2800	1000

Being a production riser, the safety class is set to high and the required wall thickness calculated for the different failure modes are shown in Table 13. From these results, the propagating buckling yields the highest required minimum wall thickness. Usually this is not taken into consideration, since it can be controlled using buckle arrestors fitted along the length of the riser. This means that a wall thickness of 25 mm will be sufficient, in terms pressure loads. Complete reports for pressure containment, collapse and propagating buckling assessment is given in Appendix A – Wall Thickness Calculation.

Table 13: Pipeline Engineering Tool results

Failure Mode	Condition	Safety Class	Required thickness	Utilisation
Burst	Operation	High	11.84	0.498
Burst	System test	System test	10.38	0.439
Collapse	Empty	High	24.29	0.966
Propagating buckling	Empty	High	31.97	1.657

4.4.1 Riser fatigue

Due to time constraints, only the wave induced fatigue damage is calculated in this study, whereas the fatigue caused by Vortex-Induced Vibrations (VIV) is briefly described.

Since the wave induced fatigue is mainly caused by the vessels motion in response to the sea state, typical wave data from the Santos basin are implemented in the fatigue analysis. The distribution of total significant wave heights and primary spectral peak periods are based on data tabulated at 3 hours interval of a total of 227136 hours. The data is confidential and is not shown in its entirety in this work.

The wave scatter diagram arranges the number of occurrences with regards to Hs and Tp intervals, ranging from 0-11m and 3-21s respectively. For the wave directions, the 13 most prevailing ones are used. The occurrence frequency and directions used, are listed in Table 14, where the direction of the wave is in reference to the global coordinate system in Orcaflex as stated in *Section 4.5*.

Table 14: Wave directions and occurrence frequencies

Wave direction		Frequency
NorthEast	330°	20.37%
East-NorthEast	307.5°	14.87%
East	285°	6.69%
Beam Port -10	280°	2.43%
Beam Port -5	275°	2.37%
Beam Port	270°	2.16%
Beam Port +5	265°	2.16%
Beam Port +10	260°	2.16%
East-SouthEast	250°	2.73%
SouthEast	240°	8.94%
South-SouthEast	217.5°	9.12%
South	195°	10.97%
South-SouthWest	182.5°	15.03%
	Total:	**100%**

The wave scatter diagram is grouped into 21 blocks, where the highest occurring sea state in each block is selected to represent all sea states within its block and is marked by a red X, as shown in Figure 13.The lumped probability of occurrence for each block is calculated and implemented in the fatigue analysis, in accordance with procedure in the reference standard, where the fatigue damage from each blocked sea state is calculated for all directions in .

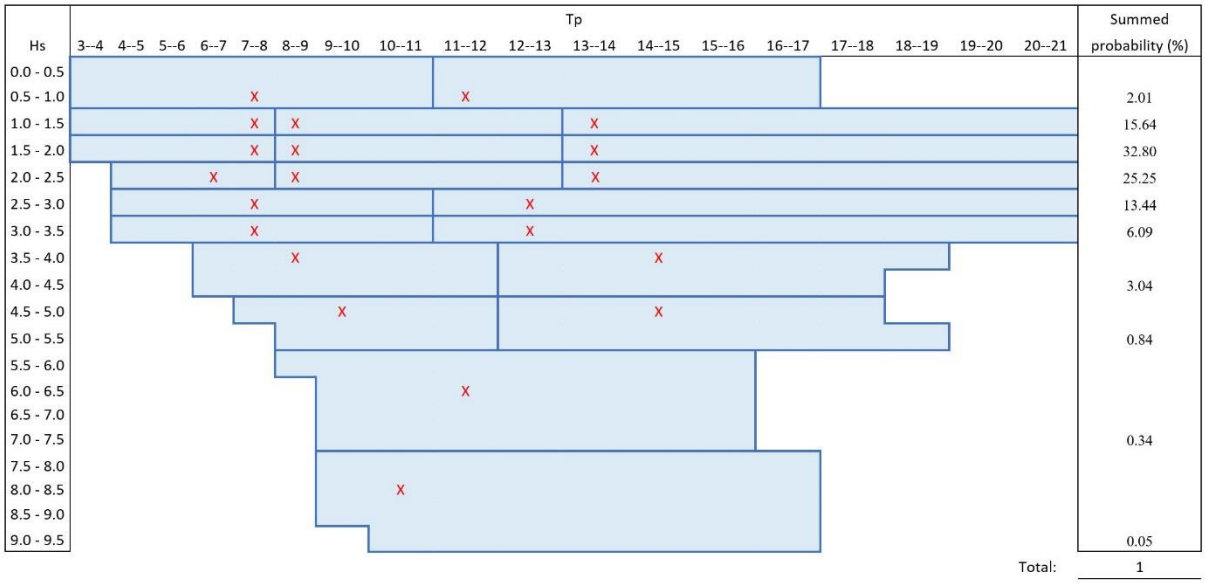

Figure 13: Blocked sea states

The fatigue capacity will be estimated by use of S-N curves, which expresses how many stress cycles it takes until failure under a constant stress range, and is expressed as followed:

$$N = \bar{a} * S^{-m} \qquad \textit{Eq. 8}$$

Or equivalently as:

$$\log(N) = \log(\bar{a}) - m * \log(S) \qquad \textit{Eq. 9}$$

Where:

N = Number of stress cycles to failure

$\bar{a}$ = Empirical constant derived from experiments

m = Empirical constant derived from experiments

S = Stress range

The stress range is determined by use of stress concentration factor and thickness correction factor to the nominal stress range:

$$S = S_0 * SCF * \left(\frac{t_3}{t_{ref}}\right)^k \qquad \textit{Eq. 10}$$

Where:

S_0 = Nominal stress range

SCF = Stress concentration factor

$\left(\frac{t_3}{t_{ref}}\right)^k$ = Thickness correction factor

t_3 = Pipe wall thickness

t_{ref} = Reference wall thickness = 25 mm

k = Thickness exponent

The Stress concentration factor is implemented to account for any geometrical imperfections that may cause stress magnification in two adjacent joints. This factor can be calculated using finite element analysis or alternatively by a closed form expression, like the following for welded riser joints:

$$SCF = 1 + \frac{3e}{t_3} * \exp\left(-\left(\frac{D}{t_3}\right)^{-0.5}\right) \quad \textit{Eq. 11}$$

Where:

e = Eccentricity caused by geometrical imperfections

The total fatigue damage will be determined by counting the stress cycles in the simulation period by the Rain Flow Counting (RFC) method.

To accumulate the fatigue damage caused by the stress cycles, the Palmer-Miner rule is used:

$$D = \sum_i \frac{n(S_i)}{N(S_i)} \quad \textit{Eq. 12}$$

Where:

$n(S_i)$ = Number of stress cycles with range S_i

$N(S_i)$ = Number of stress cycles to failure

4.4.1.1 Fatigue Calculation

The analysis will be conducted according to the S-N curve approach in the reference standard. These curves represent the magnitude of stress to the number of cycles to failure for different types of welds used for steel material based on specimens tested in laboratories (DNV, 2010c). The S-N curves in DNV-RP-C203 are based on mean-minus-two-standard-deviations curves for relevant experimental data and are associated with a 97.5% probability of survival for operation within its limits. The definition of failure is given as, the time it takes for a crack to develop through the entire material thickness at any point.

Figure 14 shows the highlighted curves that will be used in this study. The assessment of the C2-, D and E-curves, for S-N curves in seawater with cathodic protection, are selected. From the analysis, it is expected that the fatigue life for the C2-curve will yield the best performance, followed by the D- and E-curve respectively. Emphasis will be given for the D-curve by assuming that a sufficient weld quality for the cladded pipe is obtained (Legras et al., 2013).

The fatigue calculation will be conducted by the built-in fatigue analysis program in OrcaFlex, where 1 hour simulation for all 273 load cases will be implemented to provide adequately data. The total occurrence of each sea state and direction is weighted by the combined occurrence of the two, and are calculated for the total number of hours present annually. The fatigue damage is then calculated by the rainflow counting method and the cumulative fatigue is calculated for 16 circumferential points along the entire riser length. The applied parameters for the different S-N curves are given in Table 15.

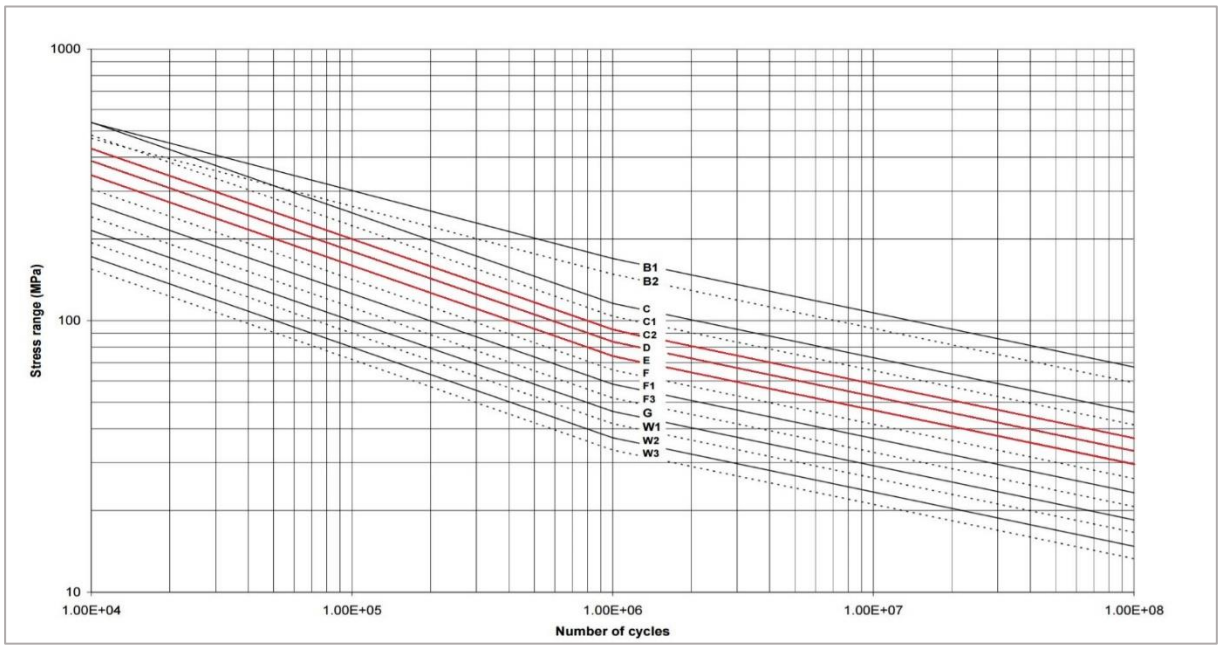

Figure 14: S-N curves in seawater with cathodic protection (DNV, 2010c).

Table 15: Stress Concentration Factor and S-N curve parameters used in the wave induced fatigue analysis

SCF	1.2
C2-Curve	
Thickness correction factor – 25 mm	1
Thickness correction factor – 28 mm	1.0059
Thickness correction factor – 30 mm	1.011
$N \leq 10^6$	m_1= 3 log$\bar{a}_1$= 11.901
$N \geq 10^6$	m_2= 5 log$\bar{a}_2$= 15.835
D-Curve	
Thickness correction factor – 25 mm	1
Thickness correction factor – 28 mm	1.008
Thickness correction factor – 30 mm	1.023
$N \leq 10^6$	m_1= 3 log$\bar{a}_1$= 11.764
$N \geq 10^6$	m_2= 5 log$\bar{a}_2$= 15.606
E-Curve	
Thickness correction factor – 25 mm	1
Thickness correction factor – 28 mm	1.008
Thickness correction factor – 30 mm	1.023
$N \leq 10^6$	m_1= 3 log$\bar{a}_1$= 11.610
$N \geq 10^6$	m_2= 5 log$\bar{a}_2$= 15.350

4.5 Design and Study Cases

Several design cases will be studied in this thesis to improve the performance of a riser configuration subjected to a 10-year current in combination with a 100-year sea state, each case will be analysed for the worst response behaviour located in simulation.

4.5.1 Initial Configuration

The initial configuration will be based on parameters listed in this Chapter and is designed in accordance with the reference standard to meet ULS and ALS design criteria, and FLS in terms of the wave induced fatigue. Results from the strength and fatigue analyses will be discussed and presented in a tabulated form for the sections listed in Table 16, along with range graphs for the entire riser length.

Table 16: Load Cases

	Offset	Results	Sections considered
Static	Nominal	• Effective tension • Bending moment • LRFD utilisation	➢ Top, sag-, hog-bend and TDP ➢ Sag-, hog-bend and TDP ➢ Top, sag-, hog-bend and TDP
Dynamic - ULS	Near & Far	• Angle variation • Effective tension • Bending moment • LRFD utilisation	➢ Hang-off point ➢ Top, sag-, hog-bend and TDP ➢ Sag-, hog-bend and TDP ➢ Top, sag-, hog-bend and TDP
Dynamic - ALS	Near & Far	• Angle variation • Effective tension • Bending moment • LRFD utilisation	➢ Hang-off point ➢ Top, sag-, hog-bend and TDP ➢ Sag-, hog-bend and TDP ➢ Top, sag-, hog-bend and TDP
Dynamic - FLS	Nominal	• Wave induced fatigue life	➢ Top, sag-, hog-bend and TDP

4.5.2 Sensitivity and Optimisation study

The objective of this thesis is to find an optimum configuration within the design premise based on the combined loading utilisation for each case. The optimisation procedure will be done by creating a set of new configurations and varying key parameters to study the extreme response behaviour for the ULS design criteria in the near and far offset position. The parameter variations to be performed are given in Table 17 and results in a total of 75 different configurations that will result in 225 different load cases, when including the nominal position.

Table 17: Parameter variation for the optimisation study

	-10%	-5%	Initial	+5%	+10%	Units
Buoyancy force	135	142.5	150	157.5	165	Tonnes
Buoyancy length	360	380	400	420	440	m
Hang-off angle	6		7	8		degrees

General observations made for these cases are presented, and the following results will be presented for the worst and best configuration, in comparison with the initial one:

- Hang-off angle: Static, maximum and minimum
- Top tension: Static, maximum and minimum
- Bending moment: Maximum and minimum
- LRFD Utilisation: Static, maximum and minimum

4.6 Software and Programming Language

The OrcaFlex software is a program for dynamic analysis of offshore marine systems, and it is provided with a programming interface for different programming languages, such as C++, Matlab and Python. This interface makes it possible to run several analyses in steps and do post-processing of the results in an automated manner.

For this thesis, the Python programming language was chosen. This open-source programming language is free-for-all to use and there are several compatible code editors available for download online. The syntax is made to be simple, easy to learn and comes with built in functions and modules for a vast range of applications. And since OrcaFlex is provided with a Dynamic Link Library (DLL), named OrcFxAPI, it can be imported in to the Python script to access some of the many functions within OrcaFlex. This makes it possible for a programmed script to both write to and read from a OrcaFlex file.

The process of making a script that performs the desired operations in an automated process is quite extensive, and requires good knowledge about programming and functional use of OrcaFlex. Consequently, a lot of work and many weeks were spent on understanding and learning the basics of Python programming language before an optimisation process could be started. By gradually learning the basic commands needed, several scripts were made to change individual parameters within a base file for OrcaFlex. These were then integrated in to one single programmed script that created all the files needed to do the optimisation study for the 225 cases listed. With very good help and instructions from in-house competence at Subsea7 the final script was made together with a second script that collects the desired results from each load case and write it to an Excel file. Figure 15 shows a very simplified flowchart for how the two scripts where used in the optimisation process, parts of the main script is given in Appendix B – Python Script.

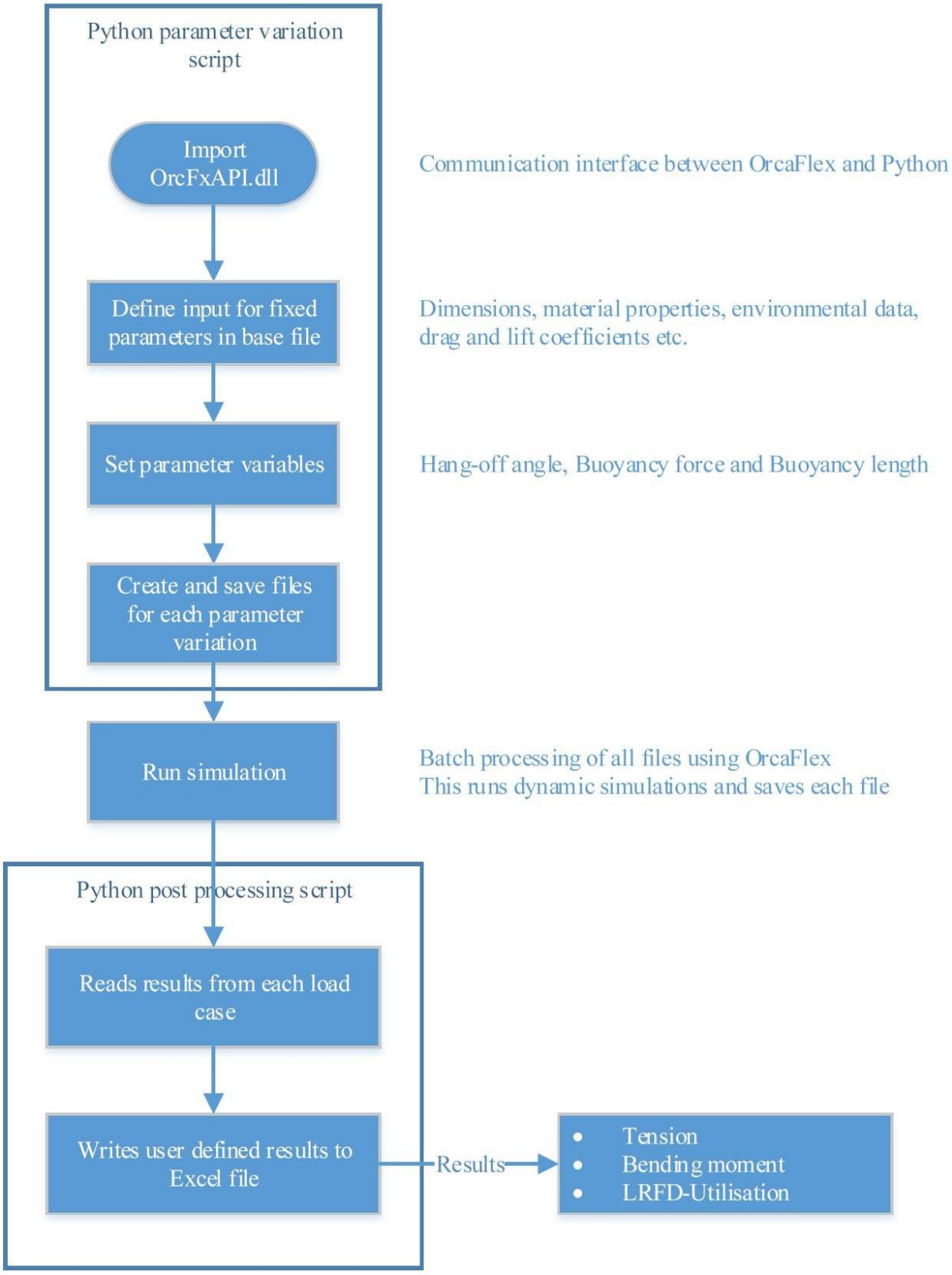

Figure 15: Optimisation process using Python

4.7 Acceptance Criteria

Combined loading:

The acceptance criteria for all cases studied in this thesis will be the combined loading criteria, which considers correlation between moment, tension and pressure differences along the entire length of the riser and is described by the following generic equation (Katla et al., 2001, DNV, 2010a):

$$g(t) = g(M_d(t), T_{ed}(t), \Delta p, \boldsymbol{R}_{\mathrm{k}}, \Lambda) \leq 1 \qquad \textit{Eq. 13}$$

For extreme value prediction:

$$g_{max} \leq 1$$

Where:

M_d = Design bending moment

T_{ed} = Design effective tension

Δp = Local difference pressure

$\boldsymbol{R}_{\mathrm{k}}$ = Vector of cross sectional capacities

Λ = Vector of safety factors

By using this approach, it will automatically account for the correlation between effective tension and bending moment, such that an optimal design can be determined that allows for a higher utilisation compared to a WSD approach.

Fatigue:

Being a production riser, the safety class is set to High with a corresponding design safety factor of 10 for the wave induced fatigue calculation. Having a design life of 25 years, this results in a minimum fatigue life of 250-years for the acceptance criteria. VIV induced fatigue is not assessed in this thesis due to time restriction.

Compression:

To avoid overall column buckling of the riser due to axial compression, the occurrence of excessive negative effective tension must be limited.

Chapter 5 Extreme Response and Fatigue Analysis

5.1 Introduction

In this chapter, the initial static configuration based on the data provided in Chapter 4 is presented and extreme response analyses conducted. All modelling, simulations and analyses were conducted in OrcaFlex and the results are presented for critical sections.

Based on all given parameters, the initial configuration was determined with emphasis on the following design philosophy:

- Low sag and hog bend curvature to reduce excessive bending forces.
- Height between seabed and sag bend must be sufficient to avoid impact loads and excessive compressive forces in all sea states, especially for the near offset case.
- Total net buoyancy force to obtain desired configuration.

5.2 Initial Static Configuration

A total net buoyancy force of 1471.5 kN was deemed suitable for this configuration and some key parameters for the layout in nominal position is presented in Table 18. A cropped picture of the sag and hog-bend area, see Figure 16, shows the wave configuration with measurements of the wave, seabed-sag and seabed-hog height.

Table 18: Details of the SLWR configuration

Description:	Value	Unit
Hang-off angle	7	°
Upper catenary length	3250	m
Buoyant section length	400	m
Lower catenary length	293	m
Bottom section length	1133	m
Total net buoyancy force	1471.5	kN
Wave height	55	m
Seabed to sag-bend height	180	m
Seabed to hog-bend height	403	m

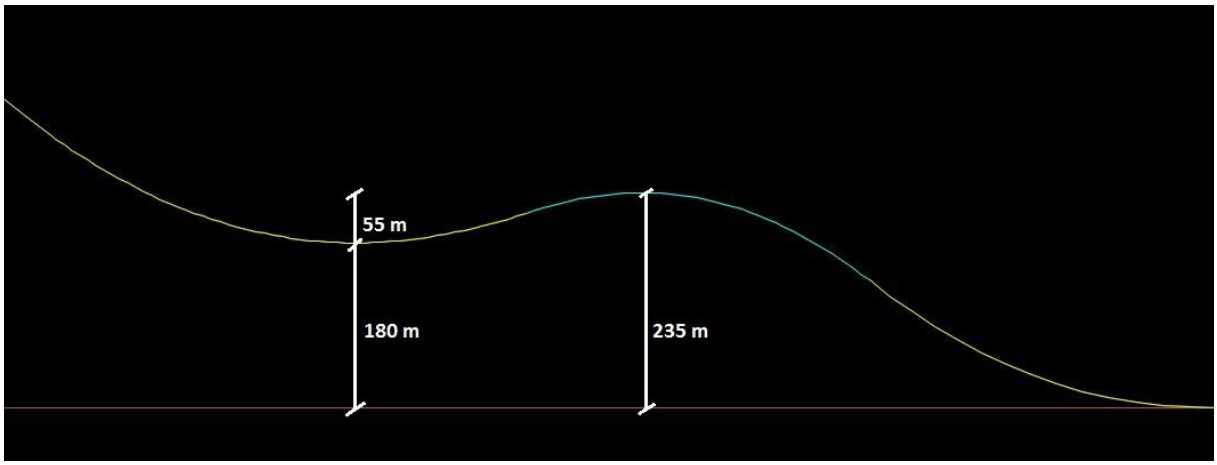

Figure 16: Sag-hog bend in static state

5.2.1 Static Analysis

Based on given parameters, a suitable static configuration of the SLWR in nominal offset position is considered. In static state, no environmental loads are present and it is only subjected to functional loads such as weight of riser, applied top tension and pressure loads. Table 19 presents the results obtained from the analysis of the static configuration.

Table 19: Static results

Effective tension (kN)	
Top	5089
Sag-bend	739
Hog-bend	739
TDP	739
Bending moment (kN*m)	
Sag-bend	95
Hog-bend	140
TDP	93
LRFD utilisation	
Top	0.30
Sag-bend	0.21
Hog-bend	0.25
TDP	0.21

5.2.2 Discussion of the Static Analysis

From the results, it is seen that the top tension is quite large, this is mainly caused by the sheer weight of the upper catenary section with content, which is suspended for a height of approximately 2620 metres. The horizontal force exerted at the top is relatively small compared to the total top tension, and can be read as the effective tension found in the sag-, hog-bend and TDP. The largest utilisation is found to be 0.30, and is also located at the top.

5.3 Dynamic Response Analyses

In dynamic analyses, both functional and environmental loads are considered to verify the integrity of the riser in extreme sea states. Each analysis was conducted by running short term simulations over the worst sea state found in Section 4.3.2.3. The analyses implemented a combination of 100-year waves and a 10-year current in-line with the riser for both ULS and ALS design conditions. Table 20 presents a summary of the applicable load factors used, together with the environmental data and vessel heading for the two design cases. For both the ULS and ALS design in this section, the increased drag coefficient is used to account for the instalment of strakes along the top section of the riser. Figure 17 illustrates a section of helical strakes fitted on a pipe length.

Table 20: Offsets, sea states and load factors used in ULS and ALS code-checks

ULS					
Position:	Offset (m)	Hs (m)	Tp (s)	Wave + Current heading	Load factors: γ_F / γ_E / γ_A
Nominal	0	6.5	12.5	270°	1.1 / 1.3 / -
Far	-154	6.5	12.5	270°	1.1 / 1.3 / -
Near	154	6.6	11.5	90°	1.1 / 1.3 / -
ALS					
Position:	Offset (m)	Hs (m)	Tp (s)	Wave + Current heading	Load factors: γ_F / γ_E / γ_A
Nominal	0	6.5 m	12.5 s	270°	1.0 / 1.0 / 1.0
Far	-184.8	6.5 m	12.5 s	270°	1.0 / 1.0 / 1.0
Near	184.8	6.6 m	11.5 s	90°	1.0 / 1.0 / 1.0

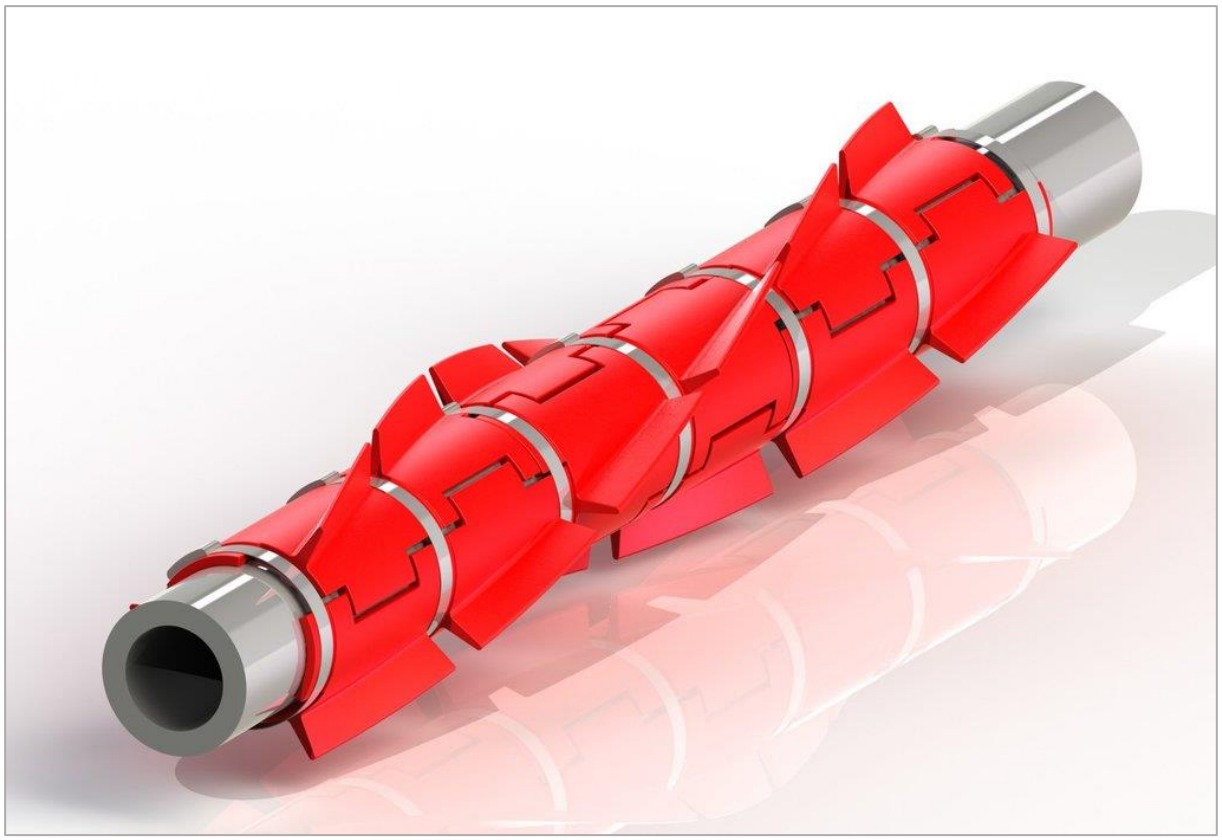

Figure 17: Helical strakes (Bardot Group, 2017).

5.3.1 Results

In this section, the results from the analyses are presented in terms of range graphs of the entire riser length and tabulated results for critical parts of the riser configuration.

5.3.1.1 ULS

Table 21 lists the results obtained for critical sections of the configuration and the complete results in terms of effective tension, bending moment and LRFD utilisation are presented in the range graphs in Figure 18, Figure 19 and Figure 20.

Table 21: Dynamic results ULS

Offset Position:	Far	Near
Hang-off angle (degrees)		
Maximum	13.8	13.5
Minimum	3.4	5.1
Variation	10.4	8.4

Max effective tension (kN)		
Static top tension	5251	4986
Top	8035	6629
Sag-bend	2350	818
Hog-bend	2474	805
TDP	2280	582
Bending moment (kN*m)		
Sag-bend	201	145
Hog-bend	293	227
TDP	121	135
LRFD utilisation		
Top	0.74	0.51
Sag-bend	0.40	0.29
Hog-bend	0.51	0.38
TDP	0.26	0.27

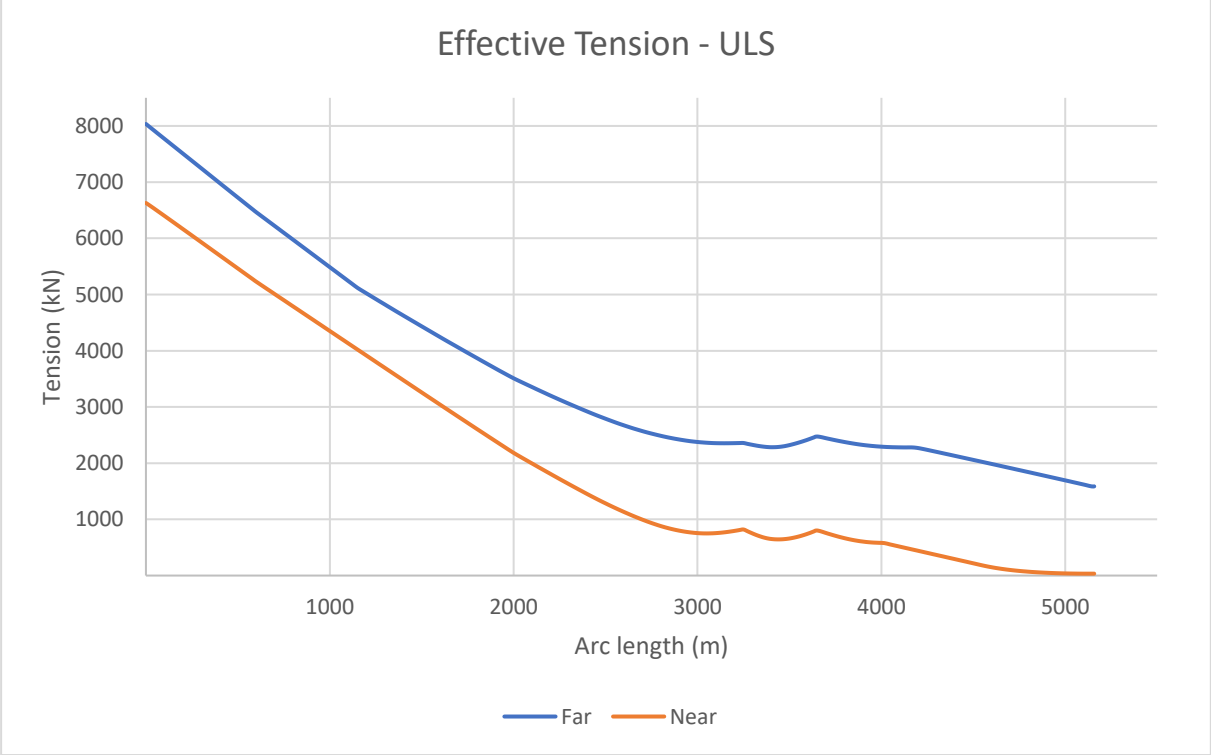

Figure 18: Range graph: Effective tension - ULS

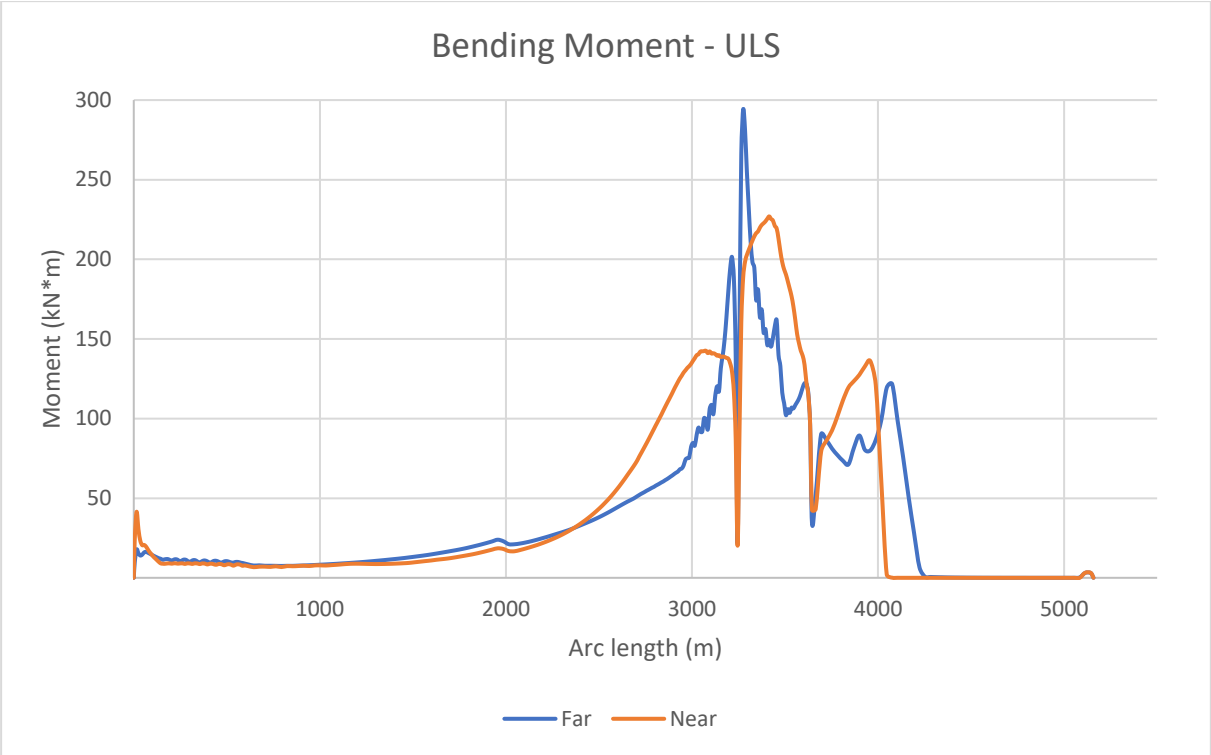

Figure 19: Range graph: Bending moment - ULS

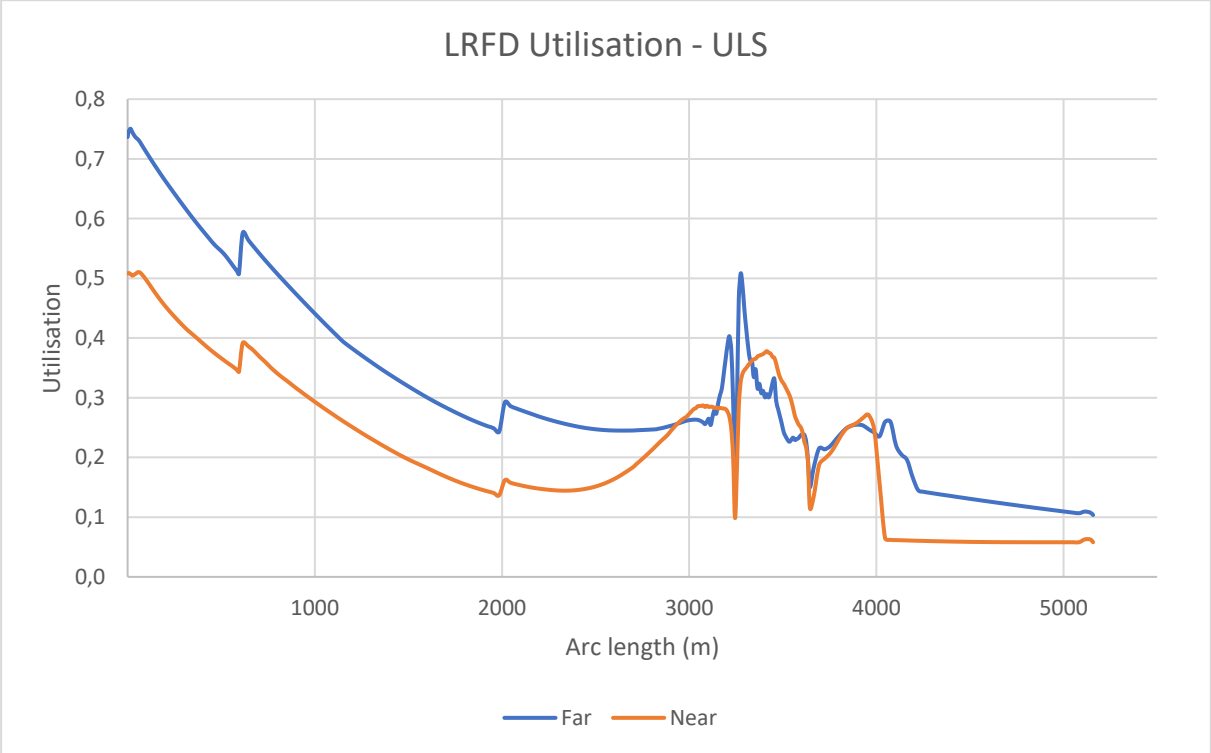

Figure 20: Range graph: LRFD utilisation - ULS

5.3.1.2 ALS

Table 22 lists the results obtained for critical sections of the configuration and the complete results in terms of effective tension, bending moment and LRFD utilisation is presented in the range graphs in Figure 21, Figure 22 and Figure 23.

Table 22: Dynamic results ALS

Offset:	Far	Near
Hang-off angle (degrees)		
Maximum	14.3	13.2
Minimum	3.9	4.9
Variation	11	8.3
Max effective tension (kN)		
Static top tension	5286	4973
Top	8127	6620
Sag-bend	2536	793
Hog-bend	2684	770
TDP	2495	538
Bending moment (kN*m)		
Sag-bend	211	148
Hog-bend	308	236
TDP	119	141
LRFD utilisation		
Top	0.57	0.40
Sag-bend	0.35	0.27
Hog-bend	0.44	0.35
TDP	0.22	0.25

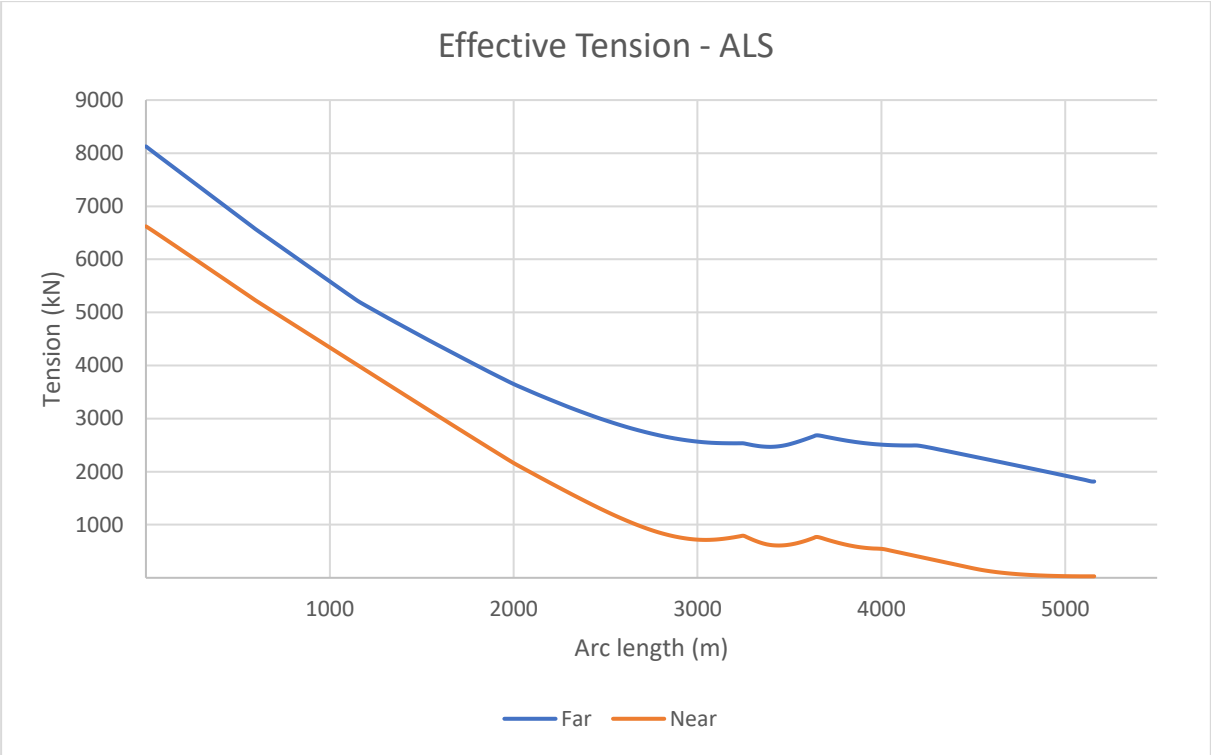

Figure 21: Range graph: Effective tension - ALS

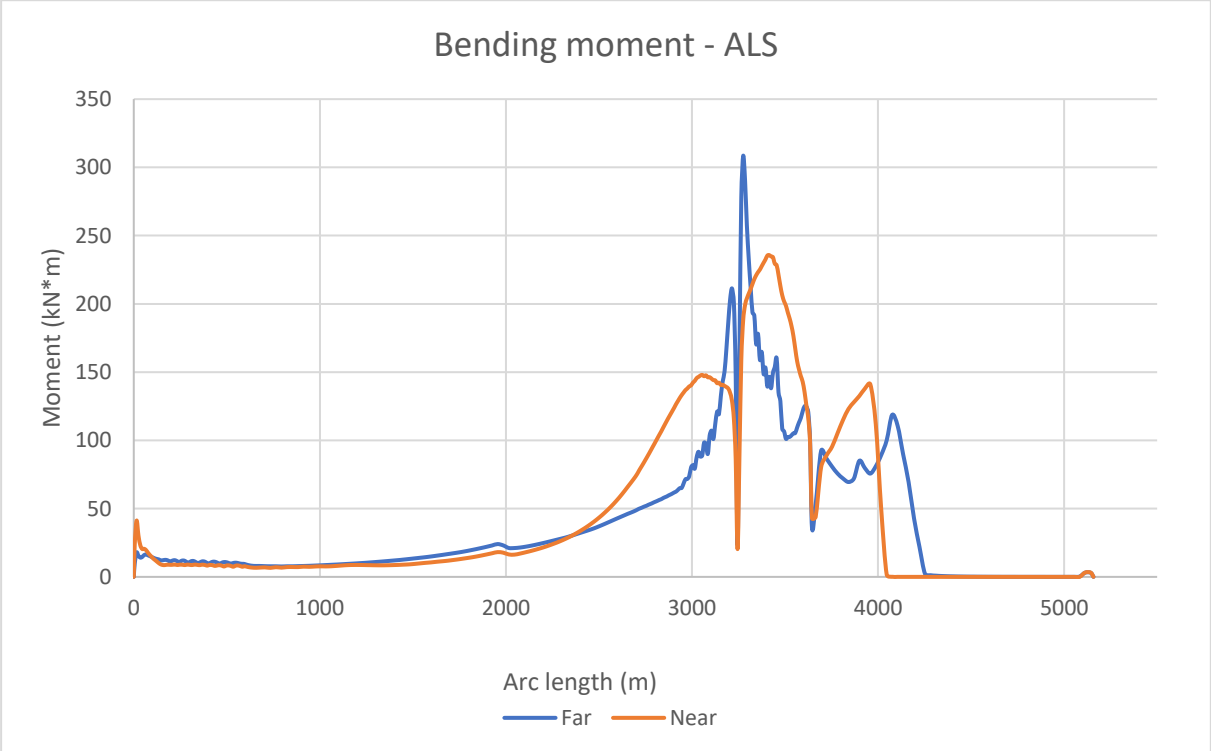

Figure 22: Range graph: Bending moment - ALS

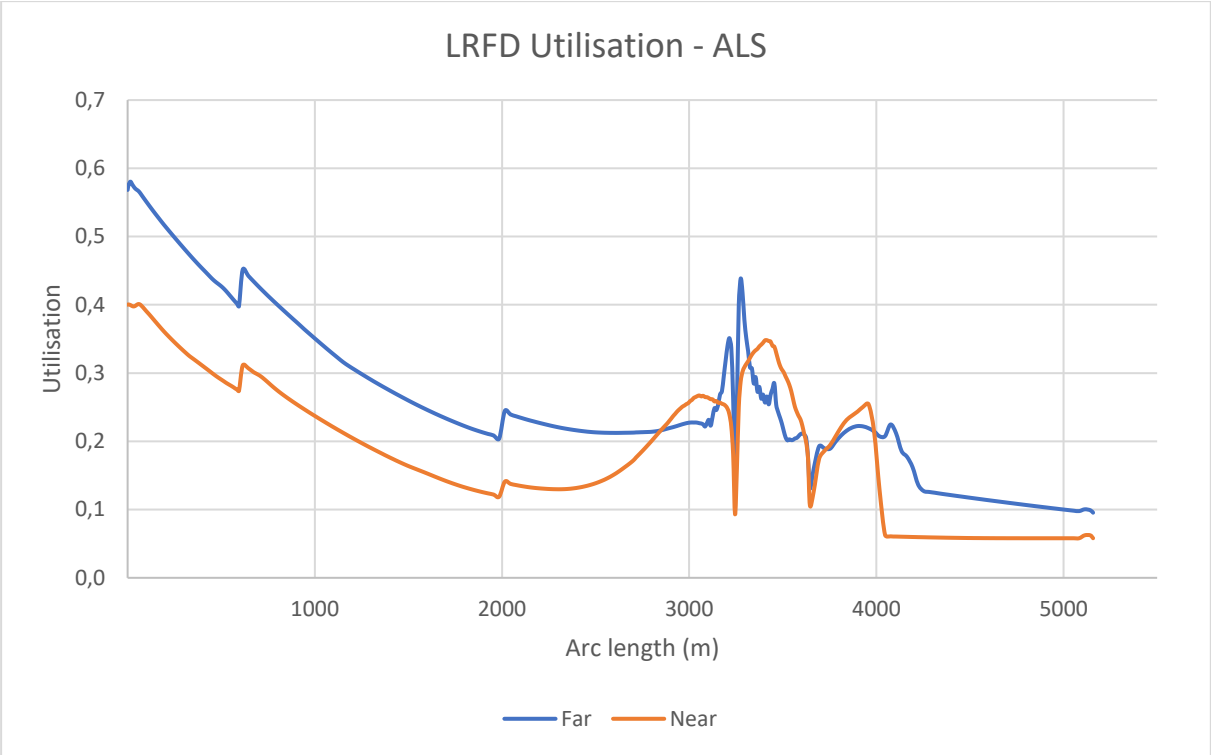

Figure 23: Range graph: LRFD utilisation - ALS

100-year wave + 10-year current	FPSO Position			
	Intact		Accidental	
	Near	Far	Near	Far
Variation in Top Angle (deg)	13.9	14.5	12.8	15.8
Max. Effective Top Tension (kN)	1854	1958	1850	1986
Sag Bend				
Max. Effective Tension (kN)	248	658	232	749
Max. Compression (kN)	50	86	46	95
Max. Bending Moment (kN.m)	425	332	445	338
Max. von Mises Stresses (MPa)	335	272	348	274
Max. DNV Utilization (LRFD)	0.77	0.65	0.73	0.56
Hog Bend				
Max. Effective Tension (kN)	159	594	146	680
Max. Compression (kN)	-	36	-	64
Max. Bending Moment (kN.m)	308	315	326	345
Max. von Mises Stresses (MPa)	264	272	271	278
Max. DNV Utilization (LRFD)	0.60	0.67	0.56	0.57
TDP				
Max. Effective Tension (kN)	111	576	97	657
Max. Compression (kN)	-	-	-	-
Max. Bending Moment (kN.m)	400	283	412	286
Max. von Mises Stresses (MPa)	314	252	322	252
Max. DNV Utilization (LRFD)	0.73	0.56	0.68	0.50

Figure 24: Extreme response summary (Orimolade et al., 2015).

5.3.2 Remarks and Discussion of the Extreme Response Results

The following observations were made from the results obtained for the extreme response analyses:

- Compared to the static configurations in the different cases, there is a significant increase in effective tension, bending moment and higher utilisation factor in the extreme response analyses. This indicates that the environmental loads have significant impact on the overall performance of the riser.
- The maximum utilisation factors observed for both ULS and ALS are below unity, which implies a safe design in accordance with the acceptance criteria for combined loading.
- Tension is the main contributor for the combined loading utilisation and is a result of the weight of riser and content in this water depth, combined with the applied top tension.
- The largest utilisation occurs at the hang-off point for the far offset position in both cases, where the far ULS resulted in 0.74 and the far ALS is 0.57. It should be noted that the maximum utilisation for the ALS is lower than ULS, despite the longer offset range and higher top tension. This is a result of the reduced load effect factors applied for the ALS design criteria.
- Maximum effective tension is observed at hang-off point in the accidental far offset position, where there is an 35% increase in tension compared to its static state.
- Maximum bending moment is experienced in the hog-bend section for the far accidental offset position. This is believed to be a result of fluctuations in the wave configuration caused by the high tension in the riser. By increasing the height between the sag- and hog-bend, see Figure 16, these rapid and dynamic bending moments can be reduced.
- The bending moment at TDP increases for the near offset positions in both cases, resulting in a higher utilisation for this section.
- There are no compressive forces observed in any of the analyses.
- The angle variations for all cases are within the limitations for the flex joint described.

Based on the extreme response analyses, it is evident that the configuration meets all acceptance criteria for both ULS and ALS, as stated in the premise.

For SLWRs in more shallow waters, the bending moment is usually the main contributor for the combined loading. As a comparison, the results from a study conducted by (Orimolade et al., 2015) is presented in

Figure 24. This table lists the extreme response results for the intact and accidental mooring condition for a similar SLWR in conjunction with a turret moored FPSO. The configuration is subjected to typical harsh environmental conditions found in the North Sea, in a water depth of 1100 meters. The intact and accidental mooring conditions for this study are 10% and 12% of the water depth, respectively.

From these results, the maximum effective tension is also experienced at hang-off in the far offset position, but are relatively small compared to the scenario in this thesis. On the contrary, the bending moments are larger for the sag-, hog-bend and TDP in the referred study. This is a result of the larger offset conditions used, but it is evident that the bending moment is the main contributor for the combined loading utilisation. Based on these observations, it can be seen that the top tension becomes the driving factor for the combined loading when moving into ultra-deep waters.

5.4 Wave induced Fatigue

Wave induced fatigue damage is calculated following the procedure described in Section 4.4.1 and the results are presented as the total fatigue life for the critical sections listed. Being a production riser, the safety class is set to high by using a factor of 10 for the wave induced fatigue calculation. Having a 25-year design life, this corresponds to a minimum fatigue life of 250-years

5.4.1 Results

Table 23: Results from the wave induced fatigue analysis

Fatigue life (years)			
	C2-Curve	**D-Curve**	**E-Curve**
15 m below flex joint	414	253	155
Sag bend	310 064	183 281	101 496
Hog bend	26 730	15 810	8 812
TDP	1 427 169	843 611	467 170

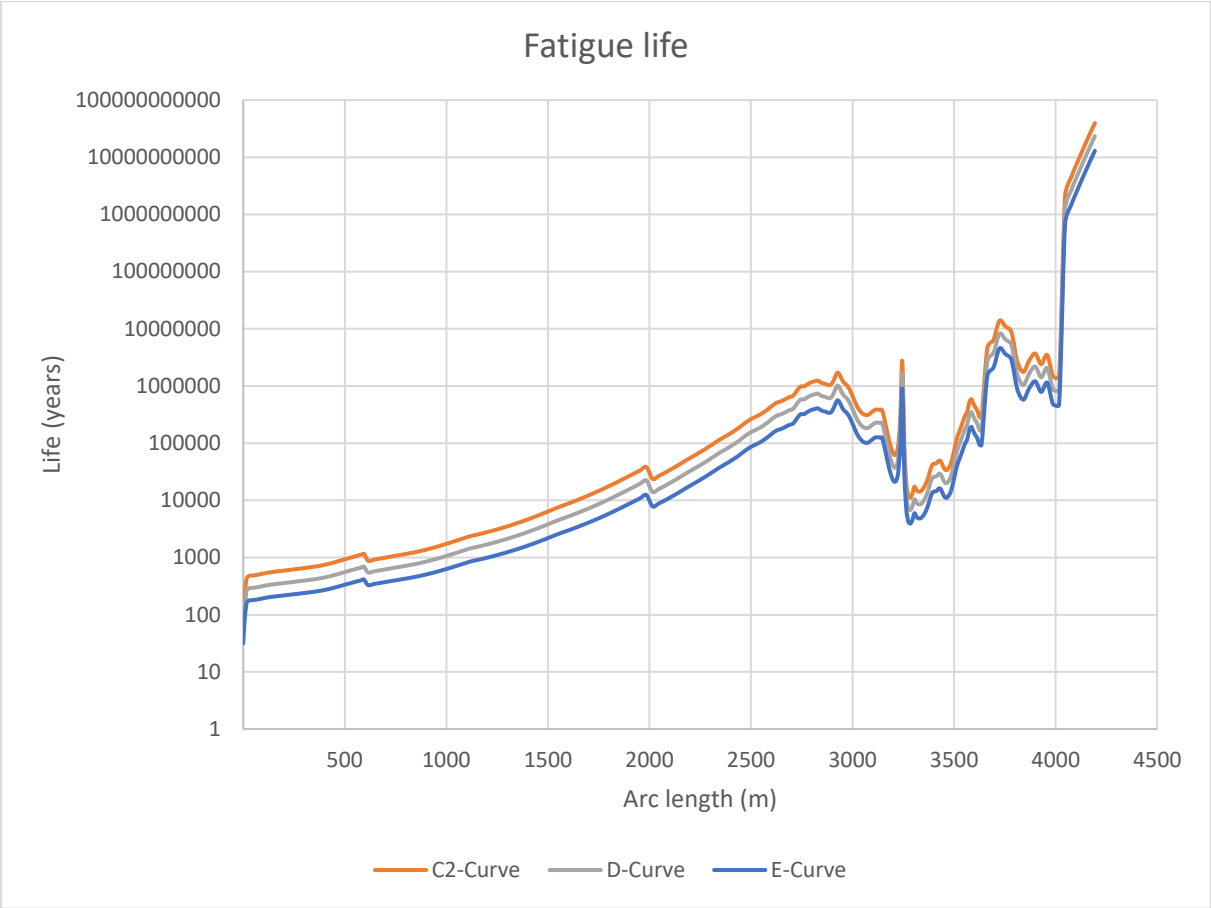

Figure 25: Range graph: Fatigue life - wave induced fatigue

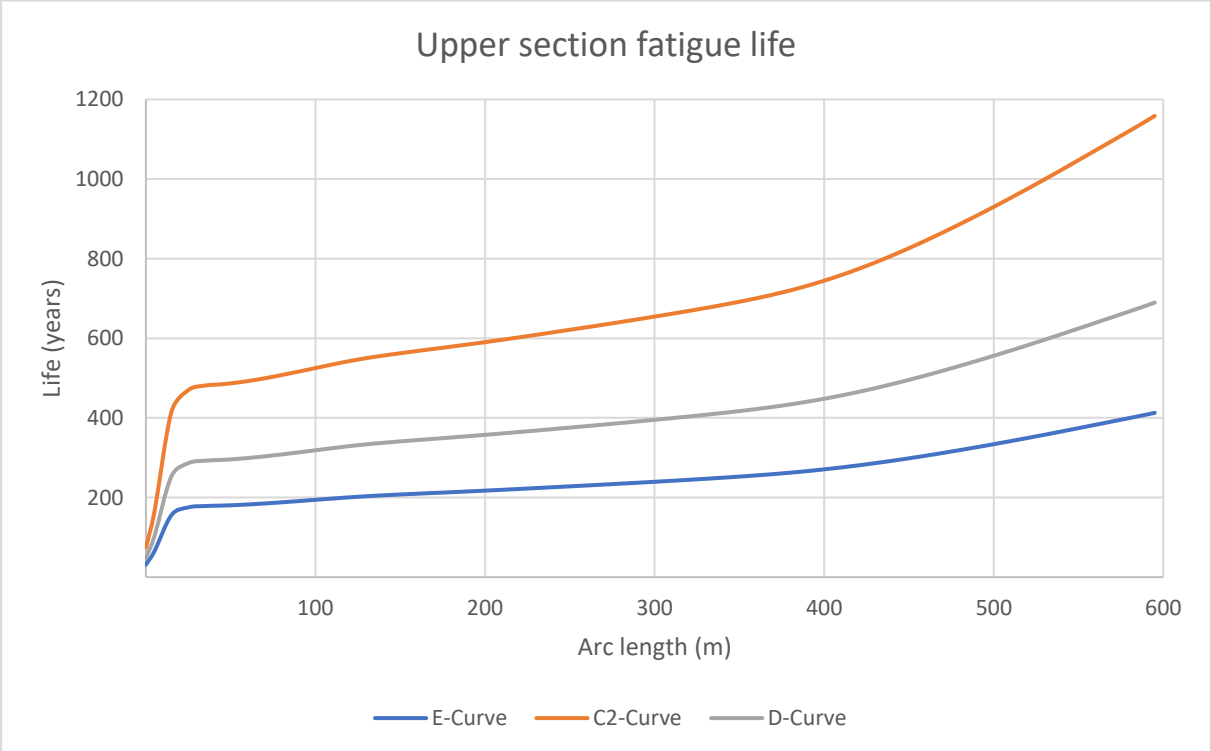

Figure 26: Range graph: Fatigue life for the upper 600 m of the riser with 30 mm wall thickness.

5.4.2 Remarks and Discussion of the Wave Induced Fatigue

Due to the large top tension caused by the weight of the riser in these water depths, the wave induced fatigue analysis turned out to be more complex and time consuming than planned. And several adjustments for the wall thickness had to be done to meet the stated acceptance criteria. Originally the wall thickness for entire riser length was set to 25 mm, but due to poor fatigue life in analysis, the upper catenary section of the configuration had to be improved.

The largest contributor to the poor fatigue performance, was the large axial forces experienced in the upper region of the riser, due to the weight of the riser and its content. The amount of top tension affects the stiffness and natural frequencies of the riser, which in turn governs the behaviour of the configuration in relation to the vessel motions, this can be compared to the pre-tensioning of SCRs. A study conducted by (Martins et al., 2000) shows that an increase in applied top-tension for a SCR increases the accumulated fatigue damage in this region.

Consequently, the wall thickness of the riser had to be increased to 30 mm for the top 600 metres and 28 mm for the following 1400 metres of the upper catenary to improve fatigue life. By doing so, the top tension increases because of the added weight of the increased wall thickness, but it provided sufficient fatigue performance in the case of the C2-curve and D-curve at 15 metres below the top termination point, as seen in Table 23. Usually the top 5 to 15 metres of the top section will be installed with a tapered pipe length to improve fatigue performance in this region, but still the upper section should be further analysed with an additional increase in wall thickness to provide sufficient fatigue life.

From the results presented in Figure 25, it is found that the sag-, hog-bend and TDP provides satisfactory fatigue life in this analysis and is well above the limit set by the acceptance criteria given in Section 4.7. For SLWRs in more shallow waters, these parts of the riser usually exhibit lower fatigue performance compared to its upper section and is more sensitive to the load transfer caused by the vessel motions. In the work conducted by (Orimolade et al., 2015), the TDP was the most sensitive region in terms of the wave induced fatigue. This fatigue study was performed for a 10" SLWR with a wall thickness of 25 mm in a water depth of 1100 metres. It is analysed in conjunction with a turret moored FPSO using typical harsh environmental conditions found in the North Sea, West of Scotland. Figure 27 shows the calculated fatigue life for that riser, where the first 1240 metres is the upper catenary section of the configuration.

Comparing the two results, it is evident that the increased axial force in the upper catenary section for the ultra-deep water configuration is a large contributor to the fatigue damage in this

region. But it should be noted that the increased stiffness of the upper section also seems to dampen the cyclic stresses experienced in the sag-, hog-bend and TDP.

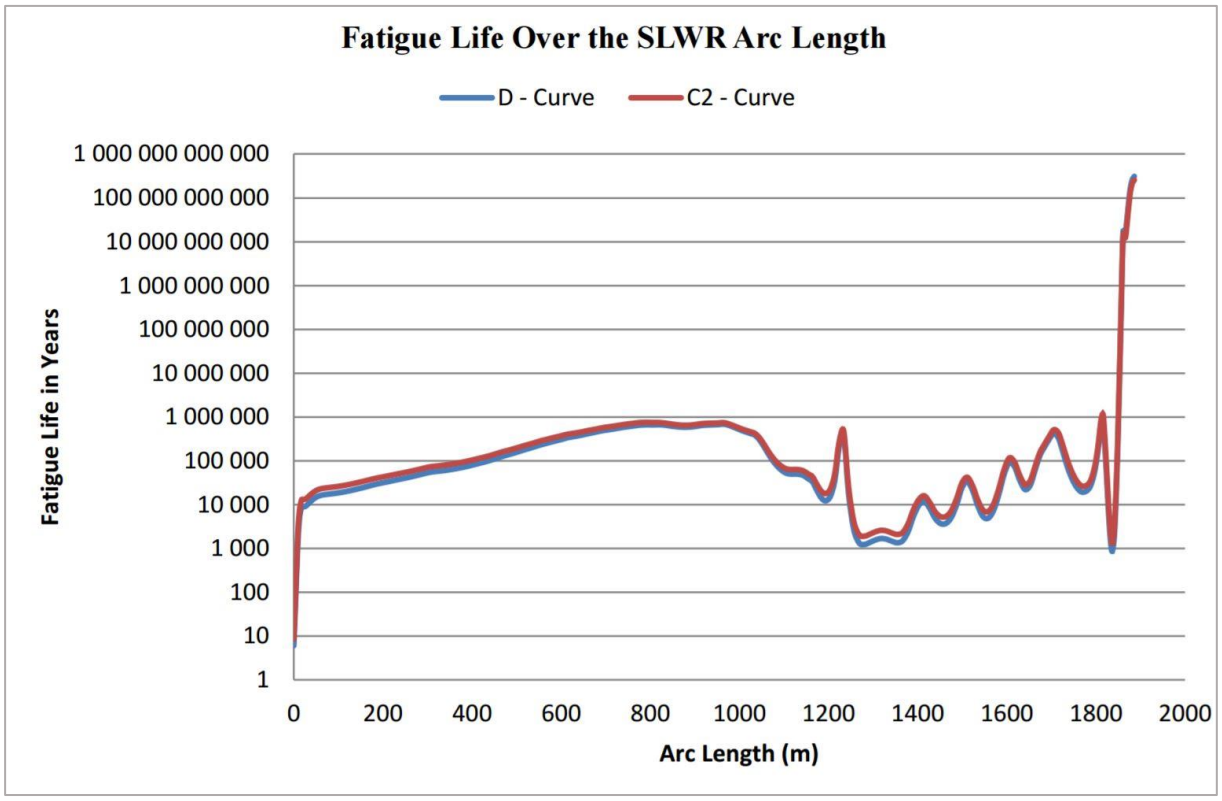

Figure 27: Wave induced fatigue for SLWR in a water depth of 1100 m (Orimolade et al., 2015).

5.5 Vortex Induced Vibration Fatigue

Since the VIV induced fatigue is not assessed in this thesis, a presentation of this phenomena is given instead. VIV occurs when the flow of fluid over a structure starts shedding vortices on the opposite side of the structure, with respect to the flow direction. This unsteady flow phenomenon can happen under certain conditions, where the vortices detach in a periodical manner from opposing sides, causing the structure to oscillate. If the vortex shedding frequency matches the resonance frequency of the structure, it will cause the structure to resonate and the oscillation can become self-sustaining (Odland, 2015). Any oscillatory motion will to some extent cause cyclic loading in the structure, thus contributing to the fatigue damage. And this is an important issue to address in riser design, especially when moving into deep waters with the presence of strong currents. Figure 28 illustrates the two directions in which the pipe will oscillate, the combination of these directions results in an 8-figure motion.

A riser suspended in deep waters will be more susceptible to VIV induced fatigue, because of (Bai and Bai, 2005):

- Strong currents are usually present in deeper waters
- Increase in riser length reduces its natural frequency, thus lowering the required fluid velocity needed to achieve exiting shedding frequencies.
- The use of FPUs eliminates the possibility of clamping the riser to a fixed structure.
- Magnitude and directional changes in the current can result in several modes of the riser that can be excitation into VIV.

To analyse the VIV induced fatigue damage, it is important to:

- Determine the eigenfrequencies and modes of the riser, for different current directions.
- Find the most dominating frequencies among the eigenfrequencies.
- Analyse the response of the frequencies when the riser is subjected to different current profiles.
- Calculate the accumulated fatigue damage from VIV using applicable methods, such as S-N curves.
- Verify if the riser configuration meets the design criteria, usually a fatigue life of more than 20 times its intended service life, or if VIV-suppressive measures needs to be implemented.
- If measures need to be taken, redo the analysis with VIV-suppressors included.

The two most common ways of suppressing VIV, is to install fairings or helical strakes for critical sections of the riser. These works by disrupting the fluid flow over the riser, and a typical helical strake is seen in Figure 17. The helical strakes are fixed in position, whereas the fairings are free to rotate depending on the direction of the current.

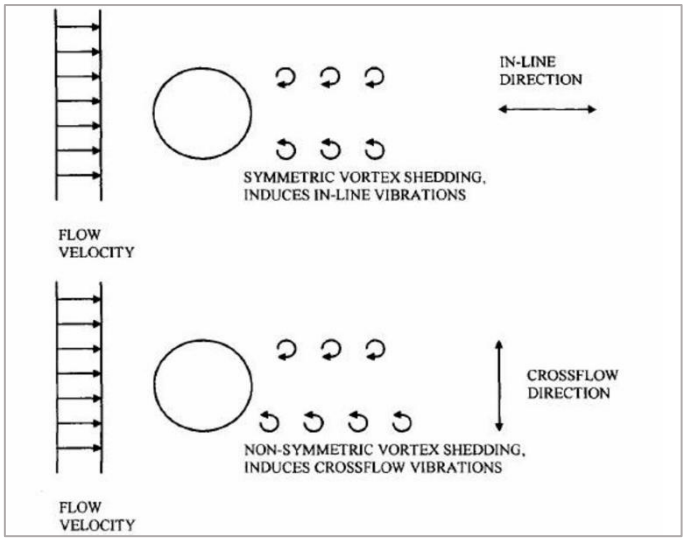

Figure 28: Vortex induced motions (Bai and Bai, 2005).

Chapter 6 Sensitivity and Optimisation

6.1 Introduction

In this Chapter, the results from the optimisation study is presented and discussed. The optimisation is based on the initial configuration with the aim of improving the overall performance within the ULS design criteria for combined loading. The procedure follows the same methodology as the initial one, apart from the increased drag coefficient, thus neglecting the presence of strakes fitted in the upper catenary section since these were not modelled in the simulations. Consequently, the dynamic response results will vary somewhat compared to the ULS results previously presented. All the files were created by use of a programmed script for the 75 configurations given in Table 17 and resulted in a total of 225 load cases. The obtained results for all load cases can be seen in its entirety in Appendix C – Optimisation Results.

6.2 Optimisation Results

From the optimisation process, it was clear that the Far offset positions resulted in the poorest performance for all configurations. Consequently, these will be compared and the maximum utilisation factor found in all the 75 Far offset cases are plotted in Figure 29. This graph shows the maximum utilisation factors found in each case, and these are plotted against the static hang-off angle for each case for the nominal offset position, represented on the x-axis. Each line represents the combination of the fixed buoyancy length and buoyancy force versus static hang-off angle for that configuration, where the marked spot on the lines highlights the individual cases.

When considering the different hang-off angles, in terms of combined loading utilisation, it is evident that the 6 degrees static hang-off resulted in the best performance in all cases. The two outer edges for this hang-off angle are highlighted in Figure 30, for the best and worst case. These are compared to the initial configuration in Table 24 to study the difference in extreme response behaviour between the three cases.

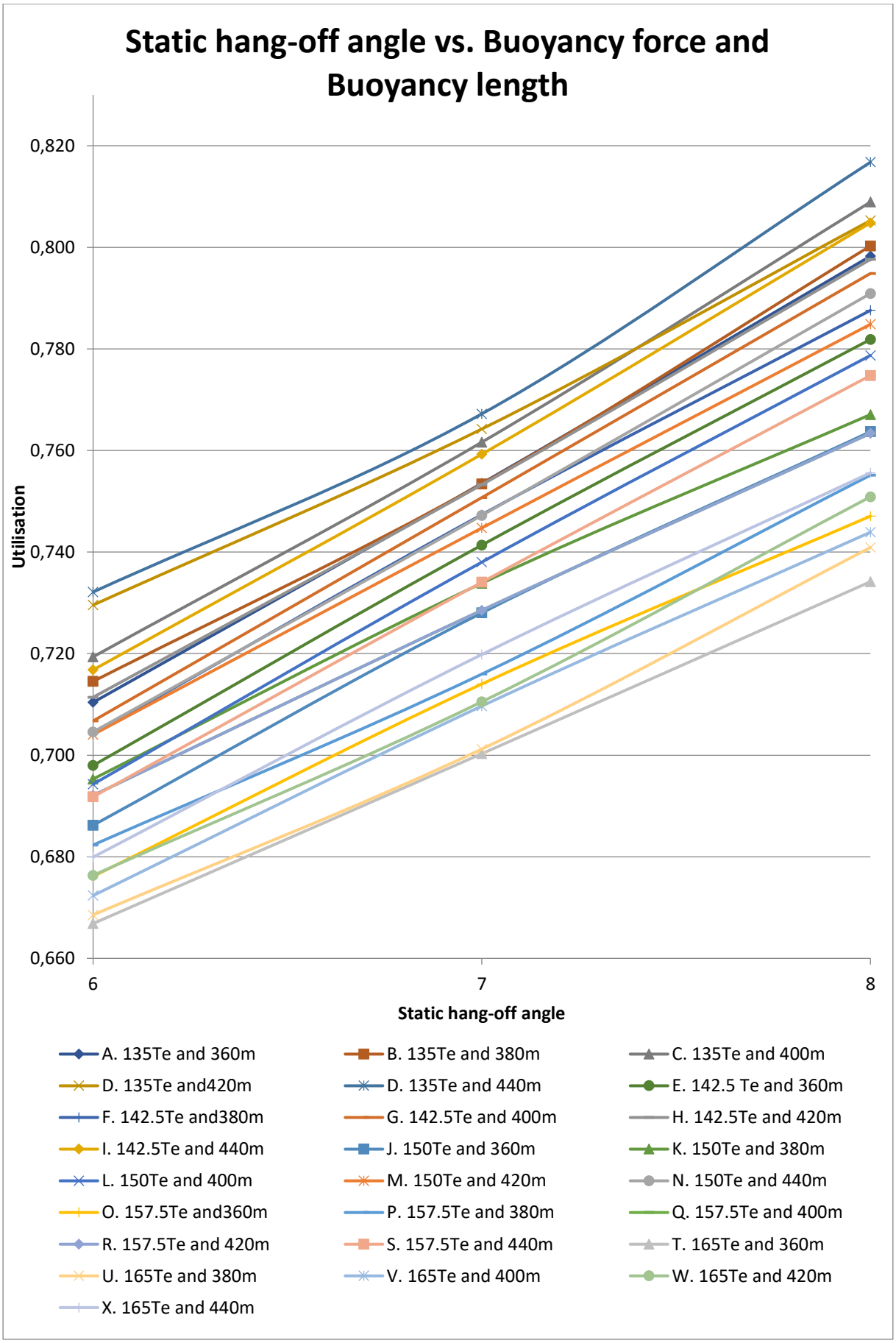

Figure 29: Optimisation results for all far offset cases

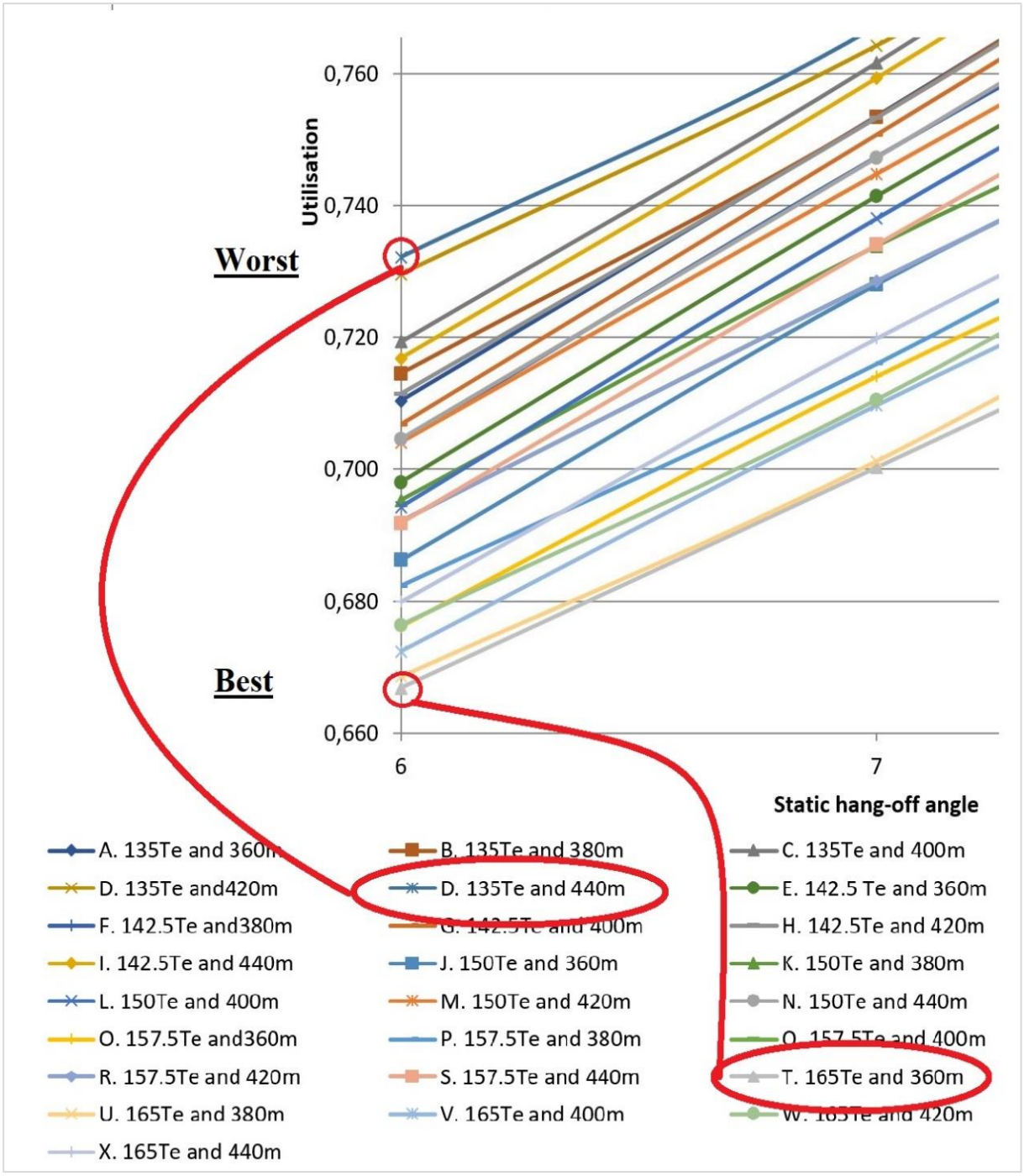

Figure 30: Detailed image of the utilisation for the 6 degrees static hang-off angle

Table 24: Performance comparison of the initial configuration versus the worst and best configuration found for the 6 degrees static hang-off angle

Design case:	6° D-configuration	Initial	6° T-configuration	Units:
Net buoyancy force	135	150	165	Tonnes
Buoyancy length	440	400	360	m
Hang-off angle static	6	7	6	Degrees
NEAR Offset position				
Hang-off angle static	6,89	7,74	7,10	Degrees
Hang-off angle max	12.08	12.97	12.31	Degrees
Hang-off angle min	3.55	4.40	3.77	Degrees
Hang-off angle range	8.54	8.57	8.54	Degrees
Top tension max	6702	6631	6510	kN
Top tension static	5019	4977	4878	kN
Top tension min	3288	3295	3276	kN
Bending moment max	196	234	340	kN ∗ m
Bending moment min	142	178	280	kN ∗ m
Utilization max	0.52	0.51	0.55	N/A
Utilization static	0.30	0.29	0.48	N/A
Utilization min	0.19	0.18	0.46	N/A
FAR Offset position				
Hang-off angle static	8.01	9.20	7.86	Degrees
Hang-off angle max	12.56	13.71	12.39	Degrees
Hang-off angle min	2.12	3.26	1.98	Degrees
Hang-off angle range	10.44	10.46	10.45	Degrees
Top tension max	7912	7939	7515	kN
Top tension static	5217	5215	5060	kN
Top tension min	1858	1880	2081	kN
Bending moment max	281	279	291	kN ∗ m
Bending moment min	27	43	88	kN ∗ m
Utilization max	0.732	0.738	0.667	N/A
Utilization static	0.33	0.33	0.31	N/A
Utilization min	0.12	0.12	0.13	N/A

6.3 Discussion of the Optimisation Results

Sensitivity study and general observations made from the optimisation study:

- Reducing the static hang-off angle reduces the maximum utilisation for all configurations. This is in accordance with the observations made in Section 5.3 and shows that decreasing the applied top tension reduces the maximum utilisation factor.
- Among all configurations, the D-configuration combined with an 8° hang-off angle resulted in the worst utilisation. This is a consequence of applied top tension, low net

buoyancy force in combination with the longest buoyancy section, causing the centre of buoyancy to be further away from the upper catenary section than for the shorter lengths.

- When reducing the buoyancy length for a fixed buoyancy force, the utilisation factor reduces in most cases. This is a result of the way this optimisation study is conducted, where the upper section has a fixed length. Such that when reducing the buoyancy length, the centre of buoyancy moves towards the upper catenary section, thus exerting more lift for this section. Though this is not the case for all configurations as seen for the top line in Figure 32. This indicates that there more factors come into play, such as bending moment becoming more prevailing for some configurations.
- An increase in buoyancy force decreases the utilisation factor for all combinations of buoyancy length and hang-off angle, again this is a result of the high tension being the main contributor in the combined loading.
- Comparing the O-configuration with the W-configuration, it is seen that the maximum utilisation is equal for the 6° hang-off case and for the 7° case, the O-configuration performs better than in the case of the W-configuration. Considering the 8° case, the opposite happens. These observations are made for other comparisons as well. And this indicates that at a certain point, the performance obtained for a large buoyancy force spread over a longer section, can be achieved by less buoyancy force spread over a shorter section. This can be seen more clearly in Figure 32, where the different combinations of static hang-off angle and buoyancy force are plotted in terms buoyancy length on the x-axis and utilisation on the y-axis.
- There are no compressive forces found in any of the configurations.
- The top angle variation for all cases are within the limitations for the flex joint.

Observations made for the comparison study in:

- The largest hang-off angle in both near and far offset position is experienced by the initial configuration, and the smallest angle is found in the far offset position for the T-configuration. The hang-off angle range variation is within the acceptable limit and is found to be the approximately the same for all configuration for the different offset positions.
- The highest tension is found at the top of the initial configuration in the far offset position, and is a consequence of this configuration having a larger static hang-off angle resulting in higher applied top tension. The maximum tension experienced is slightly higher for the initial, compared to the D-configuration for the same offset position.

- The ratio between the maximum tension and the static tension for the initial configuration in far offset position is 1.52, whereas for the T-configuration it is decreased to 1.48, indicating an important improvement in the configuration.
- The T-configuration results in the highest utilisation factor for the near offset position, this is a result of the large buoyancy force applied in combination with the shortest buoyancy length. As a result, this configuration experiences a lower curvature in the hog-bend and increased bending moment in this region, see Figure 31. Still the utilisation is within good margins at 0.55.
- The highest utilisation factor found in the comparison is 0.738, and is for the initial configuration in the far offset position. This is a result of the applied top tension, buoyancy force and buoyancy length as described earlier.

From these results, it is seen that by reducing the static hang-off angle, increasing the total net buoyancy force or moving the centre of buoyancy towards the upper catenary will all result in a lower utilisation factor. And that a combination of all these provided the best solution for the framework set for this study. For SLWRs in more shallow waters (Orimolade et al., 2015), this might not be the case since bending moments will be more dominating. Thus, the use of increased buoyancy force over a shorter section may contribute to larger bending moments, resulting in a higher utilisation factor.

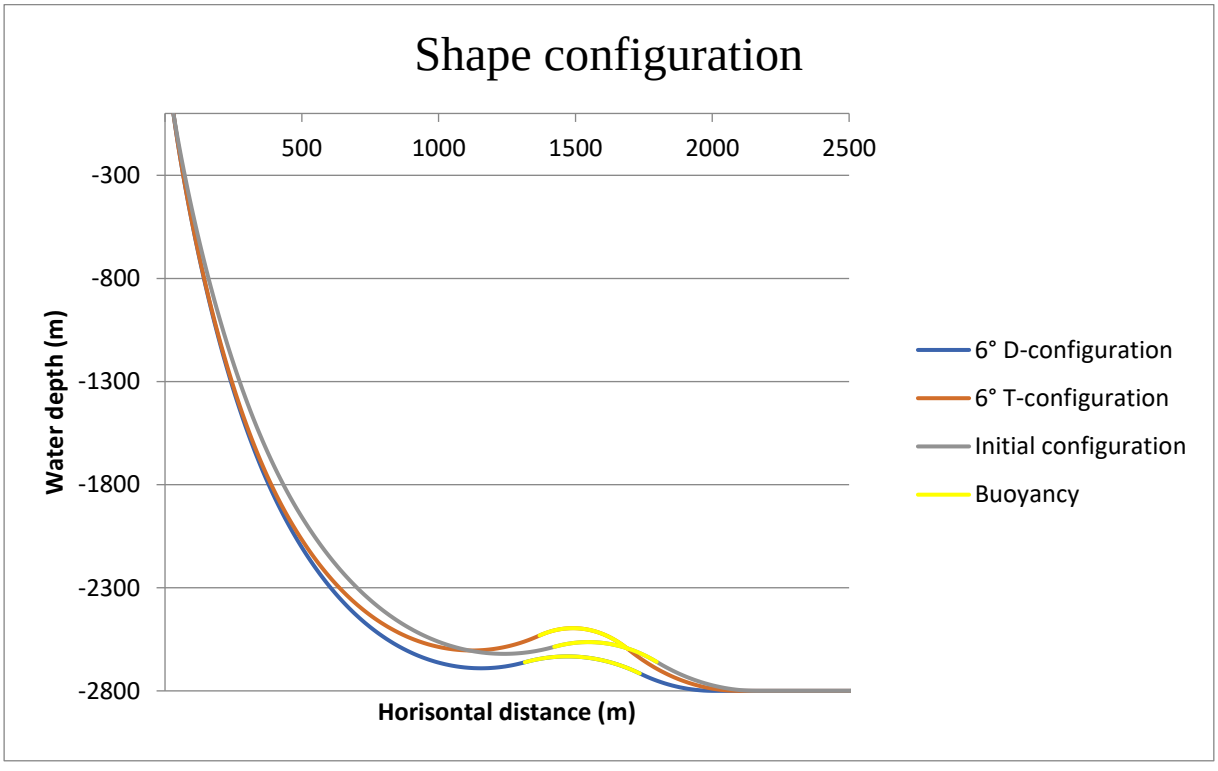

Figure 31: Comparison of the different shape configurations

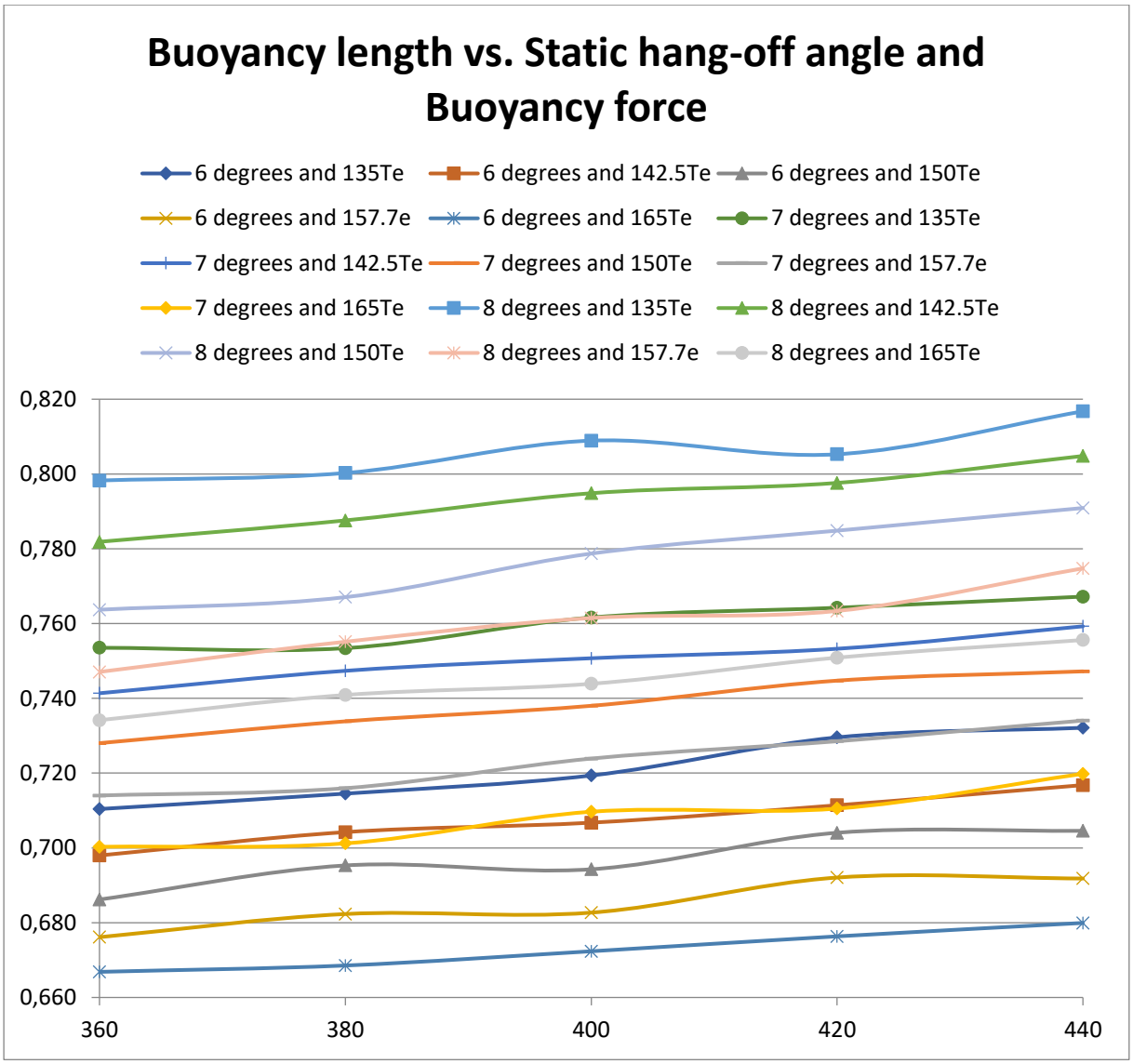

Figure 32: Utilisation for buoyancy length vs. buoyancy force and hang-off angle

6.4 Wave Induced Fatigue for the Optimised Configuration

Being the configuration with the lowest utilisation factor, the 6° T-configuration was selected for an additional wave induced fatigue analysis, to see how the riser would perform. Since the top tension is reduced compared to the initial configuration, it is expected that the fatigue life will be improved because of this. The results for the critical sections are presented in Table 25, together with the results from the initial configuration. A comparison of the calculated fatigue life over the entire arc length is shown in Figure 33.

Table 25: Comparison of the wave induced fatigue life

Fatigue life (years)			
	C2-Curve	D-Curve	E-Curve
	6° T-configuration from optimisation study		
15 m below flex joint	479	290	176
Sag bend	490 236	289 782	160 474
Hog bend	35 957	21 257	11 825
TDP	4 560 855	2 695 957	1 492 953
	Initial configuration		
15 m below flex joint	414	253	155
Sag bend	310 064	183 281	101 496
Hog bend	26 730	15 810	8 812
TDP	1 427 169	843 611	467 170

Observations made when comparing the wave induced fatigue life of the 6° T-configuration with results for the initial configuration:

- The fatigue life is improved over the entire arc length for all S-N curves in comparison to the initial configuration.
- At 15 meters below hang-off point, the calculated fatigue life is 290 years for the T-configuration following the D-curve, this is a 37-year increase compared to the initial configuration.
- The decrease in top tension results in better fatigue performance for the wave induced fatigue and the findings are in accordance with the observations and remarks made in Chapter 5.

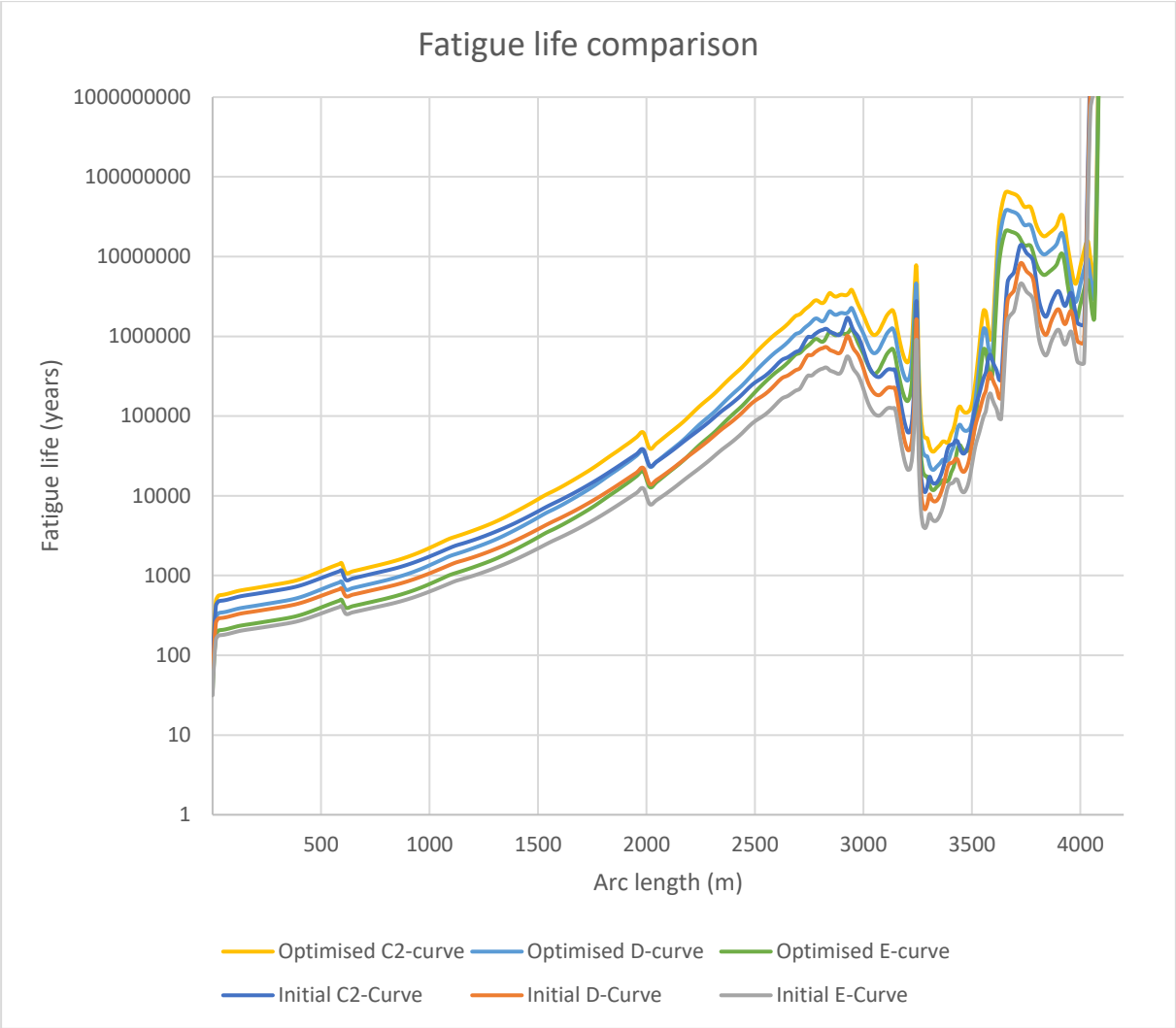

Figure 33: Fatigue life for initial and improved configuration over the entire arc length

Chapter 7 Conclusion and Recommendations

7.1 Conclusion

This thesis has presented an initial 10" production SLWR configuration that were subjected to several parameter adjustments to improve the LRFD utilisation of the configuration. All configurations were considered for deployment in the ultra-deep waters off the coast of Brazil, in conjunction with a high-motion vessel. Riser modelling and analyses have been performed by use of OrcaFlex and its programming interface.

The vessel used in the studies, is a typical spread moored FPSO with associated RAOs. As the vessel motions is the main design driver for dynamic risers, a detailed vessel response analysis is conducted for typical 100-year waves to determine the worst response. With the combination of the 100-year waves and a 10-year current, several analyses are presented to verify the integrity of the riser in extreme sea states, and the wave induced fatigue is calculated for two of the configurations.

Extreme Response Analysis

From the results of the extreme response analyses, it is shown that the SLWR can be implemented in ultra-deep waters in conjunction with a spread moored FPSO. It has been analysed under typical extreme environmental conditions found in the Santos basin off the coast of Brazil, and the results have shown that it is able to withstand the subjected loads.

The riser met both the ULS and ALS design criteria, and the highest utilisation factor was found at the top of the riser in the operational far offset position. The maximum utilisation in this case was 74%, and the main contributor is the resulting top tension due to the weight of the riser. A maximum top tension of 8127 kN was registered in the accidental far offset position. Maximum bending moment was also observed in the accidental far offset position, and was located in the hog-bend. Even though the riser were subjected to larger forces for the accidental mooring condition, the combined loading utilisation is less than for the ULS due to lower load factors being applied for the ALS design criteria.

Following the S-N curve approach in the reference standard DNV-OS-F201, the wave induced fatigue life was calculated for a total of 273 load cases. This was done by blocking the wave scatter diagram into 21 blocks with lumped probability of occurrence and calculating the total damage for the 13 most prevailing wave directions. The analysis showed that the most critical

area was the top section, which resulted in increased wall thickness for the upper catenary section of the riser.

With a design life of 25 years, the calculated fatigue life must be more than 250 years. This was not achieved for the top 15 meters, and it is assumed that this will be covered by a tapered section. The fatigue life at 15 meters was found to be 254 years for the D-curve and 414 years for the C2-curve. The rest of the riser length showed very good fatigue performance against the wave induced fatigue. The VIV induced fatigue was not assessed in this study due to time constraints, and is listed as recommendation for further work.

Sensitivity and Optimisation

After establishing an initial configuration that met the design criteria, it was subjected to several parameter changes with the aim of improving the utilisation factor. This was done by using the programming interface for the OrcaFlex software, which made it easy and quick to create a wide range of different configurations based on the initial one. By varying the net buoyancy force, buoyancy length and static hang-off angle, a total of 75 different configurations were analysed for the ULS design criteria. This resulted in a total of 225 load cases, including nominal, far and near offset position. Results from these load cases were then obtained and analysed to find an improved configuration with regard to the combined loading criteria.

The analyses showed that all configurations met the ULS design criteria. It was evident that by decreasing the static hang-off angle and shortening the buoyancy section, while increasing the total net buoyancy force, lowered the utilisation factor in nearly all cases. These results are in accordance with the observations made in the extreme response analyses, where it was concluded that the top tension was the main contributor for the combined loading utilisation. By decreasing the static hang-off angle, the applied top tension is decreased. The way the optimisation procedure was conducted in this study, the reduction in buoyancy length caused the centre of buoyancy force to be shifted toward the upper catenary section, thus reducing the top tension. Combining a shorter buoyancy length with increased buoyancy force further reduced the utilisation factor, even though this increased the maximum bending moment experienced in the hog-bend.

A comparison study between the initial configuration and the best and worst of the 6° static hang-off configuration showed how the parameter variations affected the performance of the configuration. And it was concluded that the 6° configuration with the shortest buoyancy section and largest net buoyancy force yielded the best results in terms of the objective stated

in this thesis. This configuration was analysed for wave induced fatigue, which resulted in a calculated fatigue life of 290 years at 15 meters below hang-off point.

Summary

From the extreme response and wave induced fatigue analyses it is shown that the SLWR concept can be implemented in ultra-deep waters in conjunction with a spread moored FPSO. It is found that the tension experienced in these depths is the main contributor for the combined loading, whereas for more shallow waters, the bending moment tends to be more prevailing. High tension also affects the SLWRs performance for the wave induced fatigue, resulting in increased wall thickness in the upper section.

Analyses show how parameter changes can improve the utilisation factor for a SLWR within the ULS design criteria given in the offshore standard DNV-OS-F201: Dynamic Risers. And from a total of 75 different configurations created in the optimisation study, it is established which one performs best in terms of the combined loading criteria.

Conclusive remarks made for SLWR configurations in these water depths, is that a small static hang-off angle seems to be desirable to reduce the applied top tension. A large net buoyancy force spread over a suitable section will also relieve the tension felt at the top, thus improving both the utilisation factor and the wave induced fatigue performance.

7.2 Recommendations

Based on the analyses and results presented in this thesis, a good insight in the implementation of SLWRs in ultra-deep waters is given and its integrity in extreme sea states is verified. By adjusting different parameters for the initial configuration, it is shown that the performance of the riser is affected and that there are many considerations to take when designing a SLWR in these water depths. Even though this thesis covers the main aspects of designing and analysing a SLWR, still there are more analyses and further studies that should be conducted. And the following recommendations are made:

- Perform VIV-induced fatigue analysis for SLWRs in these water depths and asses the need of VIV suppressive devices to verify sufficient fatigue life.
- Wall thickness sizing in the upper catenary section. Do analyses with varying wall thicknesses and section length to improve fatigue life, and to determining a better sectioning of the upper catenary.

- Increase the number of parameter variables in the optimisation study. Further work should be conducted by altering the height of the upper catenary and including more design parameters in the optimisation study.
- Perform analyses with varying water depth to determine when the effective tension becomes the main contributor in the combined loading criteria.
- Do optimisation study where cost, installation and riser performance are all included.

References

ANDRADE, E. Q. D., AGUIAR, L. L. D., SENRA, S. F., SIQUEIRA, E. F. N., TORRES, A. L. F. L. & MOURELLE, M. M. 2010. Optimization procedures of steel lazy wave riser configuration for spread moored FPSOs in deepwater offshore Brazil. *Offshore technology conference.* Houston, Texas, USA.

BAI, Y. & BAI, Q. 2005. *Subsea Pipelines and Risers,* Jordan Hill, UNKNOWN, Elsevier Science.

BAI, Y. & BAI, Q. 2012. *Subsea engineering handbook,* Oxford, UK, Elsevier.

BARDOT GROUP. 2017. *Helical strakes [Picture]* [Online]. Available: http://www.bardotgroup.com/fr/solutions-surf/stabilisationlde-lignes/viv-strakes [Accessed 5.5.2017].

CARTER, B. A. & RONALDS, B. F. 1998. Deepwater Riser Technology. Society of Petroleum Engineers.

CHAKRABARTI, S. 2005. *Handbook of Offshore Engineering (2-volume set),* St. Louis, UNKNOWN, Elsevier Science.

DNV 2010a. DNV-OS-F201: Dynamic Risers.

DNV 2010b. DNV-OSS-302: Offshore Riser Systems.

DNV 2010c. DNV-RP-C203: Fatigue Design of Offshore Steel Structures.

FELISITA, A. 2016. *On the Application of Steel Lazy Wave Riser for Deepwater Locations with Harsh Environments.* Philosophiae Doctor, Faculty of Science and Technology, University of Stavanger.

FISHER, E. A. & BERNER, P. C. 1988. Non-Integral Production Riser For Green Canyon Block 29 Development. Offshore Technology Conference.

GEMILANG, G. M. 2015. *Feasibility study of selected riser concepts in deep water and harsh environment [Master thesis]*. University of Stavanger.

GREALISH, F., KAVANAGH, K., CONNAIRE, A. & BATTY, P. 2007. Advanced Nonlinear Analysis Methodologies for SCRs. Offshore Technology Conference.

HOFFMAN, J., YUN, H., MODI, A. & PEARCE, R. 2010. Parque das Conchas Pipeline, Flowline and Riser System Design, Installation and Challenges. Offshore Technology Conference.

HUTCHINSON OIL & GAS. 2017. *Flex Joint [Picture]* [Online]. Available: http://oil-gas.hutchinsonworldwide.com/applications/riser-connection [Accessed 31.5.2017].

KALMAN, M., YU, L., DURR, C. & SUAREZ, J. 2014. Qualification of Unbonded Flexible Pipe to API and DNV Standards. Offshore Technology Conference.

KARUNAKARAN, D., DUTTA, A., CLAUSEN, T. & LUND, K. M. 2002. Steel Catenary Riser Configurations for Large Motion Semi Submersibles with Lightweight Coating. *Deep Offshore Technology Conference* New Orleans.

KARUNAKARAN, D. & FRØNSDAL, M. 2016. Steel Lazy Wave Riser with Tether for FPSO with Dis-Connectable Turret for Iceberg Conditions. Offshore Technology Conference.

KARUNAKARAN, D., MELING, T. S., KRISTOFFERSEN, S. & LUND, K. M. 2005. Weight-Optimized SCRs For Deepwater Harsh Environments. Offshore Technology Conference.

KARUNAKARAN, D., NORDSVE, N. T. & OLUFSEN, A. 1996. An Efficient Metal Riser Configuration For Ship And Semi Based Production Systems. International Society of Offshore and Polar Engineers.

KATLA, E., MORK, K. & HANSEN, V. 2001. Dynamic Risers: Introduction and Background to the New DNV Offshore Standard (OS-F201). Offshore Technology Conference.

KAVANAGH, W. K., LOU, J. & HAYS, P. K. 2003. Design of Steel Risers in Ultra Deep Water-The Influence of Recent Code Requirements on Wall Thickness Design for 10,000ft Water Depth. Offshore Technology Conference.
KIM, S. & KIM, M.-H. 2015. Dynamic behaviors of conventional SCR and lazy-wave SCR for FPSOs in deepwater. *Ocean Engineering,* 106**,** 396-414.
KIRKEMO, F., MØRK, K. J., SØDAHL, N. & LEIRA, B. 1999. Design of Deepwater Metallic Risers. International Society of Offshore and Polar Engineers.
LEGRAS, J.-L., KARUNAKARAN, D. N. & JONES, R. L. 2013. Fatigue Enhancement of SCRs: Design Applying Weight Distribution and Optimized Fabrication. Offshore Technology Conference.
LUPPI, A., COUSIN, G. & O'SULLIVAN, R. 2014. Deepwater Hybrid Riser Systems. Offshore Technology Conference.
MARTINS, C. A., HIGASHI, E. & SILVA, R. M. C. 2000. A Parametric Analysis of Steel Catenary Risers: Fatigue Behavior Near the Top. International Society of Offshore and Polar Engineers.
NOV. 2017. *Multilayer Flexible Pipe [Picture]* [Online]. Available: http://www.nov.com/Segments/Completion_and_Production_Solutions/Subsea_Production_Systems/Flexible_Pipe_Systems/Designing_Flexible_Pipes/Materials_and_Profiles/Materials_and_Profiles.aspx [Accessed 12.6.2017].
ODLAND, J. 2015. Platform design issues. *Offshore field development.* Stavanger: Universitet i Stavanger.
OFFSHORE MAGAZINE. 2015. *Deepwater solutions & records for concept selection [PDF]* [Online]. Offshore magazine. Available: http://www.offshore-mag.com/content/dam/offshore/print-articles/volume-75/05/0515-DeepwaterPoster040815ADS.pdf [Accessed 2.3.2017].
ORIMOLADE, A. P. 2014. *Steel lazy wave risers from turret moored FPSO [Master thesis]*. University of Stavanger.
ORIMOLADE, A. P., KARUNAKARAN, D. & MELING, T. S. 2015. Steel lazy wave risers from turret moored FPSO for deepwater harsh environment. *International conferance on ocean, offshore and arctic engineering.* St. John's, Newfoundland, Canada.
PHIFER, E. H., KOPP, F., SWANSON, R. C., ALLEN, D. W. & LANGNER, C. G. 1994. Design And Installation Of Auger Steel Catenary Risers. Offshore Technology Conference.
SPE INTERNATIONAL. 2015. *History of offshore drilling units* [Online]. Available: http://petrowiki.org/History_of_offshore_drilling_units [Accessed 4.4.2017].
SUBSEA7 FOR PETROBRAS. 2015. *Buoy-Supported Riser [Picture]* [Online]. Available: http://offshore.worleyparsons.com/project/subsea-7-riser-buoys/ [Accessed 9.5.2017].
SWORN, A. 2005. Hybrid Riser Towers from an Operator's Perspective. Offshore Technology Conference.
U.S. ENERGY INFORMATION ADMINISTRATION 2016. International Energy Outlook 2016 *In:* ENERGY, U. S. D. O. (ed.). Washington, DC 20585: Office of Energy Analysis.
VOIE, P. E. & SØDAHL, N. 2013. Optimisation of Steel Catenary Risers. *International Conference on Ocean, Offshoreand Arctic Engineering.* Nantes, France.

Appendices

Appendix A – Wall Thickness Calculation

PET Design Inputs and Code Check Results

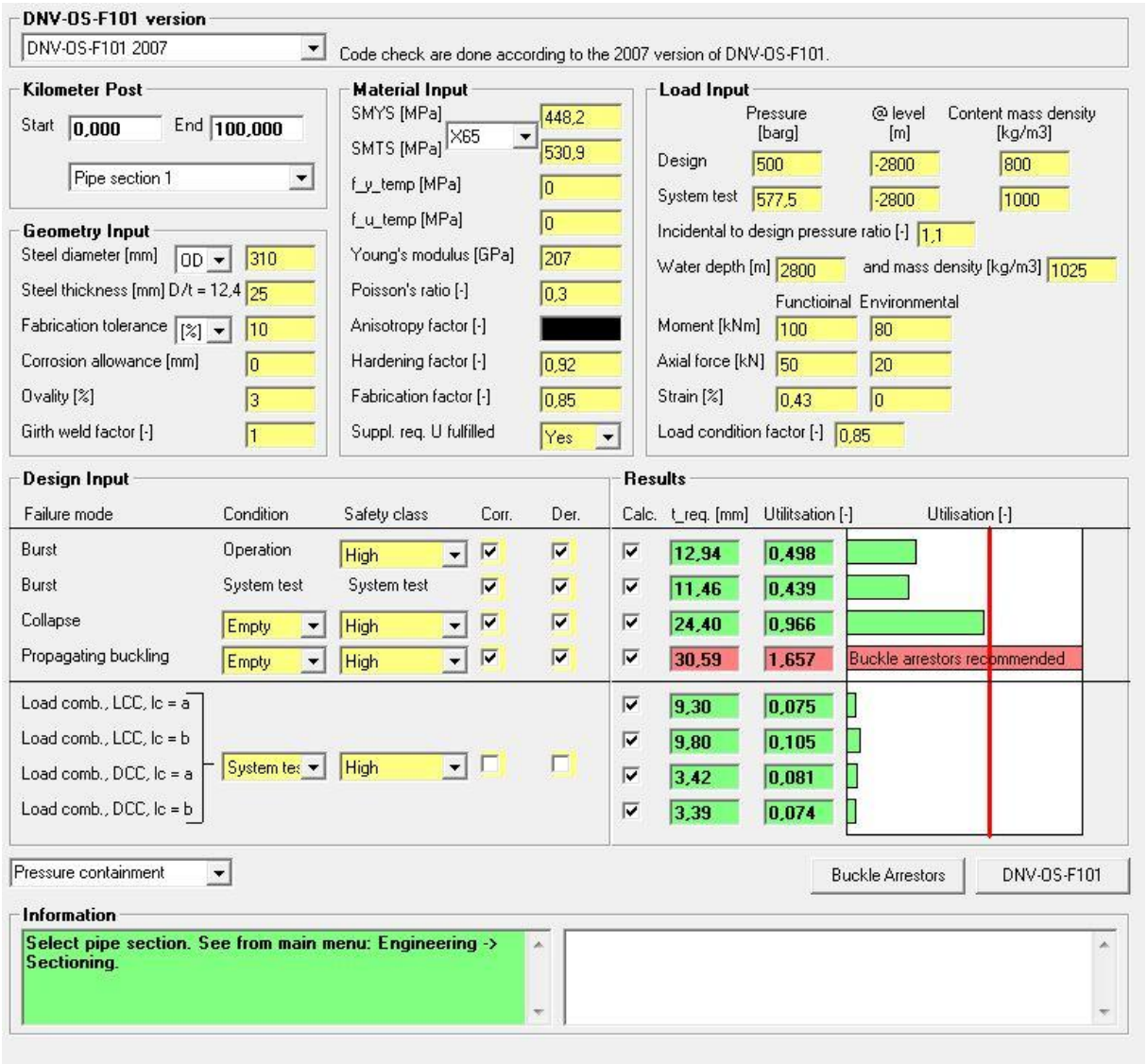

PET Pressure Containment Report:

DNV-OS-F101 - SUBMARINE PIPELINE SYSTEMS - 2007

Pipeline Engineering Tool (PET)

Pressure Containment (bursting) report

Project: Pipe

Section: Pipe section 1

KP Start: 0,000 ***KP End:*** 100,000 ***Date:*** 04.07.2017

RELEVANT INPUT PARAMETERS:	Operation	System test
Nominal outer steel diameter [mm]:	310,00	
Nominal steel wall thickness [mm]:	25,00	
Fabrication tolerance [%]:	10,00	
Corrosion allowance [mm]:	0,00	
Specified minimum yield stress [MPa]:	448,2	
Specified minimum tensile strength [MPa]:	530,9	
Derating in yield stress due to temperature [MPa]:	0,0	
Derating in tensile strength due to temperature [MPa]:	0,0	
Depth [m]:	2800,0	
Density of external fluid [kg/m^3]:	1025,0	
Material strength factor [-]:	1,00	1,00
Internal pressure at reference level [bar]:	500,0	577,5
Reference level for internal pressure [m]:	-2800,0	-2800,0
Density of internal fluid [kg/m^3]:	800,0	1000,0
Incidental to design pressure ratio [-]:	1,10	1,00
Safety Class:	HIGH	SYSTEM TEST
Corroded wall thickness:	YES	YES
Derated material properties:	YES	YES
INTERMEDIATE RESULTS:	**Operation**	**System test**
Characteristic yield stress [MPa]:	448,2	448,2
Characteristic ultimate strength [MPa]:	530,9	530,9
Steel wall thickness used in code check [mm]:	22,50	22,50
Pressure containment resistance, yielding limit state [bar]:	810,1	810,1
Pressure containment resistance, ultimate [bar]:	834,4	834,4
Pressure containment resistance, minimum [bar]:	810,1	810,1
Local design pressure [bar]:	500,0	577,5
Local incidental pressure [bar]:	550,0	577,5
External pressure [bar]:	281,5	281,5
Pressure difference [bar]:	268,5	296,0
Material resistance factor [-]:	1,15	1,15
Safety class resistance factor [-]:	1,308	1,046
FINAL RESULTS:	**Operation**	**System test**
Code check, utility with given wall thickness [-]:	0,50	0,44
Required nominal wall thicness [mm]:	12,94	11,46

Appendix B – Python Script

Parameter variation script:

```
from OrcFxAPI import *
from numpy import sign
import numpy as np
from math import *
import pylab as plt
from os import system
from scipy.optimize import fmin as cg

def setBuoyancyProperties(m):

  global normPip,buoyPip,riserName

  #
  # INPUT
  #
  pipMass = m[normPip].MassPerUnitLength
  pipSteelOD = m[normPip].OD
  pipID = m[normPip].ID - 2*m[normPip].LiningThickness #SJEKK ENDRING
  pipCD = m[normPip].Cdx
  pipCDa = m[normPip].Cdz
  pipAM = m[normPip].Cax
  coatingT = m[normPip].CoatingThickness
  pipOD = pipSteelOD + 2.*coatingT

  #
  # Buoyancy modules fixed properties
  #
  buyMassHdw = 0.025                  #Buoy hardware mass
  buyMassDens = 0.395                 #Buoy material density
  buyLen = 3.0                        #Buoyant Length

  buyCDaf = 1.0                       #Axial form buoy
  buyCDas = 0.01                      #Axial skin buoy
  buyCD = 1.0                         #Drag coeff buoy
  buyAM = 1.0                         #Added mass buoy
  buyAMa = 0.5                        #Axial added mass buoy
  buyOD = 1.3                         #Initial Buoyant Diameter

  #
  # Calculate the pitch of the buoyancy modules
  #
  #Find length of buoyancy section
  lenBuySection = 0.
  for i in range(len(m[riserName].Length)):
    if m[riserName].LineType[i] == buoyPip:
      lenBuySection += m[riserName].Length[i]

  #Find total net buoyancy
  netBuoyancy = calcNetBuoyancy(m)
  volPerBuoy = (buyLen*pi/4.)*(buyOD**2 - pipOD**2)
  massPerBuoy = volPerBuoy*buyMassDens + buyMassHdw
  dispPerBuoy = volPerBuoy*1.025
  netBuoyancyPerBuoy = dispPerBuoy - massPerBuoy

  nBuoys = netBuoyancy/netBuoyancyPerBuoy
  buyPitch = lenBuySection/nBuoys

  #Calculate useful values
  buyLenFac = buyLen/buyPitch
  pipLenFac = 1.-buyLenFac
  buyArea = 0.25*pi*buyOD**2-0.25*pi*pipOD**2
  buyVol = 0.25*pi*buyOD**2*buyLenFac
  pipVol = 0.25*pi*pipOD**2*pipLenFac
  nBuyModules = 1/buyPitch

  #Calculate equivalent properties
  eqvOD = sqrt(pipLenFac*pipOD**2 + buyLenFac*buyOD**2)
  dragOD = pipOD
  eqvCD = (pipOD*pipCD*pipLenFac + buyOD*buyCD*buyLenFac)/dragOD
  eqvCDa        =        (pipOD*pipCDa*pipLenFac        +        buyOD*buyCDas*buyLenFac        +
nBuyModules*buyArea*buyCDaf/pi)/dragOD
```

```
    eqvAM = (buyAM*buyVol + pipAM*pipVol) / (buyVol+pipVol)
    eqvAMa = buyAMa*buyVol/(buyVol+pipVol)
    eqvM = pipMass + (buyMassHdw + buyLen*buyArea*buyMassDens)*nBuyModules

    #Set outer diameter
    m[buoyPip].OD = eqvOD
    #Set inner diameter
    m[buoyPip].ID = pipID
    #Set mass per unit length
    m[buoyPip].MassPerUnitLength = eqvM
    #Set outer stress diameter
    m[buoyPip].StressOD = pipSteelOD
    #Set inner stress diameter
    m[buoyPip].StressID = pipID
    #Set contact diameter
    m[buoyPip].ContactDiameter = buyOD
    #Set drag diameter normal
    m[buoyPip].NormalDragLiftDiameter = pipOD
    #Set drag diameter axial
    m[buoyPip].AxialDragLiftDiameter = pipOD
    #Set drag coefficient normal
    m[buoyPip].Cdx = eqvCD
    #m[buoyPip].Cdy = "~"
    #Set drag coefficient axial
    m[buoyPip].Cdz = eqvCDa
    #Set added mass coefficient normal x
    m[buoyPip].Cax = eqvAM
    #Set added mass coefficient normal y
    #m[buoyPip].Cay = "~"
    #Set added mass coefficient axial
    m[buoyPip].Caz = eqvAMa

    #Set structural parameters equal
    m[buoyPip].EIx = m[normPip].EIx
    m[buoyPip].EA = m[normPip].EA
    m[buoyPip].PoissonRatio = m[normPip].PoissonRatio
    m[buoyPip].GJ = m[normPip].GJ

    return m

def setNetBuoyancy(m,newNetBuoyancy):

    """Updates the net buoyancy"""

    #Get id's for normal and buoyant pipes
    global normPip,buoyPip

    #Calculate the current net buoyancy
    oldNetBuoyancy = calcNetBuoyancy(m)

    #Find the ratio between the new net buoyancy and
    #the old net buoyancy
    r = newNetBuoyancy/oldNetBuoyancy

    #Get the type id's
    typ0 = m[normPip]
    typB = m[buoyPip]

    #Find the difference in volume between normal pipe and buoyancy section
    dV0 = pi*(typB.OD**2 - (typ0.OD + 2*typ0.CoatingThickness)**2)/4.

    #Find the difference in mass between normal pipe and buoyancy section
    dM0 = (typB.MassPerUnitLength - typ0.MassPerUnitLength)

    #Find the updated differences based on the ratio
    dV1 = dV0*r
    dM1 = dM0*r

    #Calculate the updated OD
    typB.OD = sqrt((4.*dV1/pi) + (typ0.OD + 2*typ0.CoatingThickness)**2)

    #Calculate the updated mass
    typB.MassPerUnitLength = dM1 + typ0.MassPerUnitLength

    #Set correct properties for buoyancy section
    m = setBuoyancyProperties(m)
```

```
  #Return updated model
  return m

def calcNetBuoyancy(m,content=0.):

  global normPip,buoyPip,riserName

  def getWeight(typ,m,content):

    #Calculate the weight in air
    dm = typ.MassPerUnitLength
    dm_content = content*pi*typ.ID**2/4.
    dm_tot = dm + dm_content

    #Calculate the displacement
    CoatingThickness = 0.
    if typ.CoatingThickness != None:
      CoatingThickness = typ.CoatingThickness
    disp = 1.025*pi*(typ.OD+2*CoatingThickness)**2/4

    #Calculate the weight in water
    dmW = dm_tot - disp

    return dmW

  wgt0 = getWeight(m[normPip],m,content)
  wgt1 = getWeight(m[buoyPip],m,content)
  LB = 0.
  for i in range(len(m[riserName].LineType)):
    if m[riserName].LineType[i] == buoyPip:
      LB += m[riserName].Length[i]
  return LB*(wgt0 - wgt1)

def getBuoyantLength(m):
  global buoyPip,riserName
  Ltot = 0.
  for i in range(len(m[riserName].LineType)):
    if m[riserName].LineType[i] == buoyPip:
      Ltot += m[riserName].Length[i]
  return Ltot

def getTopLength(m):
  global buoyPip,riserName
  Ltot = 0.
  for i in range(len(m[riserName].LineType)):
    if m[riserName].LineType[i] == buoyPip:
      break
    Ltot += m[riserName].Length[i]
  return Ltot

def changeBuoyantLength(m,newTopLength,newBuoyantLength):

  """Change the length of the buoyant section"""

  #Import the identifiers for normal pipe and buoyant pipe
  global normPip,buoyPip,topLengthI,riserName

  #Update the top length
  oldTopLength = getTopLength(m)
  m[riserName].Length[topLengthI] += newTopLength - oldTopLength
  m[riserName].Length[-1] -= newTopLength - oldTopLength

  #Find the current length of the buoyant section
  oldBuoyantLength = getBuoyantLength(m)

  #Calculate the ratio of the new length and the old length
  r = newBuoyantLength/oldBuoyantLength

  #Adjust the length of the buoyant section
  for i in range(len(m[riserName].LineType)):
    if m[riserName].LineType[i] == buoyPip:
      m[riserName].Length[i] *= r

  #-----------------------------------------------------
  # Adjust the properties of the  buoyant section pipe
  #-----------------------------------------------------
  #Id the types
```

```
  typ0 = m[normPip]
  typB = m[buoyPip]

  #Find the difference in volume between the buoyant and non-buoyant type
  dV0 = pi*(typB.OD**2 - (typ0.OD + 2*typ0.CoatingThickness)**2)/4.

  #Find the difference in weight between the buoyant and non-buoyant type
  dM0 = (typB.MassPerUnitLength - typ0.MassPerUnitLength)

  #Calculate the updated differential volume and mass, based on new length
  dV1 = dV0/r
  dM1 = dM0/r

  #Calculate the updated outer diameter and mass, with the same density as before
  typB.OD = sqrt((4.*dV1/pi) + (typ0.OD + 2*typ0.CoatingThickness)**2)
  typB.MassPerUnitLength = dM1 + typ0.MassPerUnitLength


  #Adjust the length of the bottom section so that the total
  #riser length remains the same
  dL = newBuoyantLength - oldBuoyantLength
  m[riserName].Length[-1] -= dL

  #Set correct properties for buoyancy section
  #I.e. equivalent added mass and drag coefficients
  #volume and mass based on density, etc.
  m = setBuoyancyProperties(m)

  #Return the model
  return m

def setOffsetAndEnvironment(m,offset,envIn):

  """Set the environment and vessel offset"""

  global vesselName

  #Get the environment object
  env = m['Environment']

  #Set the wave
  env.WaveHs = envIn['Hs']
  env.WaveGamma = envIn['Gamma']
  env.WaveTp = envIn['Tp']
  env.WaveDirection = envIn['WaveDir']
  env.WaveSeed = envIn['seed']
  env.SimulationTimeOrigin = envIn['time']
  env.WaveOriginX = offset[0]
  env.WaveOriginY = offset[1]

  #Set the current
  env.CurrentDepth = [v[0] for v in envIn['CurrentTab']]
  env.CurrentFactor = [v[1] for v in envIn['CurrentTab']]
  env.RefCurrentSpeed = envIn['CurrentSpeed']
  env.RefCurrentDirection = envIn['CurrentDir']

  #Set the vessel offset
  m[vesselName].InitialX = offset[0]
  m[vesselName].InitialY = offset[1]

  #Return updated model
  return m

#-----------------------------------------------------
# INPUT - MODEL DEFINITIONS
#-----------------------------------------------------
m = Model("BaseFile.dat")
normPip = 'Line Type1'
buoyPip = 'Line Type2'
vesselName = "Cidade de Sao Paulo"
riserName = "Riser"

#Index defining the segment where the
#top length should be adjusted.
#Note that first segment is 0
topLengthI = 0
```

```
#Horizontal distance from vessel center to hangoff point
hangoffPoint = (0., 31.)


#-----------------------------------------------------
# INPUT - Parameter variations
#-----------------------------------------------------

#Name, content density [Te/m3]
contentVariation = [
#Normal must be first since this defines the lead angle!!!
("Normal",0.8),
#The others can follow
#("Heavy",1.0),
#("Light",0.8),
]

#Name, (x-offset, y-offset), Wave Dir, Current Dir
offsetVariation = [
#Nominal must be first since this defines the functional
#loadcase!!!
("Nominal", (0.,   0.) ,     270.,     270. ),
#Then you can provide the others
("Near",     (0., 154.4) ,    90.,      90. ),
("Far",      (0.,-154.4) ,     270.,     270. ),
]

#Name, buoyancy [Te]
buoyancyVariaton = [
("B150Te",150.),
("B157.5Te",157.5),
("B165Te",165.),
("B142.5Te",142.5),
("B135Te",135.),
]

#Name, (top section length, buoyant section length)
buoyantLengthVariation = [
("BL400m",(3250.,400.)),
("BL420m",(3250.,420.)),
("BL440m",(3250.,440.)),
("BL380m",(3250.,380.)),
("BL360m",(3250.,360.)),
]

#Target declination
targetDeclinationVariaton = [
("LA8deg",172.),
("LA7deg",173.),
("LA6deg",174.),
]

#-----------------------------------------------------
# INPUT - ENVIRONMENT
#-----------------------------------------------------
currentTab = [
(0    ,1      ),
(50   ,1      ),
(100  ,0.875  ),
(150  ,0.7426),
(200  ,0.6323),
(250  ,0.5735),
(300  ,0.5073),
(350  ,0.4338),
(375  ,0.4117),
(800  ,0.2867),
(1200,0.2279),
(1600,0.2205),
(2000,0.2353),
(2200,0.2353),
]

env = {"Hs":6.5,"Tp":12.5,"Gamma":1.851813124,"seed":415,"time":5013.,
       "CurrentSpeed":1.36,"CurrentTab":currentTab}
```

```
#-----------------------------------------------------
# INPUT - FINISHED
#-----------------------------------------------------

#Generate buoyancy cases
cases = []
iCase = 0
for buoy in buoyancyVariaton:
  for bLen in buoyantLengthVariation:
    for ola in targetDeclinationVariaton:

      for off in offsetVariation:
        for cont in contentVariation:

              caseName = "C%003i %s %s %s %s %s"%(iCase,off[0],cont[0],buoy[0],bLen[0],ola[0])
              funcNameID                                                                    =
"%s_%s_%s_%s_%s"%(offsetVariation[0][0],cont[0],buoy[0],bLen[0],ola[0])
              nomNameID                                                                     =
"%s_%s_%s_%s_%s"%(offsetVariation[0][0],contentVariation[0][0],buoy[0],bLen[0],ola[0])
              if funcNameID not in caseName:
                for case in cases:
                  if funcNameID in case['name']:
                    funcName = case['name']
                    break
              else:
                funcName = caseName

              cases.append({
              "name": caseName,
              "funcName": funcName,
              "nomNameID": nomNameID,
              "content":cont,
              "offset":off,
              "buoyancy":buoy,
              "buoyantLength":bLen,
              "declinationTarget":ola,
              }
              )
              iCase += 1


#Update and save OrcaFlex files
for case in cases:

  #Print
  print case['name']

  #Update the buoyancy
  m = setNetBuoyancy(m,case['buoyancy'][1])

  #Update the buoyant length
  m = changeBuoyantLength(m,*case['buoyantLength'][1])

  #Update vessel offset and environment
  env['WaveDir']    = case['offset'][2]
  env['CurrentDir'] = case['offset'][3]
  m = setOffsetAndEnvironment(m,case['offset'][1],env)

  #Set the content density
  m[riserName].ContentsDensity = case['content'][1]

  #Set functional case
  if case['funcName'] == case['name']:
    m['Code Checks'].DNVFunctionalLoadSpecifiedBy = "Current model"
  else:
    m['Code Checks'].DNVFunctionalLoadSpecifiedBy = "Simulation file"
    m['Code Checks'].DNVFunctionalLoadFileName = case['funcName'] + ".sim"

  #Iterate the hangoff angle for the nominal case, else; adapt nominal bottom length
  if case['nomNameID'] in case['name']:
    print "Running line setup wizard..."
    #m.general.LineSetupCalculationMode = 'Calculate Anchor Positions'
    m.general.LineSetupCalculationMode = 'Calculate Line Lengths'
    m[riserName].LineSetupIncluded = 'Yes'
    m[riserName].LineSetupTargetVariable = 'Declination'
    m[riserName].LineSetupTargetValue = case['declinationTarget'][1]
```

```
    m[riserName].LineSetupLineEnd = "End A"
    m[riserName].LineSetupArclength = 0.
    m[riserName].LineSetupSectionToBeModified = len(m[riserName].Length)
    m.InvokeLineSetupWizard()
    case['bottomSegmentLength'] = m[riserName].Length[-1]
    print "...done"
  else:
    for caseNom in cases:
      if case['nomNameID'] in caseNom['name']:
        m[riserName].Length[-1] = caseNom['bottomSegmentLength']
        break


#Save the model
m.CalculateStatics()
m.SaveSimulation(case['name'] + ".sim")
```

Appendix C – Optimisation Results

Net buoyancy:	135 tonnes									
Buoyancy length:	360m			380m			400m			
Hang-off angle:	6°	7°	8°	6°	7°	8°	6°	7°	8°	
Offset Position:	NOMINAL									Unit:
Hangoff angle max	10,6	11,6	12,5	10,6	11,6	12,5	10,6	11,6	12,5	deg
Hangoff angle min	0,2	1,2	2,1	0,2	1,2	2,1	0,2	1,2	2,1	deg
Hangoff angle range	10,4	10,4	10,4	10,4	10,4	10,4	10,4	10,4	10,4	deg
Top tension max	7520	7626	7784	7519	7686	7809	7564	7684	7836	kN
Top tension static	5076	5126	5182	5085	5135	5191	5094	5144	5199	kN
Top tension min	2127	2048	1965	2111	2025	1925	2098	2011	1915	kN
Bend. moment max	276	280	289	266	272	283	258	266	280	kN*m
Bend. moment static	143	125	115	130	114	105	119	104	95	kN*m
Bend. moment min	74	58	49	63	50	42	54	43	36	kN*m
Utilization max	0,66	0,68	0,71	0,66	0,69	0,71	0,67	0,69	0,72	N/A
Utilization static	0,31	0,31	0,32	0,31	0,32	0,32	0,31	0,32	0,32	N/A
Utilization min	0,13	0,12	0,12	0,13	0,12	0,12	0,13	0,12	0,12	N/A
Offset Position	NEAR									Unit:
Hangoff angle max	12,1	12,9	13,6	12,1	12,9	13,6	12,1	12,9	13,6	deg
Hangoff angle static	6,9	7,7	8,4	6,9	7,6	8,4	6,9	7,6	8,4	deg
Hangoff angle min	3,6	4,3	5,0	3,6	4,3	5,0	3,6	4,3	5,0	deg
Hangoff angle range	8,5	8,6	8,6	8,5	8,6	8,6	8,5	8,6	8,6	deg
Top tension max	6646	6661	6691	6658	6680	6695	6671	6683	6738	kN
Top tension static	4979	5009	5042	4989	5018	5051	4999	5027	5060	kN
Top tension min	3296	3301	3303	3296	3299	3312	3290	3304	3308	kN
Bend. moment max	265	238	217	244	221	202	226	205	189	kN*m
Bend. moment static	217	189	167	199	172	152	180	157	138	kN*m
Bend. moment min	207	178	155	187	163	141	172	147	126	kN*m
Utilization max	0,51	0,51	0,52	0,51	0,51	0,52	0,51	0,51	0,52	N/A
Utilization static	0,29	0,30	0,30	0,30	0,30	0,30	0,30	0,30	0,30	N/A
Utilization min	0,18	0,19	0,19	0,18	0,19	0,19	0,19	0,19	0,18	N/A
Offset Position	FAR									Unit:
Hangoff angle max	12,5	13,8	15,1	12,5	13,8	15,0	12,6	13,8	15,1	deg
Hangoff angle static	8,0	9,3	10,5	8,0	9,3	10,5	8,0	9,3	10,5	deg
Hangoff angle min	2,1	3,3	4,6	2,1	3,3	4,6	2,1	3,3	4,6	deg
Hangoff angle range	10	10	10	10	10	10	10	10	10	deg
Top tension max	7784	8030	8266	7809	8031	8278	7838	8078	8325	kN
Top tension static	5182	5261	5349	5191	5269	5357	5200	5277	5364	kN
Top tension min	1964	1842	1720	1925	1816	1711	1913	1797	1692	kN
Bend. moment max	289	309	358	282	310	369	280	314	382	kN*m
Bend. moment static	115	103	92	105	94	84	95	85	76	kN*m
Bend. moment min	49	40	33	43	34	28	36	29	24	kN*m
Utilization max	0,71	0,75	0,80	0,71	0,75	0,80	0,72	0,76	0,81	N/A
Utilization static	0,32	0,33	0,34	0,32	0,33	0,34	0,32	0,33	0,34	N/A
Utilization min	0,12	0,12	0,12	0,12	0,12	0,12	0,12	0,12	0,12	N/A

Net buoyancy:	135 tonnes						
Buoyancy length:	420m			440m			
Hang-off angle:	6°	7°	8°	6°	7°	8°	
Offset Position:	NOMINAL						Unit:
Hangoff angle max	10,6	11,6	12,6	10,6	11,6	12,6	deg
Hangoff angle min	0,2	1,2	2,1	0,2	1,2	2,1	deg
Hangoff angle range	10,4	10,4	10,4	10,4	10,4	10,4	deg
Top tension max	7563	7738	7897	7623	7747	7915	kN
Top tension static	5104	5153	5208	5113	5162	5217	kN
Top tension min	2078	1992	1876	2067	1970	1861	kN
Bend. moment max	252	262	279	247	261	281	kN*m
Bend. moment static	109	95	87	100	91	79	kN*m
Bend. moment min	46	37	31	40	33	27	kN*m
Utilization max	0,67	0,70	0,73	0,68	0,70	0,73	N/A
Utilization static	0,31	0,32	0,32	0,31	0,32	0,32	N/A
Utilization min	0,13	0,12	0,12	0,13	0,12	0,12	N/A
Offset Position	NEAR						Unit:
Hangoff angle max	12,1	12,8	13,6	12,1	12,8	13,6	deg
Hangoff angle static	6,9	7,6	8,4	6,9	7,6	8,3	deg
Hangoff angle min	3,6	4,3	5,0	3,5	4,3	5,0	deg
Hangoff angle range	8,5	8,6	8,6	8,5	8,6	8,6	deg
Top tension max	6679	6720	6721	6702	6708	6775	kN
Top tension static	5009	5037	5069	5019	5047	5079	kN
Top tension min	3296	3309	3315	3288	3308	3319	kN
Bend. moment max	209	191	177	196	176	166	kN*m
Bend. moment static	166	143	126	152	132	107	kN*m
Bend. moment min	156	132	114	142	122	74	kN*m
Utilization max	0,51	0,52	0,52	0,52	0,52	0,53	N/A
Utilization static	0,30	0,30	0,30	0,30	0,30	0,31	N/A
Utilization min	0,19	0,18	0,18	0,19	0,18	0,19	N/A
Offset Position	FAR						Unit:
Hangoff angle max	12,6	13,8	15,0	12,6	13,8	15,0	deg
Hangoff angle static	8,0	9,3	10,5	8,0	9,3	10,5	deg
Hangoff angle min	2,1	3,3	4,6	2,1	3,3	4,6	deg
Hangoff angle range	10	10	10	10	10	10	deg
Top tension max	7896	8082	8308	7912	8111	8370	kN
Top tension static	5208	5286	5373	5217	5294	5380	kN
Top tension min	1874	1760	1686	1858	1747	1669	kN
Bend. moment max	279	321	398	281	332	419	kN*m
Bend. moment static	87	78	69	79	71	63	kN*m
Bend. moment min	32	26	21	27	22	18	kN*m
Utilization max	0,73	0,76	0,81	0,73	0,77	0,82	N/A
Utilization static	0,32	0,33	0,34	0,33	0,33	0,34	N/A
Utilization min	0,12	0,12	0,12	0,12	0,12	0,12	N/A

Net buoyancy;	142.5 tonnes									
Buoyancy length:	360m			380m			400m			
Hang-off angle:	6°	7°	8°	6°	7°	8°	6°	7°	8°	
Offset Position:	NOMINAL									Unit:
Hangoff angle max	10,6	11,6	12,5	10,6	11,6	12,5	10,6	11,6	12,5	deg
Hangoff angle min	0,2	1,2	2,1	0,2	1,2	2,1	0,2	1,2	2,1	deg
Hangoff angle range	10,4	10,4	10,4	10,4	10,4	10,4	10,4	10,4	10,4	deg
Top tension max	7443	7594	7714	7465	7590	7761	7480	7648	7769	kN
Top tension static	5049	5099	5154	5058	5108	5162	5067	5117	5171	kN
Top tension min	2141	2086	1999	2134	2061	1977	2121	2054	1958	kN
Bend. moment max	278	281	286	268	272	279	258	264	273	kN*m
Bend. moment static	154	136	125	141	124	115	129	114	105	kN*m
Bend. moment min	85	68	58	74	59	50	64	51	44	kN*m
Utilization max	0,65	0,68	0,70	0,66	0,68	0,70	0,66	0,69	0,71	N/A
Utilization static	0,31	0,31	0,32	0,31	0,31	0,32	0,31	0,31	0,32	N/A
Utilization min	0,13	0,13	0,12	0,13	0,13	0,12	0,13	0,13	0,12	N/A
Offset Position:	NEAR									Unit:
Hangoff angle max	12,2	12,9	13,7	12,2	12,9	13,7	12,2	12,9	13,7	deg
Hangoff angle static	7,0	7,7	8,4	7,0	7,7	8,4	7,0	7,7	8,4	deg
Hangoff angle min	3,6	4,4	5,1	3,6	4,4	5,1	3,6	4,3	5,1	deg
Hangoff angle range	8,5	8,6	8,6	8,5	8,6	8,6	8,5	8,6	8,6	deg
Top tension max	6618	6636	6681	6630	6659	6668	6648	6657	6683	kN
Top tension static	4954	4984	5016	4964	4993	5025	4973	5002	5034	kN
Top tension min	3294	3299	3309	3293	3304	3309	3290	3299	3300	kN
Bend. moment max	284	256	231	263	236	215	242	218	199	kN*m
Bend. moment static	238	209	186	218	191	166	199	175	153	kN*m
Bend. moment min	221	193	172	204	176	155	188	163	126	kN*m
Utilization max	0,51	0,51	0,51	0,51	0,51	0,51	0,51	0,51	0,51	N/A
Utilization static	0,29	0,29	0,30	0,29	0,29	0,30	0,30	0,30	0,30	N/A
Utilization min	0,18	0,18	0,18	0,18	0,18	0,19	0,19	0,19	0,19	N/A
Offset Position:	FAR									Unit:
Hangoff angle max	12,5	13,7	15,0	12,5	13,8	15,0	12,5	13,8	15,0	deg
Hangoff angle static	8,0	9,2	10,5	8,0	9,2	10,5	8,0	9,2	10,5	deg
Hangoff angle min	2,1	3,3	4,5	2,1	3,3	4,5	2,1	3,3	4,5	deg
Hangoff angle range	10,4	10,5	10,5	10,4	10,5	10,5	10,4	10,5	10,5	deg
Top tension max	7709	7959	8174	7746	7994	8206	7762	8014	8246	kN
Top tension static	5152	5229	5316	5160	5238	5324	5170	5246	5332	kN
Top tension min	2003	1884	1755	1977	1861	1750	1961	1839	1715	kN
Bend. moment max	286	297	325	278	292	329	272	290	335	kN*m
Bend. moment static	126	113	101	115	103	93	105	94	85	kN*m
Bend. moment min	58	48	39	51	41	34	44	36	30	kN*m
Utilization max	0,70	0,74	0,78	0,70	0,75	0,79	0,71	0,75	0,79	N/A
Utilization static	0,32	0,33	0,34	0,32	0,33	0,34	0,32	0,33	0,34	N/A
Utilization min	0,12	0,12	0,12	0,12	0,12	0,12	0,12	0,12	0,12	N/A

Net buoyancy:	150 tonnes									
Buoyancy length:	360m			380m			400m			
Hang-off angle:	6°	7°	8°	6°	7°	8°	6°	7°	8°	
Offset Position:	NOMINAL									Unit:
Hangoff angle max	10,6	11,6	12,5	10,6	11,6	12,5	10,6	11,6	12,5	deg
Hangoff angle min	0,2	1,2	2,1	0,2	1,2	2,1	0,2	1,2	2,1	deg
Hangoff angle range	10,4	10,4	10,4	10,4	10,4	10,4	10,4	10,4	10,4	deg
Top tension max	7408	7539	7655	7425	7534	7706	7443	7582	7710	kN
Top tension static	5022	5071	5126	5031	5080	5134	5040	5089	5143	kN
Top tension min	2149	2106	2032	2148	2088	2008	2137	2079	1993	kN
Bend. moment max	282	284	287	270	274	278	260	264	270	kN*m
Bend. moment static	165	146	135	151	134	124	139	123	114	kN*m
Bend. moment min	97	78	67	85	68	59	75	60	52	kN*m
Utilization max	0,65	0,67	0,69	0,65	0,67	0,70	0,65	0,67	0,70	N/A
Utilization static	0,30	0,31	0,31	0,31	0,31	0,32	0,31	0,31	0,32	N/A
Utilization min	0,13	0,13	0,12	0,13	0,13	0,12	0,13	0,13	0,12	N/A
Offset Position:	NEAR									Unit:
Hangoff angle max	12,2	13,0	13,7	12,2	13,0	13,7	12,2	13,0	13,7	deg
Hangoff angle static	7,0	7,8	8,5	7,0	7,7	8,5	7,0	7,7	8,5	deg
Hangoff angle min	3,7	4,4	5,1	3,7	4,4	5,1	3,7	4,4	5,1	deg
Hangoff angle range	8,54	8,57	8,60	8,54	8,57	8,60	8,54	8,57	8,60	deg
Top tension max	6588	6609	6624	6598	6618	6641	6611	6631	6662	kN
Top tension static	4929	4958	4991	4938	4968	5000	4948	4977	5009	kN
Top tension min	3295	3296	3310	3291	3300	3304	3291	3295	3304	kN
Bend. moment max	305	273	248	281	254	229	261	234	213	kN*m
Bend. moment static	257	225	200	236	207	183	217	190	169	kN*m
Bend. moment min	243	211	186	222	193	171	204	178	157	kN*m
Utilization max	0,50	0,50	0,51	0,50	0,51	0,51	0,51	0,51	0,51	N/A
Utilization static	0,43	0,29	0,29	0,29	0,29	0,30	0,29	0,29	0,30	N/A
Utilization min	0,40	0,18	0,18	0,18	0,18	0,18	0,18	0,18	0,18	N/A
Offset Position:	FAR									Unit:
Hangoff angle max	12,5	13,7	15,0	12,5	13,7	15,0	12,5	13,7	15,0	deg
Hangoff angle static	7,9	9,2	10,5	7,9	9,2	10,5	7,9	9,2	10,5	deg
Hangoff angle min	2,0	3,3	4,5	2,1	3,3	4,5	2,1	3,3	4,5	deg
Hangoff angle range	10,4	10,5	10,5	10,4	10,5	10,5	10,4	10,5	10,5	deg
Top tension max	7637	7880	8071	7691	7914	8104	7686	7939	8155	kN
Top tension static	5121	5197	5282	5130	5206	5291	5139	5215	5299	kN
Top tension min	2039	1923	1809	2014	1903	1784	2000	1880	1759	kN
Bend. moment max	287	292	306	277	285	304	270	279	306	kN*m
Bend. moment static	136	123	111	125	113	101	115	103	93	kN*m
Bend. moment min	68	56	47	59	49	41	52	43	36	kN*m
Utilization max	0,69	0,73	0,76	0,70	0,73	0,77	0,69	0,74	0,78	N/A
Utilization static	0,32	0,32	0,33	0,32	0,33	0,33	0,32	0,33	0,33	N/A
Utilization min	0,12	0,12	0,12	0,12	0,12	0,12	0,12	0,12	0,12	N/A

Net buoyancy;	150 tonnes						
Buoyancy length:	420m			440m			
Hang-off angle:	6°	7°	8°	6°	7°	8°	
Offset Position:	NOMINAL						Unit:
Hangoff angle max	10,6	11,6	12,5	10,6	11,6	12,5	deg
Hangoff angle min	0,2	1,2	2,1	0,2	1,2	2,1	deg
Hangoff angle range	10,4	10,4	10,4	10,4	10,4	10,4	deg
Top tension max	7448	7581	7763	7488	7632	7767	kN
Top tension static	5050	5098	5152	5059	5107	5161	kN
Top tension min	2129	2060	1970	2118	2045	1955	kN
Bend. moment max	251	257	265	243	251	260	kN*m
Bend. moment static	128	113	105	118	109	96	kN*m
Bend. moment min	66	53	45	58	49	40	kN*m
Utilization max	0,65	0,67	0,70	0,66	0,68	0,71	N/A
Utilization static	0,31	0,31	0,32	0,31	0,31	0,32	N/A
Utilization min	0,13	0,13	0,12	0,13	0,12	0,12	N/A
Offset Position:	NEAR						Unit:
Hangoff angle max	12,2	13,0	13,7	12,2	12,9	12,2	deg
Hangoff angle static	7,0	7,7	8,4	7,0	7,7	7,0	deg
Hangoff angle min	3,7	4,4	5,1	3,7	4,4	3,7	deg
Hangoff angle range	8,54	8,57	8,60	8,54	8,57	8,54	deg
Top tension max	6624	6640	6665	6636	6652	6636	kN
Top tension static	4958	4986	5018	4967	4996	4967	kN
Top tension min	3289	3293	3306	3289	3295	3289	kN
Bend. moment max	241	219	197	224	201	224	kN*m
Bend. moment static	200	175	155	184	161	184	kN*m
Bend. moment min	190	164	144	175	151	175	kN*m
Utilization max	0,51	0,51	0,51	0,51	0,51	0,51	N/A
Utilization static	0,29	0,30	0,30	0,29	0,30	0,29	N/A
Utilization min	0,18	0,19	0,18	0,18	0,19	0,18	N/A
Offset Position:	FAR						Unit:
Hangoff angle max	12,5	13,7	15,0	12,5	13,7	15,0	deg
Hangoff angle static	7,9	9,2	10,5	7,9	9,2	10,5	deg
Hangoff angle min	2,1	3,3	4,5	2,1	3,3	4,5	deg
Hangoff angle range	10,4	10,5	10,5	10,4	10,5	10,5	deg
Top tension max	7744	7978	8190	7748	7993	8224	kN
Top tension static	5148	5224	5308	5157	5232	5316	kN
Top tension min	1975	1857	1750	1959	1834	1713	kN
Bend. moment max	264	277	309	259	276	316	kN*m
Bend. moment static	105	95	85	97	87	78	kN*m
Bend. moment min	45	37	31	40	33	27	kN*m
Utilization max	0,70	0,74	0,78	0,70	0,75	0,79	N/A
Utilization static	0,32	0,33	0,34	0,32	0,33	0,34	N/A
Utilization min	0,12	0,12	0,12	0,12	0,12	0,12	N/A

Net buoyancy;	157.5 tonnes									
Buoyancy length:	360m			380m			400m			
Hang-off angle:	6°	7°	8°	6°	7°	8°	6°	7°	8°	
Offset Position:	NOMINAL									Unit:
Hangoff angle max	10,6	11,6	12,5	10,6	11,6	12,5	10,6	11,6	12,5	deg
Hangoff angle min	0,2	1,2	2,1	0,2	1,2	2,1	0,2	1,2	2,1	deg
Hangoff angle range	10,3	10,4	10,4	10,3	10,4	10,4	10,3	10,4	10,4	deg
Top tension max	7360	7463	7597	7379	7478	7614	7390	7492	7653	kN
Top tension static	4995	5043	5097	5004	5052	5106	5013	5061	5115	kN
Top tension min	2153	2106	2057	2155	2108	2038	2144	2090	2028	kN
Bend. moment max	286	287	289	273	276	279	262	265	270	kN*m
Bend. moment static	175	155	145	161	143	133	148	132	123	kN*m
Bend. moment min	108	88	76	96	78	68	85	69	60	kN*m
Utilization max	0,64	0,66	0,68	0,64	0,66	0,68	0,64	0,66	0,69	N/A
Utilization static	0,30	0,31	0,31	0,30	0,31	0,31	0,30	0,31	0,31	N/A
Utilization min	0,13	0,13	0,13	0,13	0,13	0,12	0,13	0,13	0,12	N/A
Offset Position:	NEAR									Unit:
Hangoff angle max	12,3	13,1	13,8	12,3	13,0	13,8	12,3	13,0	13,8	deg
Hangoff angle static	7,1	7,8	8,5	7,1	7,8	8,5	7,1	7,8	8,5	deg
Hangoff angle min	3,8	4,5	5,2	3,7	4,5	5,2	3,7	4,5	5,2	deg
Hangoff angle range	8,5	8,6	8,6	8,5	8,6	8,6	8,5	8,6	8,6	deg
Top tension max	6549	6578	6604	6563	6590	6614	6577	6602	6625	kN
Top tension static	4904	4933	4966	4913	4942	4975	4923	4952	4984	kN
Top tension min	3286	3292	3300	3287	3292	3300	3287	3292	3300	kN
Bend. moment max	323	289	262	299	269	243	277	250	227	kN*m
Bend. moment static	276	242,7	216	254	222	198	234	206	182	kN*m
Bend. moment min	261	226	200	241	208	184	223	193	169	kN*m
Utilization max	0,53	0,50	0,50	0,50	0,50	0,50	0,50	0,50	0,51	N/A
Utilization static	0,45	0,29	0,29	0,29	0,29	0,29	0,29	0,29	0,29	N/A
Utilization min	0,43	0,18	0,18	0,18	0,18	0,18	0,18	0,18	0,18	N/A
Offset Position:	FAR									Unit:
Hangoff angle max	12,4	13,7	14,9	12,4	13,7	14,9	12,4	13,7	14,9	deg
Hangoff angle static	7,9	9,1	10,4	7,9	9,2	10,4	7,9	9,2	10,4	deg
Hangoff angle min	2,0	3,2	4,4	2,0	3,2	4,4	2,0	3,2	4,4	deg
Hangoff angle range	10,4	10,4	10,5	10,4	10,4	10,5	10,4	10,5	10,5	deg
Top tension max	7574	7797	7988	7611	7810	8034	7615	7856	8057	kN
Top tension static	5090	5165	5249	5099	5174	5258	5109	5183	5266	kN
Top tension min	2063	1961	1843	2047	1942	1820	2036	1920	1807	kN
Bend. moment max	289	290	297	278	282	290	270	274	289	kN*m
Bend. moment static	146	133	120	134	122	110	124	112	101	kN*m
Bend. moment min	78	65	54	69	57	48	61	50	42	kN*m
Utilization max	0,68	0,71	0,75	0,68	0,72	0,76	0,68	0,72	0,76	N/A
Utilization static	0,31	0,32	0,33	0,31	0,32	0,33	0,32	0,32	0,33	N/A
Utilization min	0,13	0,12	0,12	0,12	0,12	0,12	0,12	0,12	0,12	N/A

Net buoyancy;	157.5 tonnes						
Buoyancy length:	420m			440m			
Hang-off angle:	6°	7°	8°	6°	7°	8°	
Offset Position:	NOMINAL						Unit:
Hangoff angle max	10,6	11,6	12,5	10,6	11,6	12,5	deg
Hangoff angle min	0,2	1,2	2,1	0,2	1,2	2,1	deg
Hangoff angle range	10,4	10,4	10,4	10,4	10,4	10,4	deg
Top tension max	7421	7524	7664	7426	7527	7711	kN
Top tension static	5022	5070	5123	5032	5079	5132	kN
Top tension min	2148	2085	2007	2130	2068	1991	kN
Bend. moment max	252	258	263	244	250	257	kN*m
Bend. moment static	137	122	113	127	112	104	kN*m
Bend. moment min	76	61	53	67	54	46	kN*m
Utilization max	0,65	0,67	0,69	0,65	0,67	0,70	N/A
Utilization static	0,30	0,31	0,31	0,31	0,31	0,32	N/A
Utilization min	0,13	0,13	0,12	0,13	0,13	0,12	N/A
Offset Position:	NEAR						Unit:
Hangoff angle max	12,3	13,0	13,8	12,3	13,0	13,8	deg
Hangoff angle static	7,1	7,8	8,5	7,0	7,8	8,5	deg
Hangoff angle min	3,7	4,4	5,2	3,7	4,4	5,2	deg
Hangoff angle range	8,5	8,6	8,6	8,5	8,6	8,6	deg
Top tension max	6591	6614	6637	6604	6624	6648	kN
Top tension static	4932	4961	4993	4942	4970	5002	kN
Top tension min	3287	3291	3300	3287	3291	3300	kN
Bend. moment max	258	233	211	239	216	197	kN*m
Bend. moment static	216	190	169	200	175	155	kN*m
Bend. moment min	207	178	157	191	165	144	kN*m
Utilization max	0,50	0,51	0,51	0,50	0,51	0,51	N/A
Utilization static	0,29	0,29	0,29	0,29	0,29	0,30	N/A
Utilization min	0,18	0,18	0,18	0,18	0,18	0,18	N/A
Offset Position:	FAR						Unit:
Hangoff angle max	12,4	13,7	14,9	12,4	13,7	14,9	deg
Hangoff angle static	7,9	9,2	10,4	7,9	9,2	10,4	deg
Hangoff angle min	2,0	3,2	4,4	2,0	3,2	4,4	deg
Hangoff angle range	10,4	10,5	10,5	10,4	10,5	10,5	deg
Top tension max	7671	7883	8082	7670	7916	8132	kN
Top tension static	5118	5192	5275	5127	5201	5283	kN
Top tension min	2014	1901	1784	1998	1874	1757	kN
Bend. moment max	262	270	287	256	266	289	kN*m
Bend. moment static	114	103	93	105	95	86	kN*m
Bend. moment min	53	44	37	47	39	33	kN*m
Utilization max	0,69	0,73	0,76	0,69	0,73	0,77	N/A
Utilization static	0,32	0,32	0,33	0,32	0,32	0,33	N/A
Utilization min	0,12	0,12	0,12	0,12	0,12	0,12	N/A

Net buoyancy;	165 tonnes									
Buoyancy length:	360m			380m			400m			
Hang-off angle:	6°	7°	8°	6°	7°	8°	6°	7°	8°	
Offset Position:	NOMINAL									Unit:
Hangoff angle max	10,6	11,5	12,5	10,6	11,5	12,5	10,6	11,5	12,5	deg
Hangoff angle min	0,2	1,2	2,1	0,2	1,2	2,1	0,2	1,2	2,1	deg
Hangoff angle range	10,3	10,4	10,4	10,3	10,4	10,4	10,3	10,4	10,4	deg
Top tension max	7317	7403	7543	7329	7424	7555	7348	7441	7593	kN
Top tension static	4967	5016	5069	4977	5024	5077	4986	5033	5086	kN
Top tension min	2153	2123	2073	2155	2121	2059	2146	2111	2053	kN
Bend. moment max	290	290	292	276	278	281	264	267	271	kN*m
Bend. moment static	185	174	154	170	160	142	157	147	131	kN*m
Bend. moment min	119	106	86	107	94	76	95	84	68	kN*m
Utilization max	0,63	0,65	0,67	0,63	0,65	0,67	0,64	0,65	0,68	N/A
Utilization static	0,30	0,30	0,31	0,30	0,31	0,31	0,30	0,31	0,31	N/A
Utilization min	0,13	0,13	0,13	0,13	0,13	0,13	0,13	0,13	0,13	N/A
Offset Position:	NEAR									Unit:
Hangoff angle max	12,4	13,1	13,9	12,3	13,1	13,9	12,3	13,1	13,8	deg
Hangoff angle static	7,1	7,9	8,6	7,1	7,9	8,6	7,1	7,8	8,6	deg
Hangoff angle min	3,8	4,5	5,3	3,8	4,5	5,2	3,8	4,5	5,2	deg
Hangoff angle range	8,5	8,6	8,6	8,5	8,6	8,6	8,5	8,6	8,6	deg
Top tension max	6510	6544	6574	6525	6557	6585	6540	6570	6596	kN
Top tension static	4878	4908	4941	4888	4917	4949	4897	4926	4958	kN
Top tension min	3276	3288	3296	3279	3288	3295	3281	3288	3295	kN
Bend. moment max	340	306	276	316	283	257	294	265	239	kN*m
Bend. moment static	294	259	229	271	239	212	251	221	196	kN*m
Bend. moment min	280	243	214	260	224	198	240	208	183	kN*m
Utilization max	0,55	0,51	0,50	0,52	0,50	0,50	0,50	0,50	0,50	N/A
Utilization static	0,48	0,43	0,29	0,45	0,29	0,29	0,29	0,29	0,29	N/A
Utilization min	0,46	0,40	0,18	0,43	0,18	0,18	0,18	0,18	0,18	N/A
Offset Position:	FAR									Unit:
Hangoff angle max	12,4	13,6	14,9	12,4	13,6	14,9	12,4	13,6	14,9	deg
Hangoff angle static	7,8	9,1	10,4	7,8	9,1	10,4	7,8	9,1	10,4	deg
Hangoff angle min	2,0	3,2	4,4	2,0	3,2	4,4	2,0	3,2	4,4	deg
Hangoff angle range	10,4	10,4	10,5	10,4	10,4	10,5	10,4	10,4	10,5	deg
Top tension max	7515	7715	7912	7526	7721	7951	7550	7771	7969	kN
Top tension static	5060	5133	5215	5068	5142	5224	5078	5151	5233	kN
Top tension min	2081	1992	1876	2070	1968	1860	2059	1956	1837	kN
Bend. moment max	291	292	294	280	283	286	271	273	280	kN*m
Bend. moment static	156	143	130	144	131	119	133	121	110	kN*m
Bend. moment min	88	74	62	78	66	55	69	58	49	kN*m
Utilization max	0,67	0,70	0,73	0,67	0,70	0,74	0,67	0,71	0,74	N/A
Utilization static	0,31	0,32	0,33	0,31	0,32	0,33	0,31	0,32	0,33	N/A
Utilization min	0,13	0,12	0,12	0,13	0,12	0,12	0,13	0,12	0,12	N/A

Net buoyancy;	165 tonnes						
Buoyancy length:	420m			440m			
Hang-off angle:	6°	7°	8°	6°	7°	8°	
Offset Position:	NOMINAL						Unit:
Hangoff angle max	10,6	11,5	12,5	10,6	11,6	12,5	deg
Hangoff angle min	0,2	1,2	2,1	0,2	1,2	2,1	deg
Hangoff angle range	10,3	10,4	10,4	10,3	10,4	10,4	deg
Top tension max	7372	7469	7602	7381	7489	7648	kN
Top tension static	4995	5042	5095	5004	5052	5104	kN
Top tension min	2145	2102	2033	2137	2091	2026	kN
Bend. moment max	254	258	263	245	250	256	kN*m
Bend. moment static	145	130	121	135	120	112	kN*m
Bend. moment min	85	69	60	76	62	54	kN*m
Utilization max	0,64	0,66	0,68	0,64	0,66	0,69	N/A
Utilization static	0,30	0,31	0,31	0,30	0,31	0,31	N/A
Utilization min	0,13	0,13	0,12	0,13	0,13	0,12	N/A
Offset Position:	NEAR						Unit:
Hangoff angle max	12,3	13,1	13,8	12,3	13,1	13,8	deg
Hangoff angle static	7,1	7,8	8,6	7,1	7,8	8,5	deg
Hangoff angle min	3,8	4,5	5,2	3,8	4,5	5,2	deg
Hangoff angle range	8,5	8,6	8,6	8,5	8,6	8,6	deg
Top tension max	6555	6582	6608	6568	6594	6618	kN
Top tension static	4907	4936	4967	4916	4945	4976	kN
Top tension min	3282	3288	3295	3283	3287	3295	kN
Bend. moment max	273	246	224	255	230	209	kN*m
Bend. moment static	233	204	181	215	189	168	kN*m
Bend. moment min	223	193	169	207	179	157	kN*m
Utilization max	0,50	0,50	0,50	0,50	0,50	0,50	N/A
Utilization static	0,29	0,29	0,29	0,29	0,29	0,29	N/A
Utilization min	0,18	0,18	0,18	0,18	0,18	0,18	N/A
Offset Position:	FAR						Unit:
Hangoff angle max	12,4	13,6	14,9	12,4	13,6	14,9	deg
Hangoff angle static	7,9	9,1	10,4	7,9	9,1	10,4	deg
Hangoff angle min	2,0	3,2	4,4	2,0	3,2	4,4	deg
Hangoff angle range	10,4	10,4	10,5	10,4	10,4	10,5	deg
Top tension max	7575	7777	8009	7598	7831	8036	kN
Top tension static	5087	5160	5242	5096	5169	5250	kN
Top tension min	2043	1935	1819	2033	1914	1797	kN
Bend. moment max	262	268	275	255	261	274	kN*m
Bend. moment static	123	112	101	113	103	94	kN*m
Bend. moment min	62	52	43	55	46	38	kN*m
Utilization max	0,68	0,71	0,75	0,68	0,72	0,76	N/A
Utilization static	0,31	0,32	0,33	0,31	0,32	0,33	N/A
Utilization min	0,12	0,12	0,12	0,12	0,12	0,12	N/A